A characterization of the expression, regulation, and function of the mouse voltage-sensitive phosphatase, Mm-VSP

Mario Giavonni Rosasco

A dissertation

submitted in partial fulfillment of the

requirements for the degree of

Doctor of Philosophy

University of Washington

2015

Reading Committee:

Sandra Bajjalieh, Chair

Richard Gardner

Sharona Gordon

Program Authorized to Offer Degree:

Pharmacology

©Copyright 2015

Mario Giavonni Rosasco

University of Washington

Abstract

A characterization of the expression, regulation, and function of the mouse voltage-sensitive phosphatase, Mm-VSP

Mario Giavonni Rosasco

Chair of the Supervisory Committee:
Professor Sandra Bajjalieh
Department of Pharmacology

Voltage-sensitive phosphatases (VSPs) are proteins that directly couple changes in membrane electrical potential to changes in the enzymatic activity of a lipid phosphatase domain. The best characterized activity of VSPs so far is dephosphorylation of the lipid substrates phosphatidylinositol 4,5-bisphosphate ($PI(4,5)P_2$), phosphatidylinositol 3,4-bisphosphate ($PI(3,4)P_2$), and phosphatidylinositol 3,4,5-trisphosphate ($PI(3,4,5)P_3$). These phospholipid signals regulate many important cellular signaling cascades that have been implicated in numerous diseases, and regulated electrical signaling is also known to play a crucial role in an equally broad variety of cell signaling events and diseases. Given that VSPs are uniquely able to directly couple these two signaling mechanisms, there is a clear biomedical motivation to fully understand the roles that VSPs play in cell signaling.

Great progress has been made using VSPs as tools to investigate phosphoinositide signaling pathways and to investigate structural mechanisms of electrochemical coupling in cells. However despite these advancements, the mammalian members of the VSP family remain poorly characterized relative to their non-mammalian counterparts, and very little is known about the

cell signaling roles that any VSP proteins serve. To address this gap in knowledge, I have characterized the expression, regulation, and activity of the VSP family member from mouse, giving particular attention to a possible role in the central nervous system. This dissertation will begin with a summary of the current state of understanding of both mammalian and non-mammalian VSPs, and then discuss what I have recently learned about the properties of the mouse VSP. In particular, I have demonstrated that the mouse protein is expressed in the central nervous system, where its expression is developmentally regulated at both the mRNA and protein levels. I have also shown that the mouse protein's transmembrane segments function as a voltage sensing domain, and that the phosphatase domain is capable of reducing the concentration of $PI(4,5)P_2$ at the plasma membrane. These properties of the mouse VSP are distinct from the reported properties of the non-mammalian VSPs, suggesting interesting and unique physiological roles for the VSPs from mammals.

Table of Contents

List of Tables and Figures

Chapter 1: Introduction

I. A tale of two signals

Cells are complex living entities that have evolved to handle the daunting task of integrating environmental stimuli in a way that promotes each cell's own survival. The mechanisms that have evolved in cells to accomplish this feat are as myriad as the stimuli to which the cells must respond, and new mechanisms are still being discovered regularly. As humans, one of the cell types that holds the greatest intrigue for us is the neuron. This amazing class of cells underlies all of our higher cognitive functions, and regulates countless other bodily processes. As would be expected for cells tasked with coordinating such varied and intricate processes, the signaling mechanisms that occur within just a single neuron are often staggeringly diverse. Two of these mechanisms – phosphoinositide signaling and changes in transmembrane voltage – will be the primary focus of this dissertation, with a particular focus on neurons.

II. Signaling through phospholipids – the phosphorylation states of phosphatidylinositol

One of the ways that neurons are able to coordinate many different signals within a single cell is by spatial separation of the signals. To a large extent, this separation is achieved through the use of lipid bilayers that form membranes to delineate different subcellular compartments, as well as to separate the inside of the cell from its surroundings. The membrane that encloses the cell is termed the plasma membrane, and the lipids on the inner leaflet (cytoplasmic side) and outer leaflet (extracellular side) serve distinct signaling roles.

Of particular importance, a small percentage of the lipids on the inner leaflet are phosphoinositides – differently phosphorylated forms of the lipid phosphatidylinositol (PI). The head group of PI can be phosphorylated at each of the third, fourth, and fifth positions of the

inositol ring by lipid kinases (Fig 1). Conversely, the phosphoinositides can be dephosphorylated by lipid phosphatases. Signaling by phosphoinositides is generally achieved by the lipids acting as second messengers, as cofactors, or as binding sites for proteins. Protein binding to phosphoinositides can be highly specific, as in the case of the pleckstrin homology protein domains (PH domains), which often specifically bind to a single phosphoinositide species (Table 1). Because of this specific binding, the differently phosphorylated forms of PI often have distinct roles in many different signaling processes, and the activities of the lipid phosphatases and kinases serve to indirectly regulate these signaling cascades.

One specific example of phospholipid signaling that is relevant to this dissertation is the pathway mediated by the lipid phosphatase PTEN. The gene encoding PTEN was originally identified as a tumor suppressor that was heavily mutated in various cancers (Li et al., 1997; Steck et al., 1997). PTEN was later shown to be a lipid phosphatase that dephosphorylates the 3' phosphate of phosphatidylinositol 3,4,5-trisphosphate ($PI(3,4,5)P_3$) (Maehama and Dixon, 1998). $PI(3,4,5)P_3$ is generated from phosphatidylinositol 4,5-bisphosphate through the enzymatic activity of the PI 3-kinase (PI3K), and then acts as a cellular growth signal by serving as a binding site for the PH domain in protein kinase B (PKB, also known as Akt). The dephosphorylation of the 3' phosphate in $PI(3,4,5)P_3$ in PTEN prevents this binding, and thereby acts to inhibit cell growth, leading to the protein's role as a tumor suppressor. The topic of PTEN's structure and enzymatic activity will arise again when we address the discovery and activity of the voltage-sensitive phosphatases.

III. Signaling through transmembrane voltage – the S4-based voltage sensor

The lipid bilayer forming the plasma membrane of neurons, in addition to containing the phosphoinositide signals described above, serves as a charge separator. Charged ions cannot

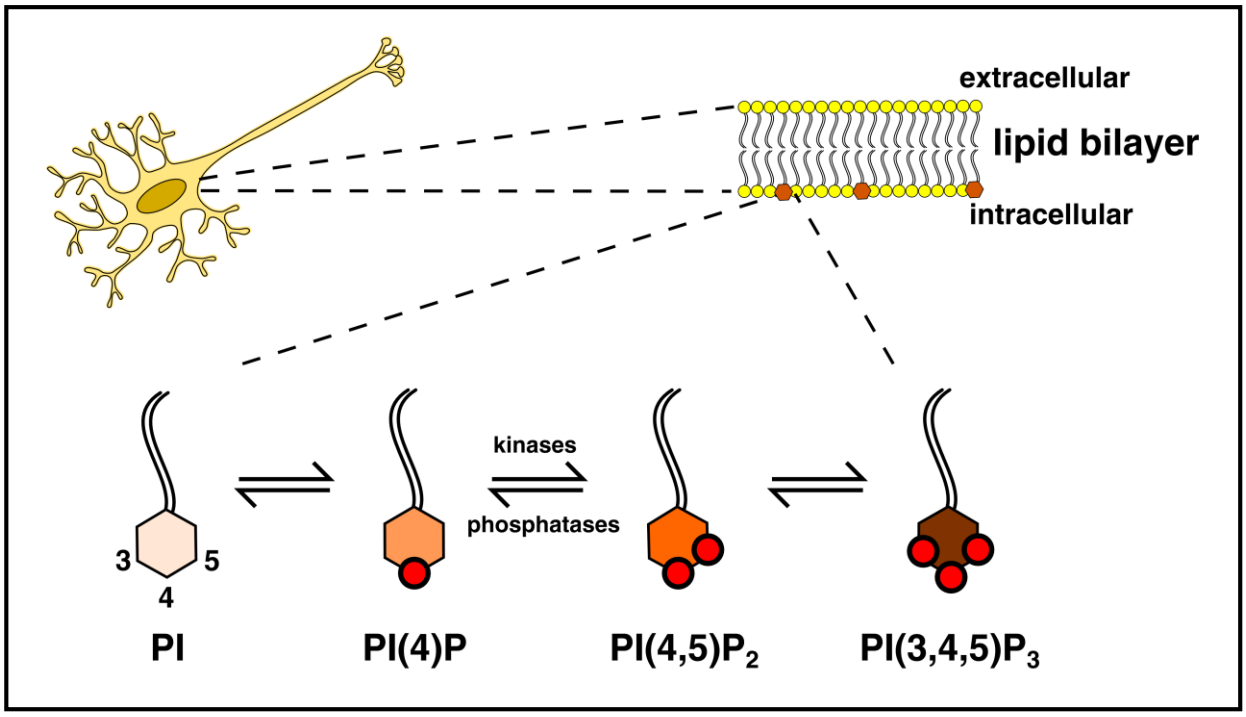

Figure 1: Phosphoinositide signaling is mediated by lipid kinases and phosphatases

A cartoon depicting the phosphoinositide signaling molecules. The plasma membrane of a cell such as a neuron (top left) is formed by a lipid bilayer (top right). Of the lipids that make up the intracellular leaflet of the bilayer, a small percentage are phosphoinositides (bottom). Phosphatidylinositol (PI, bottom left) can be phosphorylated by lipid kinases at three positions of the inositol ring (labeled 3,4,5). Conversely, phosphates can be removed by the activity of lipid phosphatases. Differently phosphorylated phosphoinositides are involved in different signaling cascades by acting as protein binding targets, cofactors, and second messengers. Other phosphorylation permutations have been identified in cells as well, but for clarity are not shown here.

PH domain	*Target Lipid*	*Reference*	*Notes*
Akt-PH	$PI(3,4,5)P_3$, $PI(3,4)P_2$	(Gray et al., 1999)	Also called PKB-PH
Btk-PH	$PI(3,4,5)P_2$	(Salim et al., 1996)	
FAPP1-PH	PI(4)P	(Levine and Munro, 2002)	
GRP1-PH	$PI(3,4,5)P_3$	(Gray et al., 1999)	
OSBP-PH	PI(4)P	(Levine and Munro, 2002)	
PLCd1-PH	$PI(4,5)P_2$	(Varnai and Balla, 1998)	
TAPP1-PH	$PI(3,4)P_2$	(Dowler et al., 2000)	

Table 1: Phosphoinositide binding specificity of pleckstrin homology domains

Pleckstrin homology (PH) domains are protein domains that have evolved to specifically recognize various lipid species in membranes. Listed here some of the PH domains that have been fluorescently labeled and used to track the presence of phosphoinositides. The proteins in which the PH domains were identified are listed on the left, with the target lipids listed to the right.

easily diffuse across the hydrophobic barrier established by the fatty acid tails of the lipids in the membrane, enabling the cell to establish different concentrations of ions inside and outside the cell. This ionic separation is largely performed through the activity of ion transporters, which use either ATP or other ionic gradients as an energy source to move ions to the opposite site of the membrane. In a resting neuron, transporters and other mechanisms lead to the intracellular side of the plasma membrane bearing a more negative charge than the extracellular side. This property is termed the resting membrane potential, and in neurons the resting membrane potential is approximately -70 mV (Kandel et al., 2000).

The membrane potential of a neuron is not static however, and many different stimuli can lead to the intracellular side of the plasma membrane becoming more negative (hyperpolarization), or less negative (depolarization) relative to the extracellular side. Many different physiological processes are affected by these fluctuations in membrane potential, and a wide variety of diseases are known to involve deregulation of these signals. For the better part of the last century, the proteins that have been best studied for their ability to respond to these changes in transmembrane voltage are the voltage-gated ion channels (Hille, 2001).

A canonical voltage-gated ion channel is made up of two different functional domains: the voltage-sensing domain (VSD) and the pore domain. The VSD comprises 4 transmembrane helical segments, termed S1 through S4, and the pore domain contains two additional transmembrane helices, S5 and S6. Four different VSD-pore pairs must assemble to form a functional channel. This assembly can take place between independent subunits, as in mammalian voltage-gated potassium channels and bacterial voltage-gated sodium channels, or between linked pseudosubunit domains, as in the mammalian voltage-gated sodium and calcium channels (Yu et al., 2005).

Within the S4 helix of the VSD, voltage-gated ion channels contain positively-charged amino acid residues. These residues are spaced three residues apart, positioning them on the same face of the helix (Fig 2). At rest, the negative resting membrane potential electrostatically attracts these positive residues towards the inside of the cell, stabilizing the S4 of the VSD in a "down" state. This down state of the VSD most commonly results in closure of the channel pore, and for this reason is also termed the resting or deactivated state. When the cell membrane is depolarized, the positive charges in S4 are electrostatically drawn towards the extracellular side of the membrane, driving the S4 of the VSD towards an "up" state. The transition of the VSD to this state is most commonly associated with the opening of the pore, and is accordingly also called the active state. The process of opening and closing the pore domain in ion channels is referred to as gating, and so the positive charges in S4 that confer voltage-sensitive gating to channels are collectively called the gating charge residues (Bezanilla, 2000).

It should be noted that while the voltage-regulated signaling discussed in this dissertation will be focused on neurons, regulated electrical signaling is essential in a wide variety of cell types and biological processes. In phenomena as diverse as conscious thought, muscle contraction, and immunological responses electrical signaling is known to play a primary role. Furthermore, although studies of the voltage-gated ion channels have explained a wide variety of voltage-sensitive physiological processes over the years, there exist a number of observed processes that are known to be voltage-dependent, but that cannot be explained by the involvement of any voltage-gated ion channels (eg: (Reddy et al., 1995; Mahaut-Smith et al., 1999; Mason and Mahaut-Smith, 2001; Billups et al., 2006)). This suggests the existence of voltage-sensitive proteins other than the ion channels. In the next chapter I will introduce one such family of proteins that has recently been discovered.

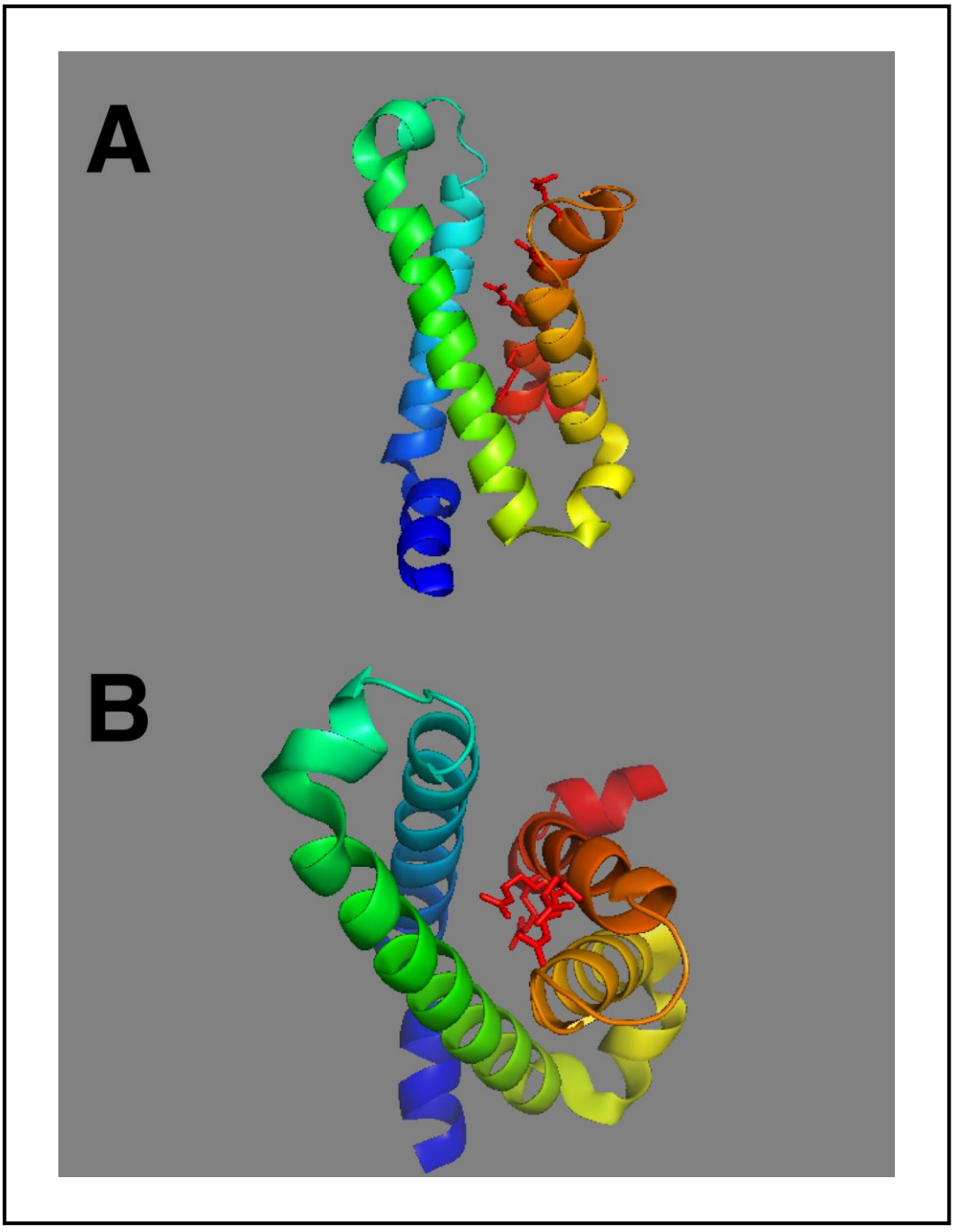

Figure 2: The S4-based voltage sensor

Shown is the crystal structure of a representative voltage sensing domain, from the structure of the bacterial voltage-gated sodium channel, NavAb (Payandeh et al., 2011). Transmembrane helices are colored from blue (S1) to red (S4). **(A)** Shows a view perpendicular to the transmembrane helices, and **(B)** shows a view from the extracellular side of the domain. The gating charge residues in S4 are the only residues depicted as stick representations, and are shown with their side chains colored red.

Chapter 2: Voltage-Sensitive Phosphatases

I. The discovery and expression of the VSPs

The voltage-sensitive phosphatases (VSPs) represent the first discovered – and so far only – proteins that directly couple changes in transmembrane voltage to enzymatic activity within a single protein (Murata et al., 2005). Like voltage-gated ion channels, VSPs contain four transmembrane segments that act as a voltage sensor (Fig 3). However, rather than coupling to the opening of an ion conducting pore, voltage sensor movements in VSPs affect the enzymatic activity of a lipid phosphatase domain on the cytoplasmic face of the protein.

The current field of VSP research has gone through two phases so far, which can be generally defined by work involving mammalian VSPs, and work involving non-mammalian VSPs. Although the mammalian VSPs were identified prior to their non-mammalian counterparts, much less is known about the mammalian VSPs. As we will see, this divide has largely been driven by differences in the functionality and accessibility of the two groups of VSPs. This is perhaps unsurprising, as a phylogenetic analysis of the VSP proteins shows that the best-studied VSPs, from sea squirt and zebrafish, are highly evolutionarily divergent from the mammalian proteins (Fig 4). Furthermore, even the characterization of the sea squirt and zebrafish VSPs has been primarily biophysical, leaving the question of what the physiological roles of VSPs are unanswered.

In this dissertation, I will present results characterizing the expression, regulation, and function of the VSP protein from mouse, to gain insight into the activity of the VSPs in mammals. To introduce the significance of this work, I will begin with a summary of the current understanding of the VSP proteins from both mammalian and non-mammalian species.

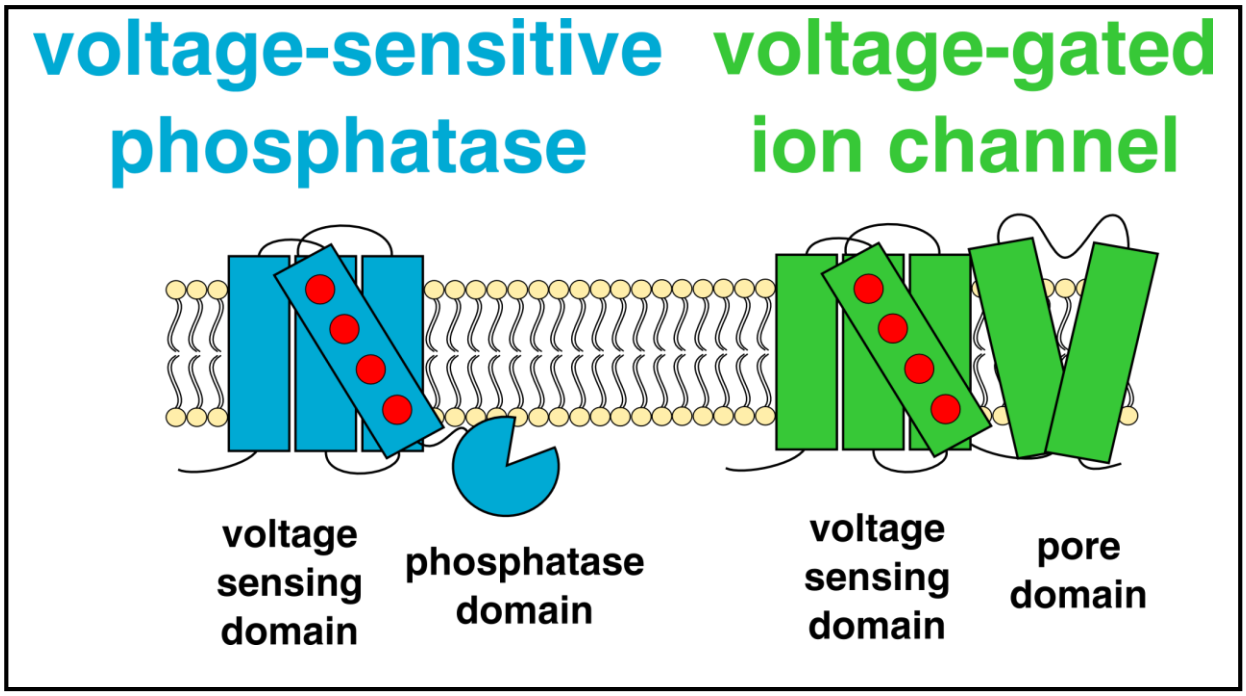

Figure 3: Topology of voltage-sensitive phosphatases and voltage-gated ion channels

A cartoon depicting the organization of voltage-sensitive phosphatases (blue) and voltage-gated ion channels (green). The positive charges in the 4th transmembrane segment (S4) that confer sensitivity to voltage are drawn as red circles.

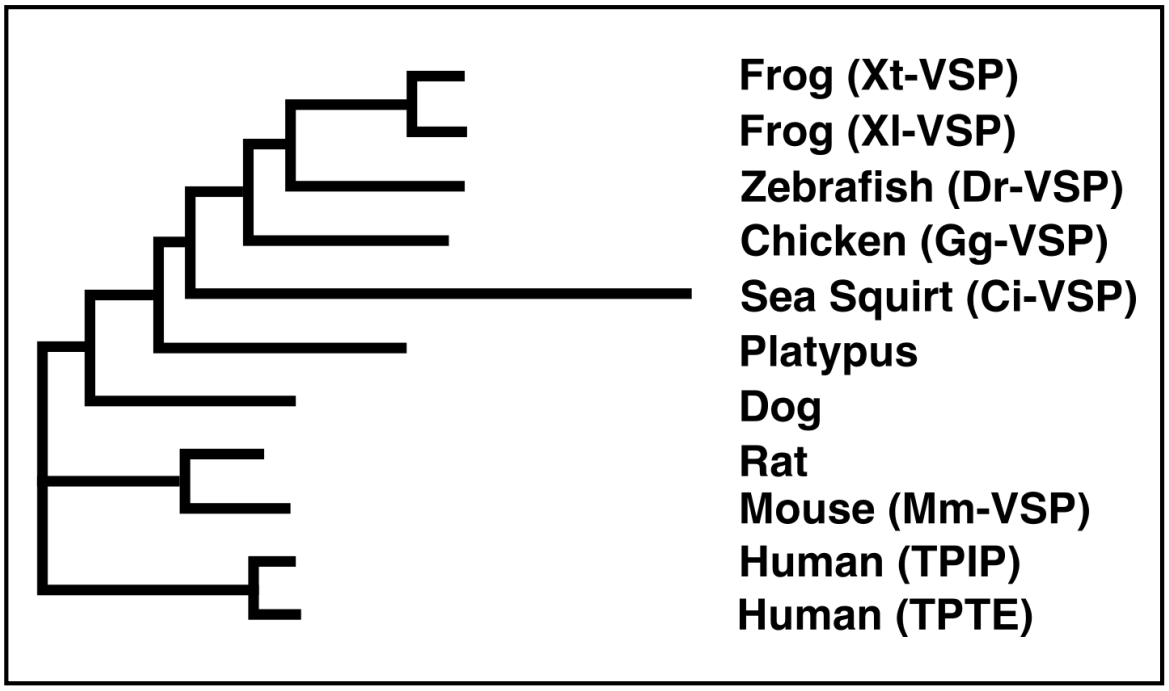

Figure 4: Phylogenetic clustering of VSP voltage sensor sequences from different species

Phylogenetic clustering was performed using the ClustalW algorithm (McWilliam et al., 2013), with protein sequences of the voltage sensor region from VSPs of various species as input. In the tree on the left, longer branch lengths indicate more divergent protein sequences. On the right are the species the VSP sequences were taken from, with proteins names (if they have been reported) listed in parentheses. From this analysis it is clear that the best-studied VSP, Ci-VSP, is highly evolutionarily divergent from the mammalian VSPs.

Discovery and expression of VSP proteins in mammals

After the discovery that the PTEN lipid phosphatase was a major tumor suppressor (Li et al., 1997; Steck et al., 1997), a number of research groups undertook to identify homologues of PTEN, predicting that such homologues might also be important signaling enzymes. One such homologue was identified in humans (Chen et al., 1999) and another in mice (Guipponi et al., 2001; Wu et al., 2001). Like PTEN these proteins were found to contain a phosphatase and tensin domain, and were accordingly named transmembrane phosphatases with tensin homology (TPTEs). The "transmembrane" part of the TPTE nomenclature refers to the presence of a domain in TPTE not found in PTEN, which was predicted to contain 4 transmembrane helices. Subsequently, a closely-related protein termed TPTE and PTEN homologous inositol lipid phosphatase (TPIP) was discovered in humans (Walker et al., 2001), which also contained a domain with 4 predicted transmembrane helices.

The transmembrane domains of TPTE and TPIP were noted to be homologous to the voltage sensors of voltage-gated ion channels (Wu et al., 2001; Kumanovics et al., 2002), predicting that the proteins would exhibit voltage-regulated activity. The discovery that the non-mammalian homologues to these proteins demonstrate voltage-dependent phosphatase activity further supported this prediction (Murata et al., 2005), and resulted in the family of proteins being renamed the voltage-sensitive phosphatases (VSPs). However until now, there has been no reported characterization of voltage-regulated activity in a VSD from TPTE or TPIP, and because of this the mammalian proteins are still frequently referred to by their original gene names. Regarding nomenclature of the mouse VSP/TPTE protein, in the third chapter of this dissertation I discuss data indicating that the protein exhibits both voltage regulation and

phosphatase activity. I will therefore refer to this protein as the voltage-sensitive phosphatase from *Mus musculus* (Mm-VSP) from hereon for clarity.

Mm-VSP, human TPTE, and human TPIP all undergo differential splicing, and are thus expressed as various isoforms. These isoforms lead primarily to differences in the amino terminal half of the proteins, and the resulting proteins show distinct subcellular localization when heterologously expressed (Walker et al., 2001; Tapparel et al., 2003). Mice contain only one gene encoding Mm-VSP, located on chromosome 8. Humans have individual genes encoding TPTE and TPIP on chromosomes 21 and 13, respectively, as well as at least two pseudogenes: ΨTPT on chromosome 13 and ΨTPTE22 on chromosome 22 (Chen et al., 1999; Walker et al., 2001; Tapparel et al., 2003). High shared synteny between the loci containing the genes for Mm-VSP and ΨTPT has led to the prediction that this pseudogene represents the ancestral mammalian VSP gene, and the multiple TPTE/TPIP genes in humans arose due to gene duplication events subsequent to the evolutionary divergence of primates and rodents. This hypothesis is further supported by the fact that the TPIP gene, also on chromosome 13, is most closely related to the Mm-VSP gene, with 71% amino acid sequence identity shared between the two proteins' phosphatase domains.

Human TPTE and TPIP are both expressed in testis, and TPIP is additionally expressed in the brain and stomach (Walker et al., 2001). Initial evidence indicated that Mm-VSP was only expressed in the testis, similarly to TPTE, however subsequent studies suggested expression in the embryonic central nervous system as well (Reymond et al., 2002). The neural expression of Mm-VSP has remained contentious though, and Mm-VSP is still often referred to as a testis-specific protein (Okamura et al., 2009). To resolve the question of neural Mm-VSP expression, I

have definitively demonstrated expression of Mm-VSP mRNA and protein in the central nervous system of both juveniles and adults (Chapter 3, Section I).

Discovery and expression of VSPs in non-mammals

In 2005 a genomic analysis of the ascidian *Ciona intestinalis* was performed to investigate the evolution of the voltage sensor domain in voltage-gated ion channels (Okamura et al., 2005). This analysis identified a gene encoding a protein that contained both a putative voltage sensing domain and a putative PTEN-like lipid phosphatase domain, and was homologous to the TPTE proteins identified in mammals (Murata et al., 2005). Electrophysiological work confirmed that changes in transmembrane potential modulated the activity of the phosphatase (see below), and so the protein was named the voltage sensor-containing phosphatase (later shortened to voltage-sensitive phosphatase) from *Ciona intestinalis* (Ci-VSP). Ci-VSP was the first protein in which voltage sensor activity was shown to be directly coupled to an enzymatic activity, and it remains the best characterized member of the VSP family.

Expression of Ci-VSP was originally identified in the testis and neural complex of *Ciona* using an RT-PCR screen (Murata et al., 2005). Further RT-PCR and *in situ* hybridization studies revealed expression in the stomach, intestine, and blood cells of juvenile *Ciona*, as well as in the blood cells of adult *Ciona* (Ogasawara et al., 2011). The population of blood cells that express Ci-VSP was found to be completely distinct from the population of blood cells that express Ci-PTEN, suggesting that these two proteins may serve similar roles for different cell types in the blood of ascidians. Notably, whereas expression of the mammalian VSP proteins was reported to be primarily limited to the intracellular membranes of the endoplasmic reticulum and Golgi (Guipponi et al., 2001; Walker et al., 2001; Tapparel et al., 2003), the Ci-VSP protein was found

to traffic readily to the plasma membrane when heterologously expressed in *Xenopus* oocytes. Furthermore, immunogold labeling of Ci-VSP indicated that the endogenous protein in sperm tails was expressed on the plasma membrane as well (Murata et al., 2005).

Continued research on VSPs has identified VSP family members from the zebrafish *Danio rerio* (Dr-VSP - (Hossain et al., 2008)), the frogs *Xenopus laevis and Xenopus tropicalis* (Xl-VSP1, Xl-VSP2, Xt-VSP - (Ratzan et al., 2011)), the chicken *Gallus gallus* (Gg-VSP - (Yamaguchi et al., 2014)), the newt *Cynops pyrrhogaster* (Cp-VSP), and the salamander *Hynobius nebulosus* (Hn-VSP) (Mutua et al., 2014). All of these species express RNA encoding the respective VSPs in the testis, and most species express VSP RNA in the kidney and liver as well. Relevant to my work on the role of Mm-VSP in the brain, RT-PCR has demonstrated that Ci-VSP, Xl-VSP2, Gg-VSP, and the human TPIP are all expressed in the central nervous system. Gg-VSP in particular has been reported to be expressed in the Purkinje neurons of the chick cerebellum (Yamaguchi et al., 2014), analogous to the expression I observe in the mouse cerebellum (Chapter 3, Section I).

II. Activities of VSPs

Given the physiological importance of both phosphoinositide signaling and signaling through membrane voltage, as well as the provocative expression profile of the VSPs that have so far been identified, one would likely predict that the VSPs play important signaling roles in the cells where they are expressed. However, just what these signaling roles are has remained a difficult question to answer. The majority of VSP research to date has been primarily biophysical, and VSP reports have focused on investigating coupling between the voltage sensor and the phosphatase, using VSPs as a biophysical platform to explore the mechanism of voltage sensation in S4-based voltage sensors, and using VSPs as a tool to experimentally regulate pools

of phosphoinositides in a voltage-controlled manner. These studies have been extremely interesting and informative, however most have focused on either Ci-VSP or Dr-VSP, due to the ease with which these proteins can be heterologously expressed on the plasma membrane of cells. As a result very little is known about the activities of the mammalian VSPs, even at a purely biophysical level. Furthermore, given the evolutionary divergence of Ci-VSP and Dr-VSP from the mammalian VSPs (Fig 4), it is not yet clear how much of what we have learned from Ci-VSP and Dr-VSP is conserved in the mammalian proteins. In the following sections of this chapter, I will summarize the current understanding of the activities of VSPs.

IIa. Voltage sensor activity

The discovery of the VSPs established that the S4-based VSD is a truly modular protein domain, capable of regulating functions other than opening of a pore domain. A question that emerges naturally from this discovery is how similar the voltage sensor activity in VSPs is to the voltage sensor activity in voltage-gated ion channels. In voltage-gated ion channels, voltage-sensitive properties can often be readily characterized by the measurement of ionic currents through the pore domain (Hodgkin and Huxley, 1952). In contrast, VSPs lack a pore domain, and hence other techniques must be utilized to characterize their voltage-dependence.

Because current is simply movement of charges, and the S4 of the VSD contains positive charges that move across the membrane in response to activation, many S4-based voltage sensors generate “gating” or “sensing” currents as they activate and deactivate. (Armstrong and Bezanilla, 1973; Schneider and Chandler, 1973; Keynes and Rojas, 1974) (Fig 5). Measurement of such sensing currents has revealed the voltage-sensitivity of a number of VSP proteins (Table 2). However, all of the VSPs that have demonstrated measurable sensing currents have been proteins from non-mammals.

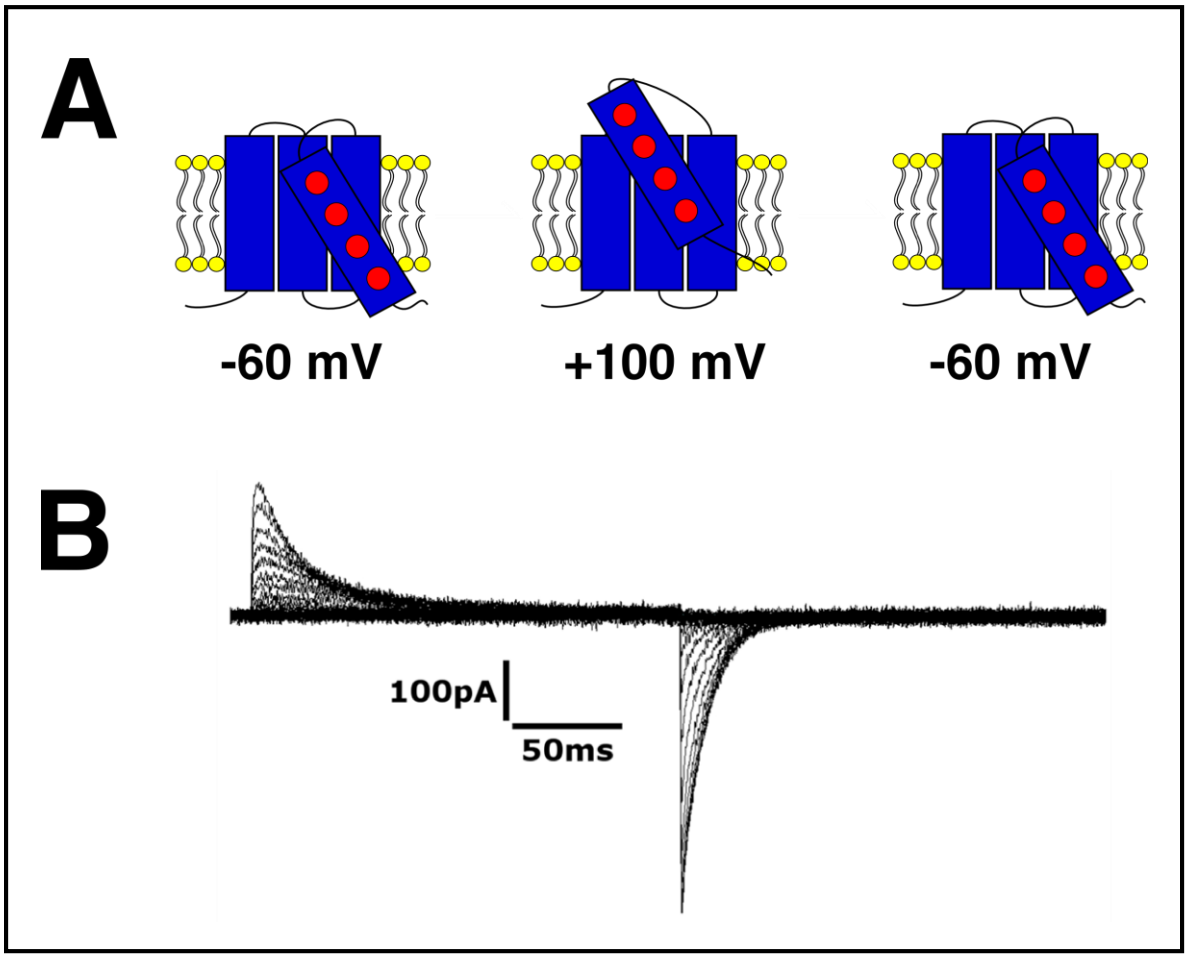

Figure 5: Sensing currents from Dr-VSP

(A) A cartoon depicting the movement of S4 across a membrane. The positive gating charge residues, depicted in red, move "up" in response to depolarization (middle), and "down" in response to repolarization (left and right).
(B) A family of sensing currents measured from an HEK293T/17 cell expressing Dr-VSP. The cell membrane was voltage-clamped in whole-cell mode at -60 mV, then pulsed in 10 mV steps from -60 mV to 160 mV to elicit sensing currents. The first outward current peak represents movement of the VSD into the "up" state as the cell is depolarized. The second, inward current peak represents return of the VSD to the "down" state as the cell is repolarized.

Protein	*Organism*	*Cell Type*	*Experiment*	*Measurement*	*Holding Potential (mV)*	*Voltage range/ΔV (mV)*	*$V_{1/2}$ (mV)*	*Z*	*Reference*
Ci-VSP	Sea squirt	*Xenopus* oocyte	TECV	Gating currents (Q-off)	-80	[-80,160] / 10	71.8	1.1	Murata et al, 2005
Dr-VSP	Zebrafish	tsA201 fibroblast	Whole-cell VC	Gating currents (Q-off)	-60	[-60,160] / 10	94	1.61	Hossain et al, 2008
Xl-VSP1	Frog	*Xenopus* oocyte	TEVC	PLCδ1-PH-GFP fluorescence changes	-80	[-60,60] / 20	NR (0-20)	NR	Ratzan et al, 2011
Xl-VSP2	Frog	*Xenopus* oocyte	TEVC	PLCδ1-PH-GFP fluorescence changes	-80	[-60,60] / 20	NR (>40)	NR	
Xt-VSP	Frog	*Xenopus* oocyte	TEVC	PLCδ1-PH-GFP fluorescence changes	-80	[-60,60] / 20	NR (0-20)	NR	
Gg-VSP	Chicken	*Xenopus* oocyte	TEVC	Gating currents (Q-off)	-60	[-60,180] / 10	97.5	0.71	Yamaguchi et al, 2013
Cp-VSP	Newt	*Xenopus* oocyte	TEVC	Gating currents (Q-off)	-60	[-60,140] / 10	NR (>100)	NR	Mutua et al, 2014
Hn-VSP	Salamander	*Xenopus* oocyte	TEVC	Gating currents (Q-off)	-60	[-60,140] / 10	NR (>100)	NR	
Mm-VSP	Mouse	HEK293T Fibroblast	Whole-cell VC	Ionic current through Kv_{SynthM} chimera	-90	[-80, 70] / 10	-10.4	0.70	Rosasco et al, 2015 *(in review)*

Table 2: Voltage sensitivity of VSPs

A list of selected voltage-sensitive properties of the VSPs that have been characterized so far. "NR" indicates a value that was not reported. Where possible, values that were not reported were estimated based on data presented in figures.

Although the mammalian VSP proteins were predicted to contain functional voltage sensing domains shortly after their discovery (Wu et al., 2001; Kumanovics et al., 2002), testing this prediction has remained difficult. This is primarily because the mammalian proteins tend to localize to intracellular membranes when heterologously expressed (Tapparel et al., 2003). However, the TPTEγ isoform does traffic readily to the plasma membrane when expressed in fibroblasts, yet still fails to generate sensing currents (Halaszovich et al., 2012). Voltage-gated proton currents were observed in a chimera in which the S3 and S4 helices of the human TPTE voltage sensor were transplanted into the Dr-VSP voltage sensor (Sutton et al., 2012), but currents resulting from the wild-type TPTE voltage sensor have not yet been reported. It has therefore remained unknown whether the transmembrane segments of the mammalian VSP family members form *bona fide* functional voltage sensing domains. I have addressed this question using the voltage sensor from Mm-VSP (Chapter 3, Section II), but for now I will focus the discussion on what has been determined about VSD activities in non-mammalian VSPs.

The generation of sensing currents by VSPs has confirmed that the voltage sensor is functionally homologous to those found in voltage-gated channels, and a recent crystal structure of Ci-VSP's VSD has confirmed that the proteins' domains are structurally homologous as well (Li et al., 2014). Whereas voltage-gated channels require co-assembly of 4 voltage sensors to produce a fully-functional protein, VSPs form functional monomers (Kohout et al., 2008). The monomeric nature of VSPs facilitates both expression of the protein and analysis of the voltage-dependent properties, and so VSPs represent an ideal reduced system in which to investigate questions of voltage sensor function.

A new conformation for voltage sensors: the relaxed state

VSPs have proven to be particularly amenable to kinetic analysis by electrophysiological approaches, and studies on Ci-VSP have led to the discovery of a new state of voltage sensor activation. In addition to the classical resting and active states of the voltage sensor, analysis of gating current and fluorometric recordings in Ci-VSP have demonstrated a third voltage and time-dependent state referred to as the "relaxed" state (Villalba-Galea et al., 2008). Kinetic models that incorporate the relaxed state accurately describe voltage sensor hysteresis, the use-dependent shifts in voltage sensitivity that have frequently been observed in voltage-gated ion channels (Fernandez et al., 1982; Shirokov et al., 1992; Olcese et al., 1997; Piper et al., 2003; Kuzmenkin et al., 2004).

In some voltage-gated ion channels, voltage sensor hysteresis was shown to be associated with slow inactivation of the channels, but this correlation does not hold in all voltage gated channels. The studies of the relaxed state in Ci-VSP have explained this variability to some extent, by demonstrating that the relaxed state is a property intrinsic to the voltage sensor itself and does not require the involvement of a pore domain. While a structural mechanism for the relaxed state has not been completely described, fluorometric recordings have demonstrated that the voltage sensor undergoes complex conformational rearrangements under conditions associated with the relaxed state (Villalba-Galea et al., 2008; Villalba-Galea et al., 2009a; Kohout et al., 2010). Furthermore, these rearrangements have been observed at both the carboxy- and amino-terminal ends of S4 (Villalba-Galea et al., 2009b). Based on the energetics of the relaxed state transition, it has been proposed that one of these rearrangements is the transition of the extracellular-facing region of the S4 from an energetically unstable 3_{10}-helix to a more stable α-helix (Villalba-Galea et al., 2008).

Kv_{Synth1} – a potassium channel gated by a VSP voltage sensor

One of the most remarkable findings regarding the modularity of the voltage sensor is the recent discovery that the VSD from Ci-VSP is capable of conferring voltage dependent gating to the Kcv potassium channel (Arrigoni et al., 2013). The Kcv channel was discovered in the genome of the cholera virus PBCV-1, and evolved as an isolated, constitutively-open pore domain, independent of any voltage-sensing domains (Plugge et al., 2000). Arrigoni et al. generated a chimera containing the Kcv pore fused to the carboxy terminus of the VSD from Ci-VSP (Fig 13) that demonstrated ion permeation properties characteristic of Kcv, but with voltage sensitive gating characteristic of Ci-VSP. This chimeric channel was accordingly named Kv_{Synth1} - the first synthetic voltage-gated potassium channel. This synthetic channel provides a platform to test the activity of a voltage-sensing domain, since potassium currents can be recorded as an indicator of voltage sensor activity. I have taken advantage of this chimera to test whether the transmembrane segments in mammalian VSPs form a functional voltage sensor (Chapter 3, Section II).

Given that the Kcv channel is constitutively open in its native context, one interesting implication of Kv_{Synth1} is that the conformation of the VSD in a resting state generates a force at the carboxy terminus to induce closure of the Kcv pore. This fact is particularly notable since Arrigoni et al. generated the Kv_{Synth1} channel using the native amino terminus of Kcv as the linker between the VSD and the pore (Fig 13). Therefore even though it is well-established that alteration of the linker following the VSD can have a pronounced effect on the functionality of both VSPs (Murata et al., 2005; Villalba-Galea et al., 2009a; Kohout et al., 2010; Hobiger et al., 2012; Hobiger et al., 2013) and channels (reviewed in (Horn, 2002)), there is no *a priori*

requirement for coevolution between the VSD and the linker in order to form a functional voltage-gated channel.

Critical residues and structure of the Ci-VSP voltage sensor

Mutational analysis has probed the role of residues in the voltage sensors of VSPs that have analogous residues known to be important for voltage-gated channel function. In particular, the R217 residue of Ci-VSP, conserved among all identified VSP family members (Fig 6), has been shown to be critical for stabilizing the resting state of the voltage sensor. This residue is positioned in the extracellular region of the S4 loop (Li et al., 2014) and the mutations R217Q and R217E drastically shift the activation of the VSD to more negative potentials (Murata et al., 2005; Villalba-Galea et al., 2013). Histidine scanning mutagenesis has shown that further down in S4, the Ci-VSP residues R223, R226, R229, and R232 are the "sensing charge residues" that traverse the lipid bilayer in response to changes in membrane potential (Villalba-Galea et al., 2013). Residues outside of S4 have also been shown to have an impact on the activation range of the VSD, such as the conserved isoleucine at position 126 in Ci-VSP (Fig 6), which acts in a steric manner to "tune" the protein's voltage sensitivity (Lacroix and Bezanilla, 2012).

Perhaps the most surprising result from studies of the Ci-VSP voltage sensor has been the discovery that voltage-dependent conformational rearrangements occur not only at the carboxy terminus of S4, but at the amino terminus of S1 as well (Tsutsui et al., 2013). Tsutsui and colleagues performed voltage-clamp fluorometry experiments using various fluorescence-based reporters of conformational arrangements fused to either the amino terminus or carboxy terminus of the Ci-VSP voltage sensor. Using these constructs, similar voltage-dependent fluorescence changes were observed when the reporters were fused to the amino terminus as

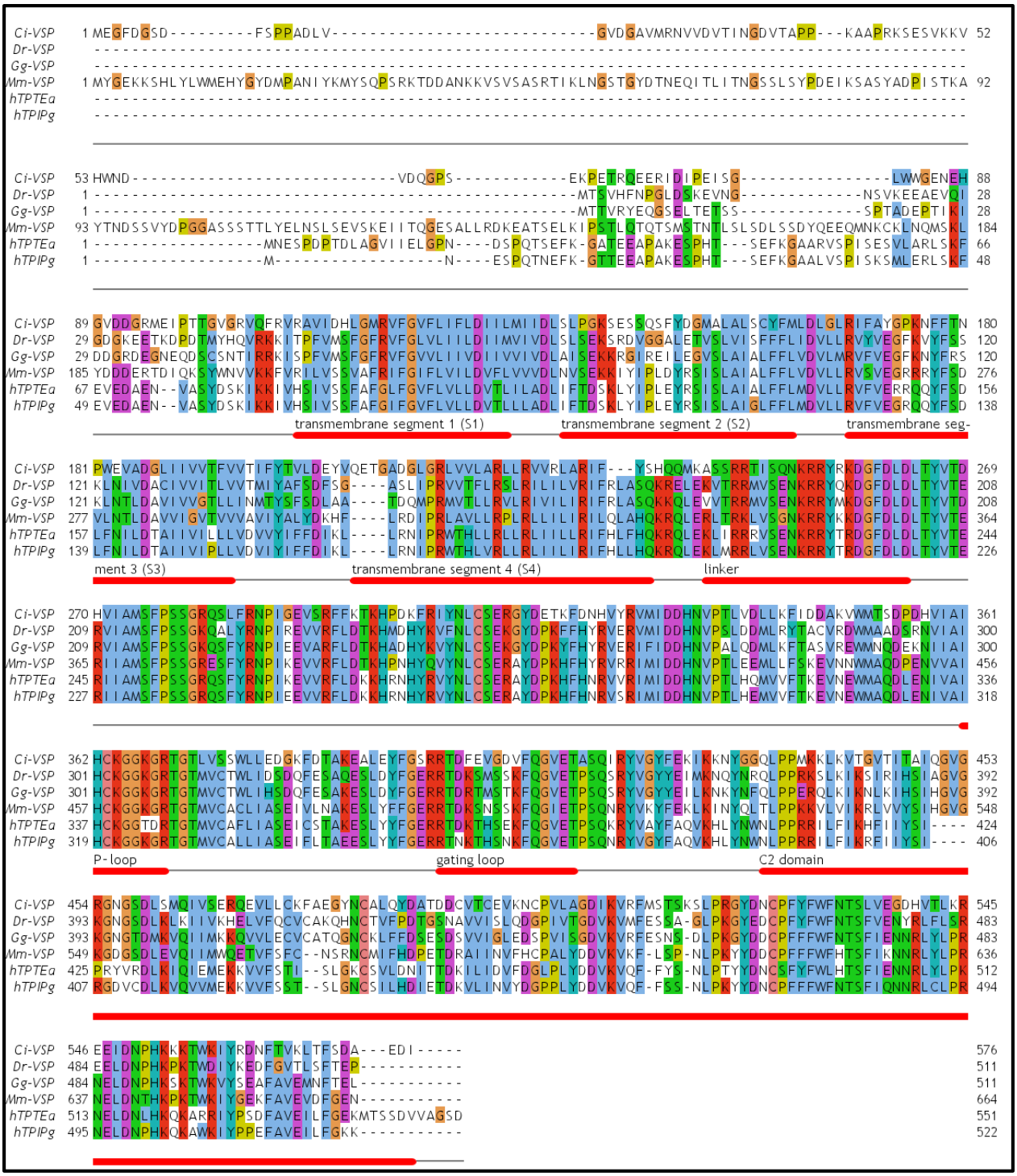

Figure 6: Amino acid sequence alignment of VSPs from various species

Shown is an alignment of the protein sequences of Ci-VSP (BAD98733.1), Dr-VSP (BAG50379.1), Gg-VSP (XP_004938794.1), Mm-VSP (NP_954866.2), hTPTEα (NP_954870.2), and hTPIPγ (AAP45146.1). Alignment was generated using COBALT, then visualized and annotated using Jalview.

when the reporters were fused to the carboxy terminus. This finding may have interesting implications for the physiological roles of VSPs, as the region amino terminal to S1 in VSPs is the most variable domain in the protein family, with regards to both length and amino acid identity (Fig 6).

Recently, the voltage sensor domain of Ci-VSP has been crystallized in putative resting and active conformations (Li et al., 2014). Because voltage could not be applied during crystallography, the two different conformations were obtained by taking advantage of the R217E mutation mentioned above. This mutation shifts the voltage dependence of Ci-VSP so that the putatively active conformation is favored at 0 mV – a voltage at which the wild-type voltage sensor favors the resting conformation. These complementary structures support many of the inferences made about the movements of VSDs based on electrophysiological and biochemical data, including the "sliding helix" or "helical screw" model proposed for the motion of S4 (Catterall, 1986; Guy and Seetharamulu, 1986).

IIb. Phosphatase activity

The cytoplasmic lipid phosphatase domain of VSPs is highly homologous to the tumor suppressor PTEN, and contains the hallmark HCXXGXXR catalytic motif shared by all protein tyrosine phosphatases (Barford et al., 1998). The phosphatase domain is entirely modular, much like the voltage sensor domain that it's attached to. This modularity is evidenced by the fact that the recombinant phosphatase domain dephosphorylates lipid substrates *in vitro* (Murata et al., 2005), and that the phosphatase domains from different species VSPs can be swapped (Halaszovich et al., 2012; Kurokawa et al., 2012). Furthermore, the functional homology of the VSP phosphatase domain to the soluble lipid phosphatase PTEN has been established by the discovery that the activity of PTEN can be controlled by a VSD (Lacroix et al., 2011).

VSP phosphatase activity against PI(4,5)P_2

Despite extensive studies, what the physiologically-relevant substrates of VSPs are remains a controversial question. PTEN is known to exert its tumor-suppressing function largely through modulation of the Akt/PKB signaling pathway, by acting to dephosphorylate the 3' phosphate of PI(3,4,5)P_3 (Maehama and Dixon, 1998), and early *in vitro* work on the mammalian proteins suggested that VSPs acted similarly as 3' phosphatases against PI(3,4,5)P_3 (Walker et al., 2001; Wu et al., 2001). Purified recombinant Ci-VSP phosphatase domain was also shown to dephosphorylate PI(3,4,5)P_3 *in vitro*, at a rate comparable to PTEN (Murata et al., 2005). However, live cell experiments using a fluorescently-labeled pleckstrin homology (PH) domain from phospholipase C delta 1 (PLCδ1) demonstrated that in response to depolarization Ci-VSP dephosphorylated PI(4,5)P_2 in the plasma membrane (Murata and Okamura, 2007). This activity was confirmed by the depolarization-induced inhibition of a number of PI(4,5)P_2-dependent potassium channels.

Dephosphorylation of PI(4,5)P_2 is the best-characterized VSP activity so far, and PI(4,5)P_2 appears to be the most broadly conserved VSP substrate across different species. In addition to Ci-VSP, depolarization-induced dephosphorylation of PI(4,5)P_2 has been demonstrated for Dr-VSP (Hossain et al., 2008), a chimera containing the phosphatase domain of TPIP (Halaszovich et al., 2012), Xl-VSP1, Xl-VSP2, Xt-VSP (Ratzan et al., 2011), and Cp-VSP (Mutua et al., 2014). Thin layer chromatography (TLC) with phosphoinositide substrates that were radiolabeled at specific positions have determined that Ci-VSP dephosphorylates the 5' position of PI(4,5)P_2 (Iwasaki et al., 2008). Further live-cell imaging experiments with various PH domains that specifically recognize different phosphoinositide confirmed these results, and

demonstrated that the same dephosphorylating activity is seen with human TPIP (Halaszovich et al., 2009; Halaszovich et al., 2012).

It is thought that the other VSPs that induce depletion of $PI(4,5)P_2$ act as 5' phosphatases as well; however, observed decreases of $PI(4,5)P_2$ concentration must be considered carefully. The pool of $PI(4,5)P_2$ exists in dynamic equilibrium with its precursor PI(4)P, and decreases in PI(4)P in various cellular compartments have been shown to cause indirect decreases in plasma membrane $PI(4,5)P_2$ (Dickson et al., 2014). Because of this, live-cell experiments that demonstrate a VSP-induced change in $PI(4,5)P_2$ can be explained by at least two possible models. In one model, $PI(4,5)P_2$ serves as a substrate for the VSP, and the observed decrease in $PI(4,5)P_2$ is a direct result of VSP activation (Fig 18). In an alternative model, PI(4)P serves as a substrate for the VSP (Fig 19). In this model, the observed decrease in $PI(4,5)P_2$ would result from the depletion of the $PI(4,5)P_2$ precursor PI(4)P. Analyzing rates of $PI(4,5)P_2$ depletion and resynthesis and performing live-cell imaging experiments using PH domains with different phospholipid binding specificities will help differentiate between these possible models.

VSP phosphatase activity against $PI(3,4,5)P_3$

Phosphatase activity against $PI(3,4,5)P_3$ has been reported for many VSPs as well (Wu et al., 2001; Murata et al., 2005; Halaszovich et al., 2012; Yamaguchi et al., 2014). In Ci-VSP, dephosphorylation of $PI(3,4,5)P_3$ has been shown to take place at the 5' position, similar to the phosphatase activity against $PI(4,5)P_2$ (Halaszovich et al., 2009). Basal $PI(3,4,5)P_3$ levels in cells are kept low in the plasma membrane by the activity of lipid phosphatases (reviewed in (Vanhaesebroeck et al., 2001; Cantley, 2002)). Because of this, most of the live-cell experiments looking at phosphatase activity against $PI(3,4,5)P_3$ have been performed under conditions where

cells have been made to generate excess $PI(3,4,5)P_3$, such as through stimulation of endogenous lipid kinases or by overexpression of a PI 3-kinase.

Interestingly, Halaszovich and colleagues have reported that when a fluorescently-tagged Btk-PH domain, which specifically binds to $PI(3,4,5)P_3$, was expressed in CHO cells, a subpopulation of cells showed the Btk-PH domain localized to the plasma membrane under resting conditions (Halaszovich et al., 2009). This localization changed in a voltage-dependent manner in cells that were coexpressing Ci-VSP, suggesting that Ci-VSP is able to regulate endogenous pools of $PI(3,4,5)P_3$ when they are present in the cell. Furthermore, studies with Gg-VSP from chicken support the possibility for a physiological role of VSPs in regulating $PI(3,4,5)P_3$. When Gg-VSP is heterologously expressed in DF-1 chicken embryonic fibroblasts, the TAPP1-PH domain, which specifically binds to $PI(3,4)P_2$, localizes more strongly to the plasma membrane. This result suggests that Gg-VSP is dephosphorylating a pool of $PI(3,4,5)P_3$ at the 5' position, to increase the membrane concentration of $PI(3,4)P_2$. This apparent increase in plasma membrane $PI(3,4)P_2$ coincides with decreased labeling by the actin marker phalloidin, and the formation of long, neurite-like outgrowths (Yamaguchi et al., 2014). The percentage of DF-1 cells that exhibit growth of the long processes can be increased by changing the properties of the Gg-VSP voltage sensor, and can be decreased by coexpressing Gg-PTEN, which depletes $PI(3,4)P_2$. Given the neural expression of many VSPs, including Gg-VSP, it is tempting to suppose that these data indicate a physiological role for VSPs in regulating neurite outgrowth.

VSP phosphatase activity at the 3' position of phosphoinositides

Recent TLC analysis of Ci-VSP activity against $PI(3,4,5)P_3$ radiolabeled specifically at either the 3', 4', or 5' position confirmed that Ci-VSP can dephosphorylate the 5' position of $PI(3,4,5)P_3$ and $PI(4,5)P_2$ as previously shown, but additionally revealed 3' phosphatase activity

against $PI(3,4)P_2$ (Kurokawa et al., 2012). In *Xenopus* oocytes expressing Ci-VSP, the relative phosphatase activities against the 3' and 5' positions were dependent on the magnitude of the depolarization used to activate the phosphatase. At membrane potentials up to 0 mV, oocytes expressing Ci-VSP and TAPP1-PH showed increased plasma membrane localization of TAPP1-PH, indicating an increased concentration of $PI(3,4)P_2$ due to dephosphorylation of $PI(3,4,5)P_3$. At 60 mV, the TAPP1-PH domain dissociated from the plasma membrane after a transient increase in localization, indicating that $PI(3,4)P_2$ was being generated and then depleted. Similar results in oocytes were obtained with a chimera containing the human TPIP phosphatase domain and the Ci-VSP voltage sensor, suggesting that this 3' phosphatase activity is a conserved feature of VSPs across species. In contrast however, studies in mammalian fibroblasts were unable to detect any 3' phosphatase activity of TPIP (Halaszovich et al., 2012). For this reason, the question of whether VSPs demonstrate physiological phosphatase activity against positions other than 5' remains open. I will consider this further in the discussion of the activity I observe with the phosphatase from Mm-VSP (Chapter 3, Section III).

Inter-species variability in VSP phosphatase domains

All current evidence indicates that the phosphatase domain of human TPTE is catalytically inactive against all phosphoinositide substrates (Walker et al., 2001). This inactivity appears to be due to two amino acids – T342 and D343 (Fig 6), which are lysine and glycine, respectively, in other VSPs. Accordingly, the double mutation T342K/D343G "restores" the activity of the human TPTE phosphatase domain (Leslie et al., 2007). These data indicate that TPIP is the functional human homologue of VSPs in other species, a possibility that is supported by genetic analysis of the genes encoding TPTE and TPIP (Tapparel et al., 2003). It remains possible that TPTE retains phosphatase activity against non-phospholipid substrates, but no such

substrates have yet been found. Another possibility is that the phosphatase and C2 domain of TPTE act in a non-catalytic manner to regulate cell signaling – a signaling paradigm that has been observed previously with PTEN (Raftopoulou et al., 2004).

The underlying cause of the apparently varied substrate specificity of VSPs from different species is still not well understood. What is known is that the presence of glycine in the substrate binding pocket at a position where PTEN contains an alanine contributes to the substrate specificity. Generating the G365A mutation in Ci-VSP results in a protein that has less phosphatase activity against $PI(4,5)P_2$ than wild-type Ci-VSP, but retains activity against $PI(3,4)P_2$, similar to PTEN (Iwasaki et al., 2008). However, this amino acid position cannot account for the species-specific differences in VSP substrate specificity noted above, as this glycine is completely conserved amongst VSPs.

IIc. VSD-phosphatase coupling

One of the major unanswered questions regarding VSPs is how movement of the voltage sensor couples to a change in enzymatic activity of the phosphatase domain. While it is well-established that depolarization increases the phosphatase activity in VSPs (Murata and Okamura, 2007) and does so extremely rapidly (Falkenburger et al., 2010), the mechanism for this regulation is unknown. Two basic coupling mechanisms have so far been proposed. In the first, the phosphatase domain is constitutively active, and the movement of the voltage sensor serves to bring the active phosphatase closer to the membrane, and consequently to its substrate. In the second model, the voltage sensor allosterically modulates the activity of the phosphatase, acting more like a switch than a positioning mechanism. These two models are not necessarily mutually exclusive, and it is entirely possible that allosteric movements that increase the activity of the

phosphatase will reposition the active site as well. Here I will consider the evidence for both models, and the role of the S4-phosphatase linker domain in both.

The idea that the phosphatase domain of VSPs might be constitutively active was suggested by data showing that the recombinant phosphatase domain and linker could be purified independently of the voltage sensor while retaining phosphatase activity (Walker et al., 2001; Wu et al., 2001; Murata et al., 2005). However, the activity of the phosphatase domain does appear to be intimately connected to the linker domain, because removing the linker residues results in a phosphatase domain that appears well-folded, but lacks any detectible phosphatase activity (Kohout et al., 2010).

Since the first report of Ci-VSP's voltage-regulated phosphatase activity, it has been noted that the linker between the carboxy terminus of S4 and the cytosolic phosphatase domain plays a role in coupling between the VSD and phosphatase. When a Ci-VSP construct lacking the first 8 residues of the linker domain was coexpressed in oocytes with $PI(4,5)P_2$-dependent potassium channels, the mutant Ci-VSP generated sensing currents comparable to wild-type, but was unable to inhibit potassium channel activity (Murata et al., 2005). The importance of the linker domain in coupling was expected, by analogy to voltage-gated channels where the linker is responsible for transducing voltage sensor movements into changes in the pore domain (Horn, 2002). Additionally, in PTEN the amino terminal residues analogous to the VSP linker serve as a phosphoinositide-binding motif (PBM). This PBM binds $PI(4,5)P_2$ to allosterically regulate the activity of PTEN (Campbell et al., 2003; Walker et al., 2004; Redfern et al., 2008).

The role of basic residues in the VSP linker

Detailed mutational analysis of the residues in the linker has generated evidence for the allosteric modulation model of VSD-phosphatase coupling. It was first noted that mutating the arginines at positions 253 and 254 in Ci-VSP both altered the kinetics of the voltage sensor, and abolished voltage-regulated phosphatase activity (Villalba-Galea et al., 2009a). Interestingly mutating these residues to lysines had a similar effect to mutating them to glutamines or alanines, indicating that the functional dependence of Ci-VSP on these residues is not solely an electrostatic effect. These residues are conserved in PTEN, where they form part of the $PI(4,5)P_2$ binding site in the PBM (Campbell et al., 2003). Another pair of arginines at positions 245 and 246, which are not conserved in PTEN, also seem to be important for coupling voltage sensor movements to phosphatase activity (Villalba-Galea et al., 2009a), presumably by also acting to bind $PI(4,5)P_2$.

To test whether the basic residues in the linker might be acting through interactions with $PI(4,5)P_2$ as in PTEN, rapamycin-inducible phosphatases or a $G\alpha_q$-coupled serotonin receptor were used to deplete $PI(4,5)P_2$ independently of Ci-VSP activity. Doing so changed the voltage sensitivity of Ci-VSP, and also inhibited a late-stage conformational rearrangement of the voltage sensor (Kohout et al., 2010). These effects of $PI(4,5)P_2$ depletion were diminished in the R253Q and R254Q Ci-VSP mutants, supporting the idea that these residues form a $PI(4,5)P_2$-binding site. Additionally, these studies revealed the importance of another basic residue, a lysine at position 252 that is also conserved in PTEN. Ci-VSP carrying the mutation K252Q showed no voltage-dependent phosphatase activity, and recombinant phosphatase carrying this mutation had significantly decreased phosphatase activity *in vitro* as well. The K252Q mutation had the most pronounced effect on voltage-dependent phosphatase activity of all the linker

mutations, which suggested that K252 occupied a unique position in coupling between the VSD and phosphatase.

A special lysine in the VSP linker

Further insight into the special role played by K252 has come from structural studies, molecular dynamics simulations, and further electrophysiological experiments. A detailed analysis of the kinetics of voltage sensor movement and voltage-gated phosphatase activity of Ci-VSP revealed a general trend, where faster "off" kinetics of the voltage sensor are correlated with weaker phosphatase activity (Hobiger et al., 2012). The authors argue that the faster off kinetics indicate weaker association of the phosphatase domain with the membrane, which in turn decreases the phosphatase activity. While this at first seems to support a model of gating where the VSD repositions the phosphatase domain nearer to its substrate, the authors go on to note that the K252C mutation completely abolishes voltage-dependent phosphatase activity, despite having almost no effect on the kinetics of the voltage sensor movement. Hobiger and colleagues therefore propose that this residue represents a unique site where the linker domain may interact directly with the phosphatase domain.

Crystal structures of the phosphatase domain of Ci-VSP have supported the conclusion that K252 can directly couple the voltage sensor movements to the phosphatase domain. In a putatively active "open" crystal structure of the phosphatase the K252 residue can be seen forming a salt bridge with the aspartate residue at position 400 (Liu et al., 2012). In contrast, a complementary structure of the putatively inactive "closed" state shows K252 instead interacting with the backbone carbonyl of glycine 365 in the active site. This dynamic interaction of K252 with D400 is significant, as the D400 residue is found in a region that the authors term the "gating loop." The gating loop contains glutamate 411, which appears to occlude the catalytic

site in the closed form structure, and moves to reveal the catalytic site in the open form structure. This indicates that the interaction between K252 and D400 is essential for stabilizing the open form of the phosphatase, and thereby allowing substrates to enter the active site. Accordingly, the mutations D400K, D400R, and D400A all abolish phosphatase activity of Ci-VSP both *in vitro* and in live cells.

The strength and stability of interactions between the linker domain and phosphatase domain were further analyzed using a 50 ns atomistic molecular dynamics simulation on a model of the whole Ci-VSP protein (Hobiger et al., 2013), and results from the simulation generally supported the conclusions based on the crystal structures. During the simulation, K252 was seen to interact with residues D400 and E402, and the neighboring residue R253 was also seen to interact strongly with D400. These results suggest a strong and direct interaction between the linker domain and the phosphatase domain mediated by K252, and electrophysiological evidence indicates that this interaction is essential for voltage sensor coupling to phosphatase activity.

The majority of data so far are consistent with allosteric regulation of the phosphatase domain by motion of the voltage sensor. However, it is impossible to ignore the fact that the phosphatase domain demonstrates catalytic activity when it is purified independent of the voltage sensor. In this context, it is interesting to once again consider that the resting conformation of the voltage sensor generates enough force to close a potassium channel that has evolved to be constitutively open ((Arrigoni et al., 2013), and Chapter 3, Section II). I speculate that perhaps the resting state of the voltage sensor in VSPs analogously serves to deactivate a phosphatase that has otherwise evolved to be constitutively active. This possibility is further supported by the finding that the activity of PTEN can be made dependent on voltage when it is fused to a VSP voltage sensor (Lacroix et al., 2011).

Bi-directional coupling between the VSD and phosphatase domains

One additional point of interest is that coupling between the VSD and the phosphatase domain of VSPs is bi-directional. Changes in the phosphatase domain can affect voltage sensor movement, just as voltage sensor movements can affect the phosphatase domain's activity. This has most clearly been demonstrated with the zebrafish VSP, Dr-VSP. Dr-VSP containing the C302S enzyme-inactivating mutation generated gating currents that decayed much more quickly than the wild-type (Hossain et al., 2008). Furthermore, pervanadate and orthovanadate, which inhibit PTPs by binding to the catalytic cysteine, were also able to induce the rapid sensing current kinetics in wild type Ci-VSP, similar to those observed in the C302S mutant. There was no further increase in kinetics when the PTP inhibitors were added to the C302S mutant, supporting the conclusion that these two manipulations speed up voltage sensor kinetics by the same mechanism.

Graded voltage-dependent phosphatase activity

As a final point regarding coupling of the voltage sensor to the phosphatase, I will note that an increase in voltage sensor movement is coupled to an increase in phosphatase activity across the entire range of voltage sensor movements (Sakata et al., 2011; Sakata and Okamura, 2014). These studies have been used to support the claim that phosphatase activity within a single VSP protein is graded, depending on the extent of voltage sensor activation. This may in fact be the case, however it is important to consider that these studies were performed using bulk measurements of many molecules of Ci-VSP acting in concert. It is therefore not possible to distinguish between a situation in which all Ci-VSP molecules are partially active, and a situation in which a fraction of the molecules are fully active. More detailed single molecule experiments will be needed to distinguish between these two possibilities.

III. Proposed Physiological Roles of VSPs

The expression of VSPs in the testis is conserved across all species in which VSPs have been identified. This together with the discovery that *Xenopus laevis* oocytes also express endogenous Xl-VSP1 (Ratzan et al., 2011; Kurokawa et al., 2012) has been used as evidence to suggest that VSPs play a role in regulating sperm-egg fusion. In many species, including *Xenopus laevis*, polyspermy is prevented by inhibition of further sperm-egg fusion after one sperm has fused. This polyspermy block is associated with a depolarization of the egg (Jaffe, 1976), and it has been noted that the voltage range in which Xl-VSP1 is able to dephosphorylate $PI(4,5)P_2$ is well-correlated with the range of voltages that inhibit sperm-egg fusion (Ratzan et al., 2011). However, the salamander *Hynobius nebulosus* expresses a VSP without detectible catalytic activity, yet still undergoes depolarization-associated polyspermy block (Mutua et al., 2014). Furthermore, not all species that express VSPs in their reproductive organs undergo voltage-dependent polyspermy block (Jaffe et al., 1983). Thus, if VSPs do act in the sperm-egg fusion pathway, this is an activity that is limited to a subset of VSP-expressing species.

As mentioned previously (Chapter 2, Section III), it has been suggested that Gg-VSP may have a role in regulating the actin cytoskeleton through the production of $PI(3,4)P_2$ (Yamaguchi et al., 2014). In DF-1 chick fibroblasts, this $PI(3,4)P_2$-producing activity was correlated with the growth of neurite-like processes. As the VSPs from humans (Walker et al., 2001) and mice (Chapter 3, Section I) are expressed in the brain, this represents an attractive possibility that could provide insight into the role of VSPs in mammals. However, to address this possibility, and any other possible role for VSPs in mammals, we must first characterize the mammalian VSPs more completely. To this end, the second half of this dissertation will summarize data I have collected to characterize a model mammalian VSP.

Chapter 3: A characterization of Mm-VSP

In the previous chapters, we have seen that while detailed biophysical analyses have been conducted on a number of VSPs, much remains unknown about their involvement in cell signaling processes. Furthermore, it is unclear how much of the functionality that has been observed in VSPs from non-mammals is conserved in the mammalian proteins. In fact, both the unique subcellular localization of the mammalian VSPs and a phylogenetic analysis of the VSP voltage sensors (Fig 4) predict that the VSPs will have very different functionality in mammals and non-mammals.

To begin to address the gap in knowledge regarding the mammalian VSPs, I have characterized the VSP from mouse, Mm-VSP. The wide variety of experimental approaches available with mice, as well as the relatively high degree of evolutionary conservation between mice and humans make this an ideal model mammalian protein. In this initial characterization of Mm-VSP, I have addressed the topics of when and where the protein is expressed, how the protein is activated, and what the phosphatase activity of the protein is. In particular, I have considered these questions in the specific context of the central nervous system. As we will see in the following sections, the data indicate that Mm-VSP behaves very differently than the non-mammalian VSPs, and likely has an important role in the central nervous system.

I. Expression and developmental regulation of Mm-VSP

Mm-VSP mRNA is expressed in brain as multiple developmentally regulated splice variants

When Mm-VSP was originally identified as a PTEN homologue, its expression was reported to be exclusive to testis (Guipponi et al., 2001; Wu et al., 2001). Expression in reproductive tissues has similarly been shown for subsequently identified VSP family members,

such as those from sea squirt, frog, chicken, and human (Walker et al., 2001; Murata et al., 2005; Ratzan et al., 2011; Yamaguchi et al., 2014). However, in all of these species, VSP expression was detected in central nervous system tissue as well. A later large-scale genomic study in mouse suggested that Mm-VSP might be expressed in the brain as well as the testis (Reymond et al., 2002). However, these results have not been confirmed, and current reports on VSP activity still refer to Mm-VSP as a testis-specific protein (Okamura et al., 2009; Ratzan et al., 2011), leaving the question of whether Mm-VSP is expressed in the brain unanswered.

As a first step to determine whether Mm-VSP is expressed in mouse brain, I designed a rigorous screen for mRNA transcripts using reverse-transcription PCR (RT-PCR). Primer pairs were designed to amplify three different regions of the Mm-VSP mRNA transcript, to decrease the possibility of generating false negatives due to expression of different isoforms. When RT-PCR was performed on RNA extracted from mouse brain, Mm-VSP transcript was detected with all three of the primer pairs (Fig. 7A). Expression of Mm-VSP mRNA could be detected in both male and female mice, at both postnatal day 0 (P0) and postnatal day 37 (P37). RT-PCR with primers against the microtubule-associate protein 2 (MAP2) transcript were used as a positive loading control (Fig 7A, bottom row). The primer pairs were used to perform RT-PCR on RNA extracted from P37 testis as a positive control for Mm-VSP expression, and were found to generate the expected amplicon. It is worth mentioning that although I did not conduct true quantitative RT-PCR, the band intensity of the amplicon from brain was much lower than the amplicon from testis. This suggests that the expression of Mm-VSP is much lower in brain than in testis, which may explain why previous RT-PCR studies failed to detect expression in brain.

Surprisingly, a primer pair that targeted the mRNA region encoding part of the amino terminus amplified two differently sized products in the brains of P0 mice (Fig 7A, second row).

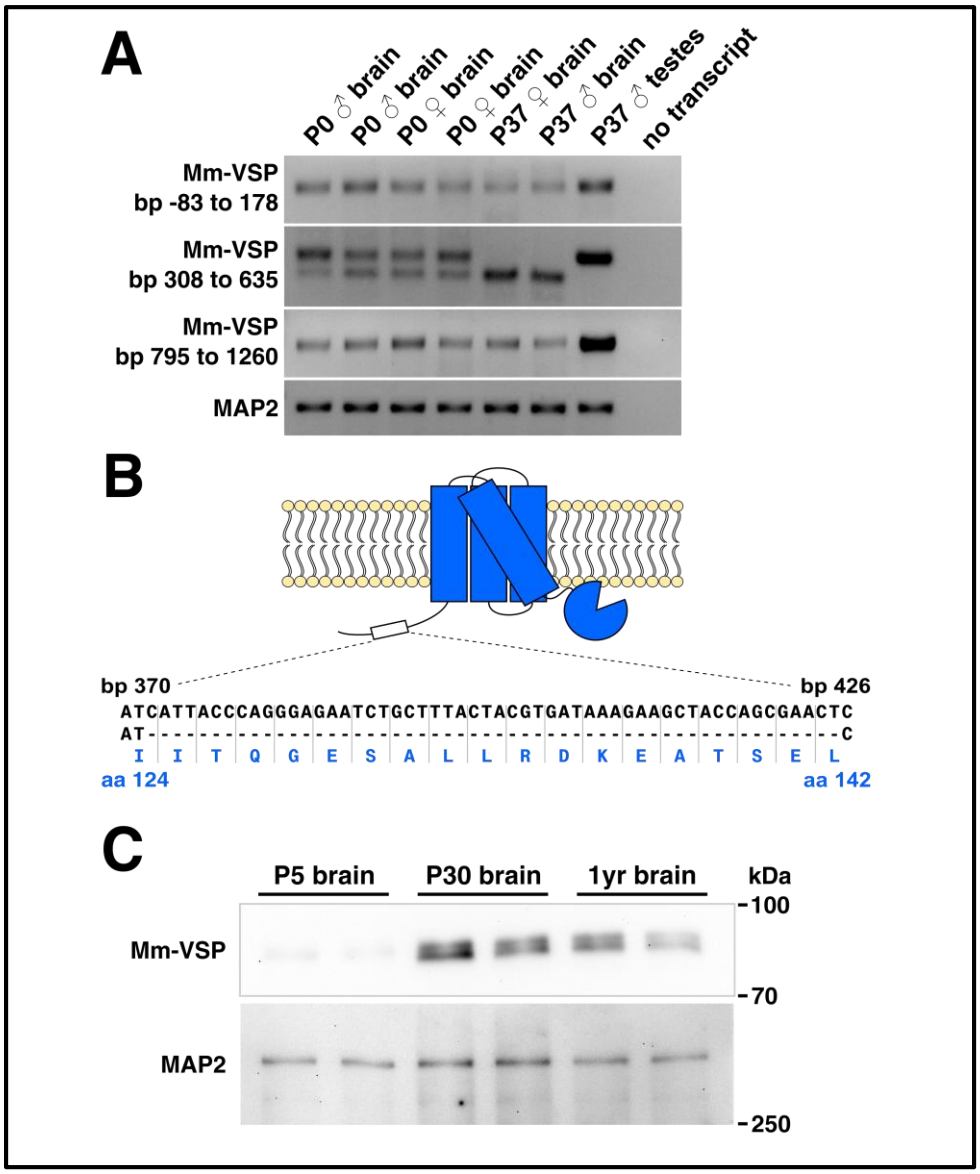

Figure 7: Mm-VSP expression is developmentally regulated

(A) RT-PCR amplicons visualized in an agarose gel using ethidium bromide. Left-hand labels indicate the base pairs of Mm-VSP's mRNA sequence amplified by each primer pair, where 0 indicates the beginning of the open reading frame. Primers against MAP2 mRNA were used as a positive loading control. Top labels indicate postnatal age in days, gender, and tissue of the mice from which RNA was collected. Each gel is representative of three replicates.
(B) Cartoon of Mm-VSP depicting the splice variant identified by amplifying the region bp 308 to bp 635, and sequencing the two differently-sized bands. The cDNA sequences with and without exon 9 are shown in black, with the amino acids encoded shown below in blue.
(C) Western blot probing for Mm-VSP in of different ages. Whole brain homogenates were probed for Mm-VSP. MAP2, probed for on the same blot, served as a loading control. Two separate mice are shown for each age. The blot is representative of three technical replicates. The predicted size of Mm-VSP is 76.71 kDa. Two bands near this size are seen to be present in whole brain homogenate, and their intensity increases with the age of the mice.

By P37, only the smaller product could be detected in the brain, while only the longer product could be detected in the testis. Sequencing of the DNA corresponding to the bands from P37 testis and brain revealed that the higher molecular weight band from adult testis corresponded to the expected sequence for full-length transcript, whereas the lower molecular weight band from adult brain corresponded to a sequence lacking the 54 bases of exon 9 (Fig. 7B). Alternate splicing of Mm-VSP has been predicted (Guipponi et al., 2001), though the exclusion of exon 9 has not been previously reported. This pattern of alternate splicing detected for Mm-VSP is mirrored by human TPIP, which is expressed as a full-length transcript in testis, and as shorter splice variants in the brain (Walker et al., 2001).

These results definitively indicate that mRNA encoding Mm-VSP is expressed in the mouse brain, and is done so in a developmentally-regulated manner. This finding does not adequately address the question of whether the Mm-VSP protein is expressed in the mouse brain though. Many factors such as efficiency of translation initiation by ribosomes, poly(A) tail length, RNA stability, post-translational modifications, and protein degradation all effect whether the presence of mRNA accurately predicts the presence of a protein in a given tissue (reviewed in (de Sousa Abreu et al., 2009)). Therefore to directly address the presence of the Mm-VSP protein in brain, I undertook to generate polyclonal antibodies against Mm-VSP.

Generation of polyclonal antibodies against Mm-VSP

For the antigen against which to develop antibodies against Mm-VSP, the first 113 amino acids of the protein were selected. This region is unique to Mm-VSP, and was predicted to be highly antigenic by hydrophilicity analysis (Hopp and Woods, 1981). A peptide containing these residues was expressed in bacteria as a recombinant protein fused to the His-MBP dual affinity fusion tag, for use in purification (Appendix I). The peptide was purified using the MBP affinity

tag, then cleaved from the tag using an engineered tobacco etched virus cleavage site. To separate the peptide from uncleaved recombinant protein, the products were separated by polyacrylamide gel electrophoresis. The protein band at the expected size of the antigenic peptide was analyzed by mass spectrometry, which confirmed its identity. The peptide was then used to immunize two rabbits to generate polyclonal antibodies.

To validate the antibodies for use in immunolabeling cells and tissue samples, Mm-VSP with the FLAG epitope fused to the amino terminus was transiently expressed in HEK293T/17 cells. Fixed cells expressing the FLAG-tagged Mm-VSP were labeled with the anti-Mm-VSP sera from either of the two immunized rabbits, and co-labeled with an anti-FLAG monoclonal antibody. This labeling was then visualized with fluorescent secondary antibodies. This resulted in almost complete overlap of the signal corresponding to anti-FLAG labeling with the signal corresponding to anti-Mm-VSP labeling (Fig 8C). These results demonstrate the specificity of the anti-Mm-VSP antibody when used for immunolabeling (Fig 8C).

Serum from one of the immunized rabbits was subjected to purification using an affinity column composed of the immunizing peptide immobilized to agarose beads. Affinity-purified antibody labeled a protein near the predicted molecular weight of Mm-VSP (76.71 kDa) when used to probe adult mouse brain homogenate in a Western blot assay (Fig 8A). Labeling of this band was blocked by pre-incubation of the antibody with the immunizing peptide, indicating that the antibody specifically labels Mm-VSP when used in Western blots.

Because the antibodies are polyclonal, and were generated using the majority of the Mm-VSP amino terminus as an antigen, they should bind to both the full-length Mm-VSP protein and the splice variant lacking exon 9. Indeed, the Western blot validation of the antibody was performed using adult brain, in which the exon 9-lacking variant appears to be the expressed

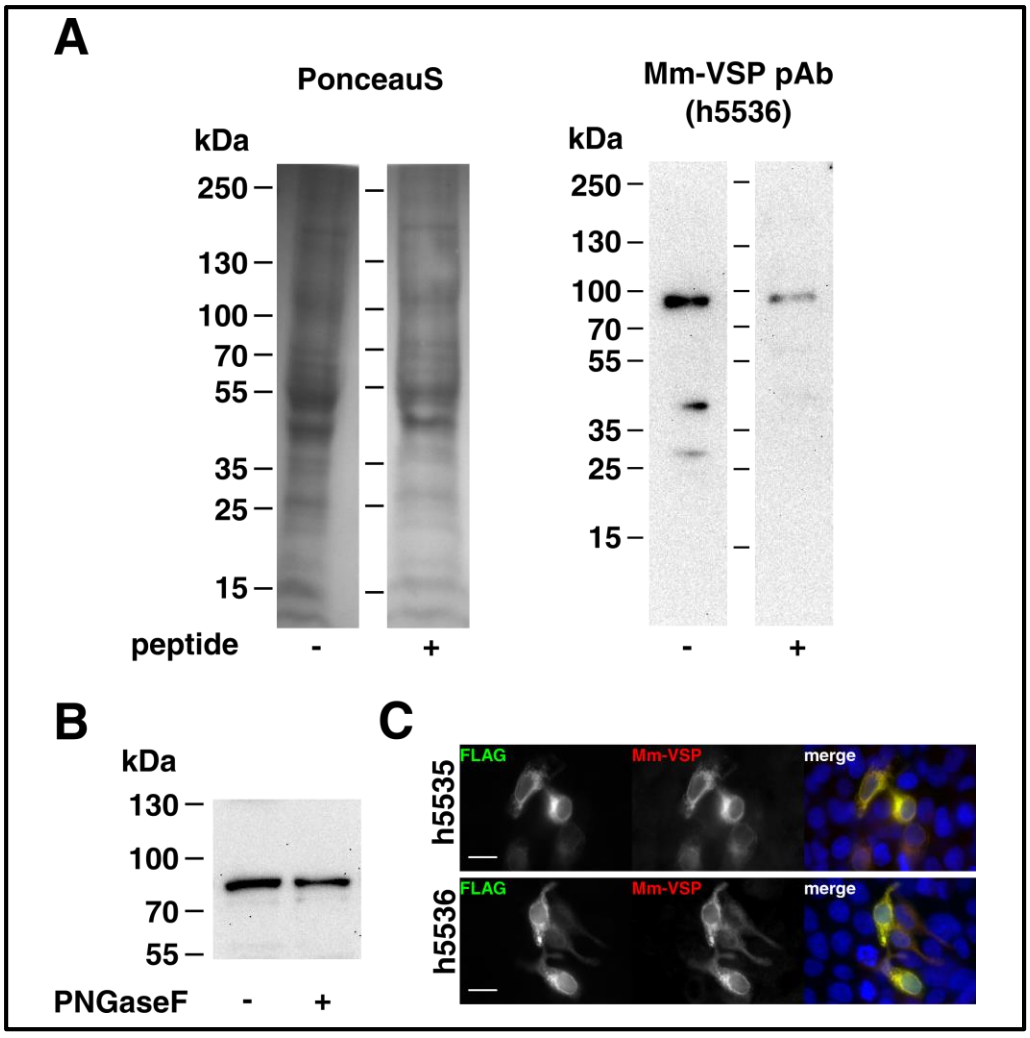

Figure 8: Validation of the rabbit polyclonal antibodies against Mm-VSP

(A) Western blot results for anti-Mm-VSP antibody h5536. Shown is a blot of whole-brain homogenate from a 1 year old mouse. Images on the left show the total protein in each lane, labeled with Ponceau S. Ponceau S was rinsed away and the blot was probed with anti-Mm-VSP antibody h5536 (right), with or without pre-incubation with the immunizing peptide (Mm-VSP a.a 1-113).
(B) Treatment with the deglycosylating enzyme PNGaseF does not affect migration of Mm-VSP in SDS-PAGE. Whole brain homogenate was incubated with the deglycosylating enzyme PNGaseF, and then probed for Mm-VSP by Western blot as in (A). No decrease of the anti-Mm-VSP labeling was observed after treatment by PNGaseF.
(C) Anti-Mm-VSP antibodies label Mm-VSP in fixed cells. Shown are fixed HEK293T/17 cells that were transfected with a construct encoding a FLAG-Mm-VSP fusion protein. Cells were co-labeled with an anti-FLAG monoclonal antibody (left panels, green in merged image) and anti-Mm-VSP sera (center panels, red in merged image). Cell nuclei were labeled with Hoechst dye (blue in merged image). Sera from two rabbits, h5535 (top) and h5536 (bottom), were tested. Scale bars indicate 15 um.

form. Conversely, validation of the antibodies for use in immunocytochemistry was done using full-length Mm-VSP. This indicates the antibodies bind both full-length and exon 9-lacking Mm-VSP, allowing me to address the question of whether Mm-VSP protein is expressed in the brain.

Mm-VSP protein is expressed in the mouse brain, and expression is developmentally regulated

To examine the time course of protein expression, the anti-Mm-VSP antibody was used to probe a Western blot with whole brain homogenates from mice of different ages. The antibody labeled two closely-spaced bands near the predicted molecular weight of Mm-VSP in tissue from animals of postnatal day 30 (P30) and 1 year of age, indicating that the Mm-VSP protein is in fact expressed in the adult mouse brain (Fig 7C). However, the intensity of both bands was so low as to be nearly undetectable in mice of postnatal day 5 (P5). Therefore not only is the Mm-VSP protein expressed in the adult mouse brain, its expression levels are also developmentally regulated in a time scale comparable to the developmental regulation of the mRNA (Fig 7A).

Regarding the presence of the two closely-spaced bands identified in the Western blot, it appears likely that these band represent additional isoforms of Mm-VSP. Neither band was abolished by pre-incubating the brain homogenate with the deglycosylating enzyme PNGaseF (Fig 8B), indicating that the presence of the second band is unlikely to be due to protein glycosylation.

Mm-VSP protein expression in the mouse brain is unique to neurons

The two predominant cell types within the brain are neurons and glia, which each express distinct cohorts of proteins and transmit cellular signals using different mechanisms. Thus, the knowledge that the Mm-VSP protein is expressed in the brain naturally leads to the question of which cell types are responsible for expressing the protein. To address whether neurons, glia, or

both cell types express Mm-VSP, I investigated protein expression in co-cultures consisting of primary mouse cortical neurons grown on a confluent layer of mouse astrocytes. Cells were fixed after cortical neurons had grown for 14 days in vitro (DIV), and the cultures were then labeled with anti-Mm-VSP antibodies. To differentiate between the cell types in the co-cultures, the fixed cells were additionally co-labeled with antibodies against protein markers to identify either neurons (MAP2), synapses (SV2), or glia (GFAP). Under these conditions, cells that demonstrated strong anti-MAP2 labeling consistently also showed high Mm-VSP labeling (Fig 9B). Conversely, cells with strong anti-GFAP labeling were consistently seen to lack Mm-VSP labeling. These data indicate that within the brain, Mm-VSP is expressed exclusively in neurons, and is absent from glia. No colocalization was observed between the anti-Mm-VSP labeling and the anti-SV2 labeling, indicating that within neurons, Mm-VSP is not present at the synapse.

All of the co-culture experiments discussed so far were performed with cortical neurons, however there are many different subtypes of neurons within the brain. Because of this these data do not address whether Mm-VSP expression is limited to the cortical neurons, or if it is broadly expressed across many neuronal populations. To determine which subpopulations of neurons within the mouse brain express Mm-VSP, I also used anti-Mm-VSP antibodies to label slices taken from the whole brain. When fixed sagittal sections of adult mouse brain were labeled with the anti-Mm-VSP antibodies, Mm-VSP expression was observed throughout neurons in the brain (Fig 10). However despite this ubiquitous expression, three populations of neurons demonstrated higher levels of anti-Mm-VSP labeling. These three populations were CA3 neurons of the hippocampus (Fig 10, red), the Purkinje neurons of the cerebellum (Fig 10, purple), and neurons throughout the cerebral cortex (Fig 10, blue). In all of these cell types, the highest Mm-VSP

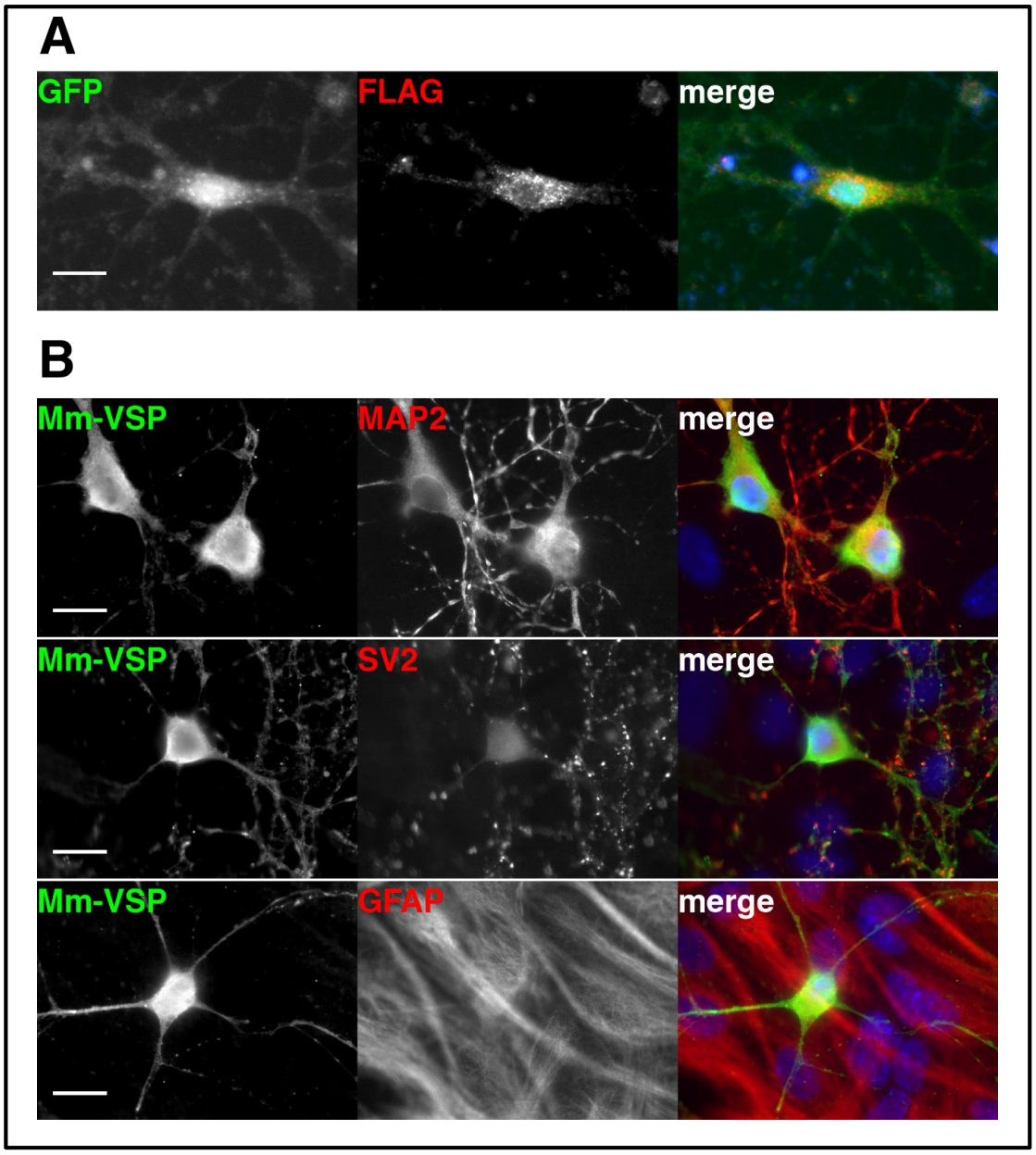

Figure 9: Mm-VSP localizes to a perinuclear region in neurons

(A) Exogenous expression of Mm-VSP in neurons. Primary cultures of cortical neurons were infected with lentivirus carrying DNA encoding both FLAG-Mm-VSP and IRES-GFP. Shown is a neuron grown for 17DIV on a feeder layer of astrocytes. The neuron was successfully infected, as determined by GFP fluorescence (left panel, green in the merged image). Labeling with an anti-FLAG antibody indicates exogenous Mm-VSP protein (center panel, red in the merged image). Cell nuclei were labeled with Hoechst dye (blue).
(B) Endogenous expression of Mm-VSP in neurons. Cortical neurons were cultured for 14DIV on a feeder layer of astrocytes. Cells were co-labeled with anti-Mm-VSP serum (left panels, green in the merged image) and an antibody against a protein marker of neurons (MAP2), synapses (SV2), or glia (GFAP) (center panels, red in the merged images). Cell nuclei were labeled with Hoechst dye (blue). Scale bars for both (A) and (B) indicate 15 um.

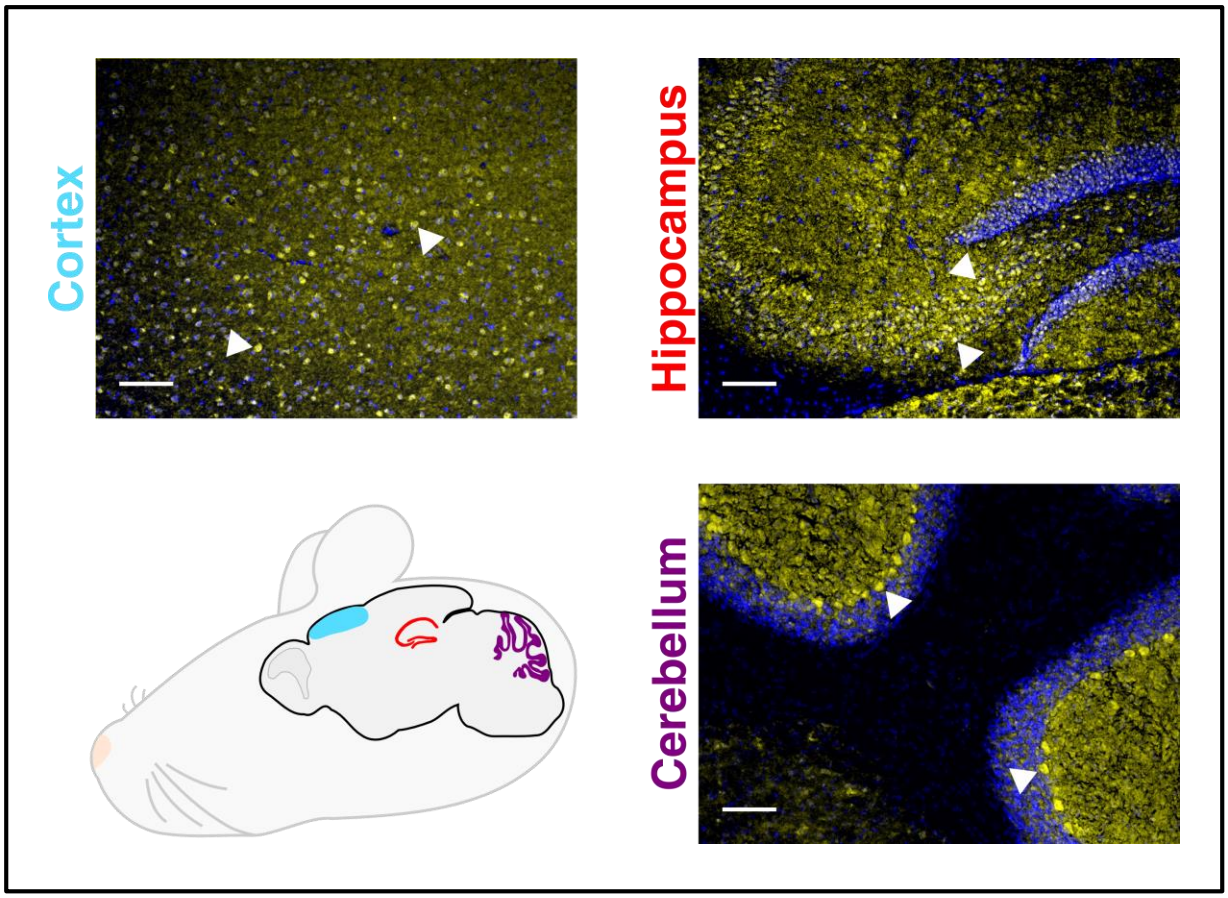

Figure 10: Mm-VSP expression is seen throughout mouse brain with higher levels in a subset of neurons

A schematic depicting color-coded regions of the mouse brain where the highest anti-Mm-VSP labeling was observed: the CA3 neurons of the hippocampus (red), Purkinje cells of the cerebellum (purple) and cells throughout the cortex (cyan). Below are images of the sections indicated in the cartoon, taken of 12.5um sagittal sections from a P43 mouse brain that was labeled with anti-Mm-VSP antibodies (yellow). Cell nuclei were stained with Hoechst dye (blue). Example cells demonstrating high anti-Mm-VSP labeling are highlighted with white arrowheads. Scale bars indicate 100 um.

labeling was seen in the soma. As in the cultured neuron experiments, the highest amount of Mm-VSP labeling was seen in neuronal cell bodies, in a subcellular compartment morphologically consistent with the Golgi and/or endoplasmic reticulum. This localization is distinct from Ci-VSP, which is found at the plasma membrane of cells in which it is naturally expressed (Murata et al., 2005).

Mm-VSP localizes to intracellular membranes, and trafficking is affected by the amino terminus and phosphatase domain

In further support of the possibility that Mm-VSP is localized to intracellular neuronal membranes, the intracellular labeling pattern of Mm-VSP closely resembles the expression pattern seen when primary mouse neurons were made to express exogenous Mm-VSP. Co-cultures of primary mouse astrocytes and cortical neurons were infected with a lentivirus encoding Mm-VSP with a FLAG epitope fused to the amino terminus. This fusion protein was expressed by a bicistrionic vector that also encoded green fluorescent protein (GFP), allowing for identification of infected neurons (Fig 9A). Infected neurons were detected by expression of GFP, and localization of the exogenous Mm-VSP protein was determined by labeling with an anti-FLAG antibody. Like the endogenous protein, exogenous FLAG-Mm-VSP was found primarily in an intracellular compartment with morphology that was consistent with the endoplasmic reticulum. This intracellular localization is also consistent with reports that Mm-VSP and the human VSPs traffic to intracellular membranes in heterologous expression systems (Guipponi et al., 2001; Walker et al., 2001; Tapparel et al., 2003).

To further investigate the intracellular localization of Mm-VSP, I generated constructs encoding either full-length Mm-VSP or exon 9-lacking Mm-VSP (Mm-VSP-Ex9). These constructs contained GFP fused to the carboxy terminus of Mm-VSP, to allow for tracking of the

proteins' localization in live cells. Because Mm-VSP was previously reported to be a Golgi-localized protein (Wu et al., 2001), these Mm-VSP constructs were coexpressed with the Golgi-localized enzyme galactosyltransferase fused to a blue fluorescent protein (GalT-oxBFP, provided by Erik Snapp, personal communication). When the two Mm-VSP constructs were expressed in HEK293T/17 cells, the two isoforms had distinct subcellular distributions. Fluorescence from full length Mm-VSP-GFP localized to a reticular compartment, morphologically consistent with localization to the endoplasmic reticulum (Fig 11, top row). In contrast, in the majority of cells expressing Mm-VSP-Ex9-GFP, fluorescence predominantly colocalized with the Golgi marker (Fig 11, middle row).

The membranes of different organelles are characterized in part by their distinct phophoinositide compositions (reviewed in (Overduin et al., 2001)). Furthermore, trafficking of proteins between organelles within the cell is known to be affected by the phospholipid compositions of these organelles' membranes (reviewed in (De Matteis et al., 2002)). Therefore one possibility for a function of Mm-VSP at intracellular membranes is regulation of protein trafficking between these compartments. One possible consequence of this function is that Mm-VSP's own trafficking may be affected by its own lipid phosphatase activity.

To investigate whether subcellular localization of Mm-VSP is dependent on the protein's lipid phosphatase activity, I mutated the cysteine residue of the active site of the phosphatase to a serine (C458S). This cysteine residue is highly conserved amongst all VSP and PTEN phosphatases (Fig 6), and has been shown to be strictly required for phosphatase activity (Maehama and Dixon, 1998; Murata et al., 2005). Introducing the C458S mutation into Mm-VSP-Ex9-GFP, which was found to traffic to the Golgi, resulted in a protein that instead

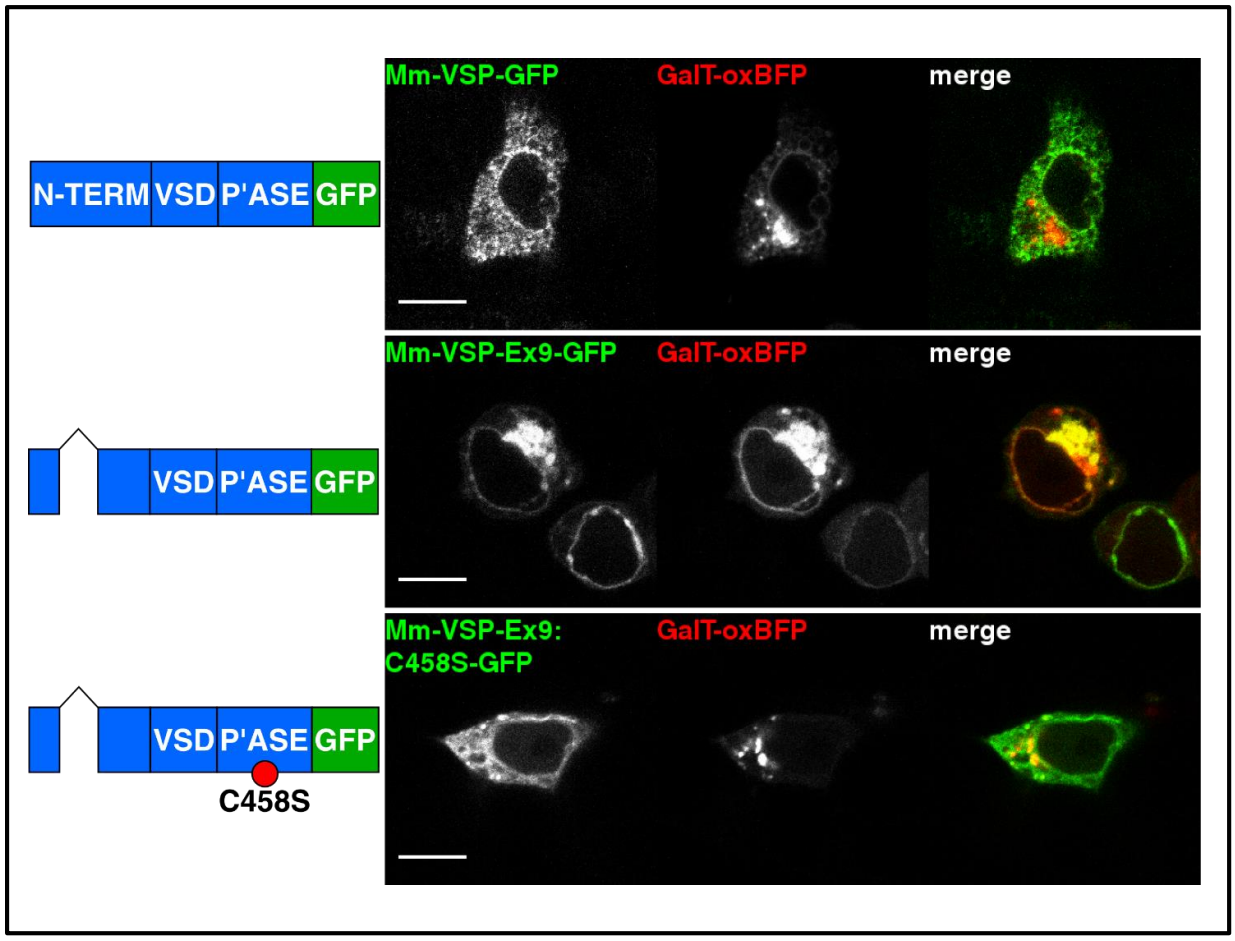

Figure 11: The amino terminus and phosphatase domain of Mm-VSP affect its trafficking

Schematics depicting Mm-VSP-GFP variants (left) are shown alongside live-cell confocal fluorescence images of HEK293T/17 cells expressing these constructs (right). Abbreviations are: N-term - amino terminal domain, VSD - voltage-sensing domain, P'ase - phosphatase domain. Removal of exon 9 is depicted as a carat connecting exons 8 and 10. Mutation of the cysteine required for phosphatase activity is indicated with a red circle. Cells were co-transfected with the indicated Mm-VSP constructs (first panel, green in the merged image) and the GalT-oxBFP construct (center panel, red in the merged image). The fluorescent GalT-oxBFP protein localizes to the Golgi apparatus (Erik Snapp, personal communication). Images were taken 24 hours after transfection. Scale bars indicate 10 um.

localized to a compartment consistent with the ER, similarly to the full-length protein (Fig 11, bottom row). This change in localization is likely not due to effects on protein folding since mutating the analogous cysteine residue in Ci-VSP results in proteins that traffic and fold normally (Villalba-Galea et al., 2009a; Liu et al., 2012). For this reason, these data are consistent with the possibility that Mm-VSP regulates trafficking between intracellular membranes through its lipid phosphatase activity. It is interesting to note that the predominant phosphoinositide in the Golgi membrane is PI(4)P, and levels of $PI(4,5)P_2$ are low, despite evidence that kinases capable of generating $PI(4,5)P_2$ are present at the Golgi membrane (Godi et al., 1999; Jones et al., 2000; Siddhanta et al., 2000; Watt et al., 2002). This suggests two possible substrates for Mm-VSP in the Golgi. Mm-VSP may be responsible for keeping $PI(4,5)P_2$ levels low by dephosphorylating $PI(4,5)P_2$ to PI(4)P, similarly to Ci-VSP. Alternatively, Mm-VSP may use the PI(4)P present in the Golgi as a substrate. I will revisit these two possibilities in my discussion of the phosphatase activity of Mm-VSP.

Conclusions regarding the expression of Mm-VSP

We can now definitively say that both Mm-VSP mRNA and the Mm-VSP protein are expressed in the brains of mice. Furthermore, the alternative splicing, developmental regulation, neuron-specific expression, and ubiquity of expression across neuronal populations suggest that Mm-VSP has an important role in neuronal physiology. To begin to address what this role is, I will now discuss experiments focused on probing the structure and function of Mm-VSP.

II. Structure and function of Mm-VSP's voltage sensor

Mm-VSP and Mm-VSP-Ex9 are both monomers in FSEC

While data indicate that Ci-VSP functions as a monomer (Kohout et al., 2008), the voltage-gated proton channel VSOP/Hv1 is known to form functional dimers (Koch et al., 2008; Lee et al., 2008; Tombola et al., 2008). This is potentially significant with regards to the subunit stoichiometry of VSPs, because like VSPs, VSOP/Hv1 subunits comprise only a single voltage sensor. Furthermore, VSOP/Hv1 is capable of functioning as a monomer, despite its natural dimerism (Koch et al., 2008; Tombola et al., 2008). The dimerization of VSOP/Hv1 was recently shown to be mediated by an extended cytoplasmic alpha helix that forms an intersubunit coiled-coil (Fujiwara et al., 2012).

The cytoplasmic amino terminus of Mm-VSP is much longer than the amino termini of other VSPs (Fig 6), and consequently may provide interprotein contacts unique to Mm-VSP. One possibility is that Mm-VSP may dimerize in a manner dependent on cytoplasmic contacts, analogously to VSOP/Hv1. If this is the case, this oligomerization may be affected by the alternative splicing observed in the mouse brain, which shortens the amino terminal tail of Mm-VSP (Fig 7). I therefore performed fluorescence-detection size exclusion chromatography (FSEC) (Kawate and Gouaux, 2006) to see whether CFP-tagged Mm-VSP and Mm-VSP-Ex9 migrated as monomers or oligomers. The predicted sizes of Mm-VSP-CFP and Mm-VSP-Ex9-CFP are 103.7 kDa and 101.7 kDa, respectively, based on average isotopic masses of amino acids (Wilkins et al., 1999). FSEC was performed on extracts from cells that had been transfected with Mm-VSP-CFP and Mm-VSP-Ex9-CFP, and clear fluorescence peaks were observed. These peaks were found very near to the expected elution volume, based on calibration with standards of known sizes (Fig 12). A moderate concentration of detergent was added to the

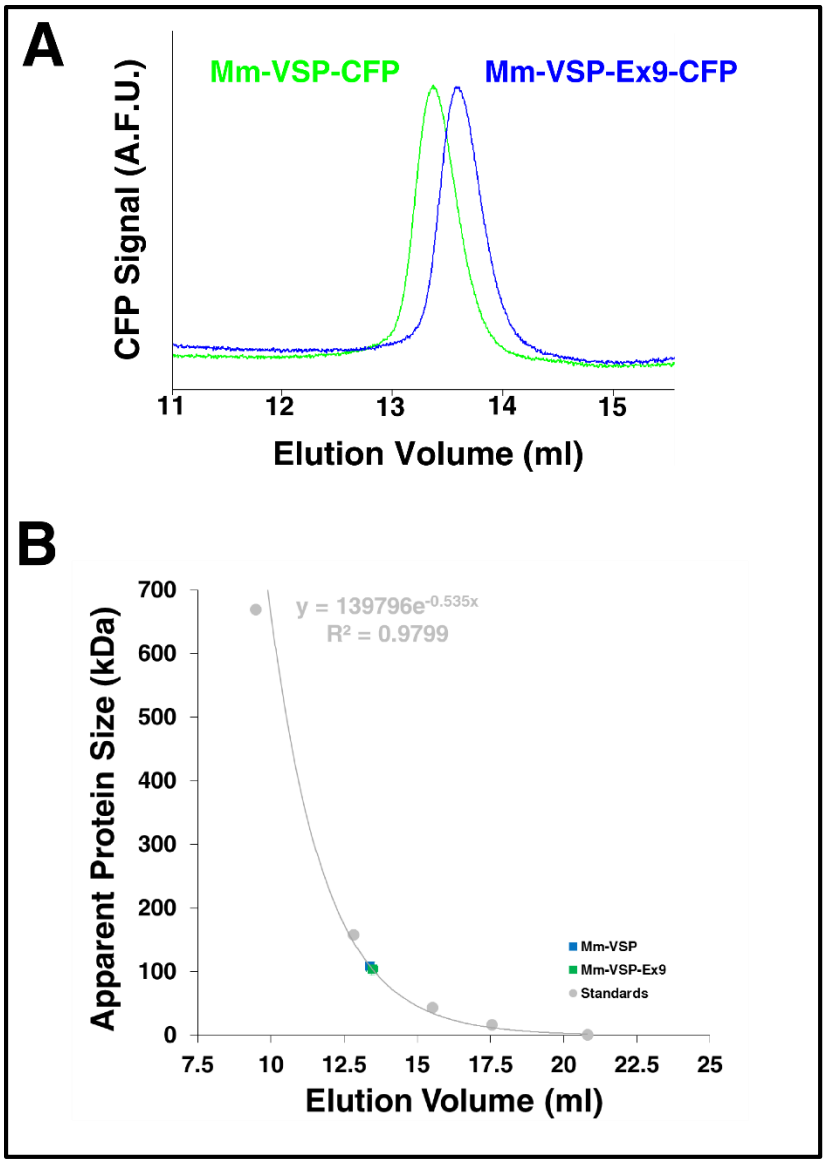

Figure 12: Mm-VSP and Mm-VSP-Ex9 appear as monomers in FSEC

(A) Fluorescence detection size exclusion chromatography elution peaks of Mm-VSP-CFP (green) and Mm-VSP-Ex9-CFP (blue). The scale of the two traces was normalized to the peak height, and the range of volumes containing the void (~8 ml) and monomeric CFP (~17 ml) peaks are excluded to facilitate comparison of the elution volumes.
(B) Protein standards of known sizes were run on the same column used to collect the data shown in (A). The protein standard sizes are plotted here against the elution volumes of the standards' peaks (grey points) and an exponential relationship relating size to elution volume was fit to the data (gray line, equation). When the exponential relationship was used to derive the apparent size of Mm-VSP-CFP and Mm-VSP-Ex9-CFP based on the elution volumes of their peaks, the resulting apparent sizes (109.5 ± 1.1 and 104.3 ± 10.6, respectively) were in good agreement with the predicted sizes for the proteins (103.7 and 101.76, respectively). Data represent averages of 2 independent runs for each protein, and error bars are ± one SD.

running buffer to maintain stability of the transmembrane domains (1.5% dodecyl maltoside, see Appendix I), and so the possibility that this detergent disrupted the formation of intersubunit contacts required for oligomer formation cannot be excluded. However, based on other groups' ability to resolve oligomers in detergent using FSEC (Kawate and Gouaux, 2006) and the previously reported monomeric nature of Ci-VSP (Kohout et al., 2008), such a disruption seems unlikely. It therefore seems most probable that Mm-VSP functions as a monomer.

The transmembrane segments of Mm-VSP form a functional voltage sensor

Although many non-mammalian VSPs have had their voltage sensitivity characterized through measurement of sensing currents (Table 2), this approach has so far been unsuccessful in characterizing the voltage sensitivity of the VSPs from mammals. This is not solely due to the intracellular localization of these proteins; a truncated Mm-VSP encoding only the transmembrane segments localizes to the plasma membrane in HEK293T/17 cells, yet still does not produce sensing currents (data not shown). Similar results were seen with one isoform of human TPTE, which traffics to the plasma membrane in HEK293 cells and also does not produce measurable sensing currents (Halaszovich et al., 2012). It has therefore remained unclear whether the transmembrane segments in human and mouse VSPs form a functional voltage sensor domain.

As a platform with which to test the functionality of the Mm-VSP voltage sensor, I turned to the recently developed Kv_{Synth} chimera channel (Arrigoni et al., 2013). In the original Kv_{Synth1} channel, the VSD of Ci-VSP was fused to the viral potassium pore Kcv (Fig 13), and the chimera was found to display properties of a voltage-gated potassium channel. Because the voltage-dependent properties of Kv_{Synth1} were found to be in good agreement with the voltage-dependent properties resulting from measurements of Ci-VSP sensing currents, it seemed that such a

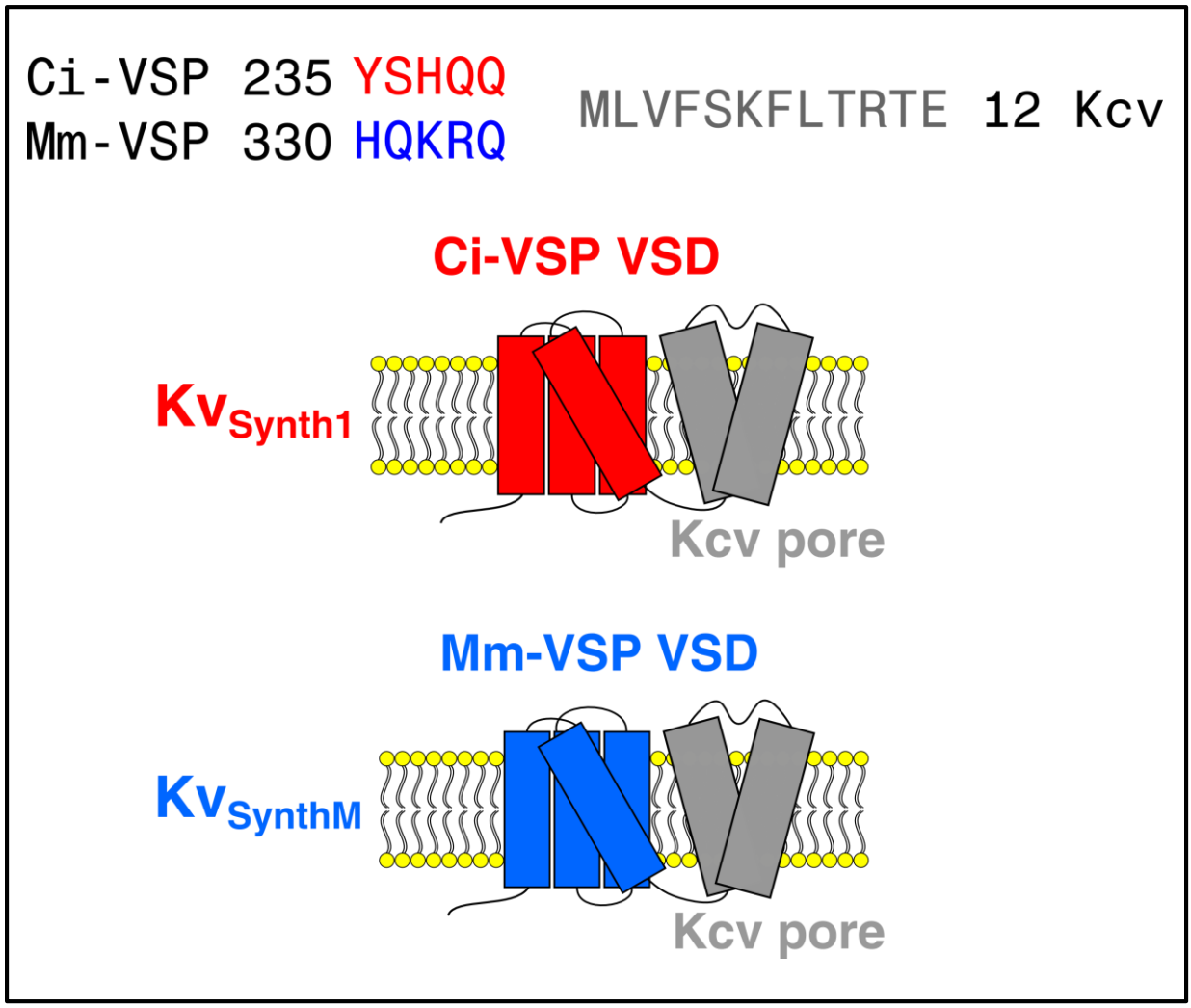

Figure 13: Construction of the Kv_{Synth} channels

Schematics depicting chimeric Kv_{Synth} channels. The original Kv_{Synth1} (Arrigoni et al., 2013) contains the voltage sensor from Ci-VSP (red) and the Kcv potassium pore from the PBCV-1 virus (gray). Kv_{SynthM} contains the voltage sensor from Mm-VSP (blue) and the Kcv potassium pore (gray). The amino acid sequences above indicate where the fusion between the two domains was made, and highlight that the linker domain of the Kv_{Synth} channels is formed by the native amino terminus of Kcv.

chimera could serve as a platform for characterizing the voltage-sensing properties of Mm-VSP. To generate an analog of Kv_{Synth1} to characterize Mm-VSP's voltage sensor, I replaced the VSD of Ci-VSP in Kv_{Synth1} with amino acids 143-334 of Mm-VSP (Fig 13). The resulting chimera was termed Kv_{SynthM}, to denote the presence of the Mm-VSP voltage sensor. To characterize the electrophysiological properties of the Kv_{Synth} channels, the chimeras were each transiently expressed in HEK293T/17 cells. Cells expressing one of the chimeras were voltage clamped in whole-cell mode, and tail currents after channel activation were measured as a readout of voltage sensor activation. The tail current amplitude was taken as an indicator of the ionic conductance (G) following voltage sensor activation, and so to evaluate voltage dependency I analyzed conductance-voltage (G-V) relationships. To measure these relationships, I applied a series of depolarizing pulses and measured instantaneous tail currents at -40 mV (Fig 14B). Normalized tail current amplitude was plotted against activating voltage, and the data were fit with a two-state Boltzmann function to derive the voltage of half-maximal activation ($V_{1/2}$) and the strength of voltage-dependence (Fig 15A). To verify that the observed currents from Kv_{SynthM} reflected potassium conductance, tail currents were measured at a variety of voltages after activating channels to steady-state at +60 mV (Fig 15B). As expected, the reversal potential of the tail currents was near the predicted equilibrium potential for potassium given the internal and external solutions used.

HEK293T/17 cells expressing Kv_{Synth1} produced voltage-dependent currents that were qualitatively similar to those originally reported when Kv_{Synth1} was expressed in *Xenopus* oocytes (Fig 14C). There was however a significant difference in the observed $V_{1/2}$ between the original experiments in oocytes (+56 mV) and the experiments in HEK293T/17 cells (-12 mV). This difference is likely due to both the difference in cell type, and the difference in holding potential

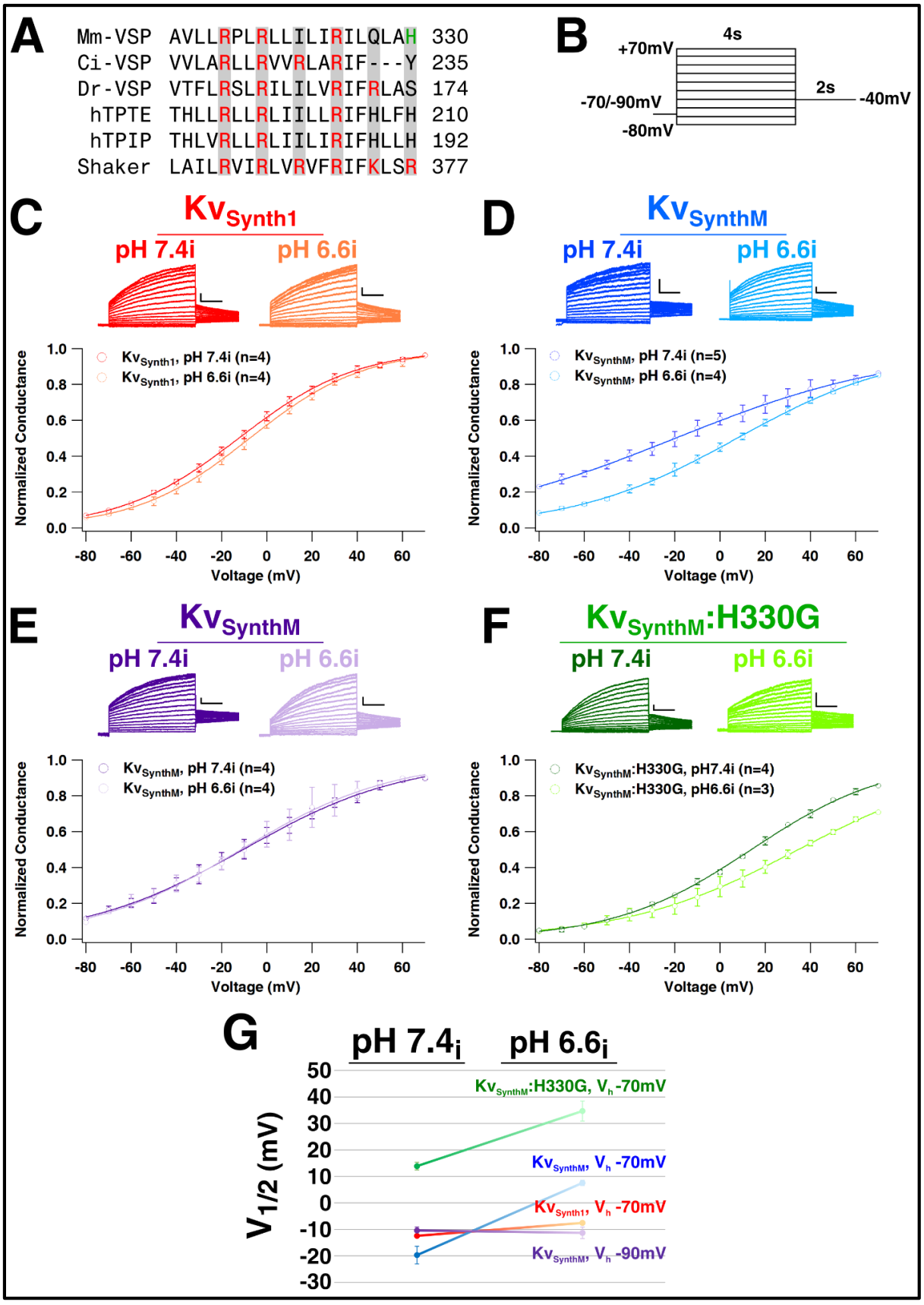
A
Mm-VSP AVLLRPLRLLILIRILQLAH 330
Ci-VSP VVLARLLRVVRLARIF---Y 235
Dr-VSP VTFLRSLRILILVRIFRLAS 174
hTPTE THLLRLLRLIILLRIFHLFH 210
hTPIP THLVRLLRLIILIRIFHLLH 192
Shaker LAILRVIRLVRVFRIFKLSR 377
B
4s
+70mV
-70/-90mV
-80mV
2s
-40mV
C
KvSynth1
pH 7.4i
pH 6.6i
KvSynth1, pH 7.4i (n=4)
KvSynth1, pH 6.6i (n=4)
Normalized Conductance
Voltage (mV)
D
KvSynthM
pH 7.4i
pH 6.6i
KvSynthM, pH 7.4i (n=5)
KvSynthM, pH 6.6i (n=4)
Normalized Conductance
Voltage (mV)
E
KvSynthM
pH 7.4i
pH 6.6i
KvSynthM, pH 7.4i (n=4)
KvSynthM, pH 6.6i (n=4)
Normalized Conductance
Voltage (mV)
F
KvSynthM:H330G
pH 7.4i
pH 6.6i
KvSynthM:H330G, pH7.4i (n=4)
KvSynthM:H330G, pH6.6i (n=3)
Normalized Conductance
Voltage (mV)
G
pH 7.4i
pH 6.6i
KvSynthM:H330G, Vh -70mV
KvSynthM, Vh -70mV
KvSynth1, Vh -70mV
KvSynthM, Vh -90mV
V1/2 (mV)

Figure 14: Kv_{Synth} channels show that the transmembrane segments of Mm-VSP sense voltage and pH

(A) An alignment of the S4 sequences of the indicated VSP family members and the *Drosophila* Shaker potassium channel. The amino acid number of the final position shown is noted on the right. Positive residues are highlighted in red, and the residue mutated to produce the Kv_{SynthM}:H330G channel is highlighted in green.
(B) The voltage protocol used to generate conductance-voltage (G-V) curves for the Kv_{Synth} channels. Cells were held at either -70 mV (C,D,F) or -90 mV (E) in whole-cell voltage clamp mode. Four second pulses from -80 mV to +70 mV were applied, increasing in 10 mV increments. Instantaneous tail currents were measured upon repolarizing to -40 mV and used as an indication of conductance. Cells were kept at their holding potential for 10 seconds between sweeps.
(C-F) Voltage and pH-dependent gating of the Kv_{Synth} channels. Representative current traces from HEK293T/17 cells transfected with the indicated Kv_{Synth} constructs are shown. Recordings were performed with intracellular solutions at pH 7.4 (darker traces) or pH 6.6 (lighter traces). Vertical scale bars indicate 500 pA, and horizontal scale bars indicate 1 second. Below the representative traces are average G-V curves, with the number of replicates indicated for each construct and condition. G-V curves were fit using a two-state Boltzmann curve, and normalized to the max and min values extrapolated from the fits for visual comparison (Fig 15A). Error bars indicate standard error of the mean. Each color-coded dataset corresponds to a given Kv_{Synth} channel and holding potential: **(C)** Kv_{Synth1}, -70 mV; **(D)** Kv_{SynthM}, -70 mV; **(E)** Kv_{SynthM}, -90 mV; **(F)** Kv_{SynthM}:H330G, -70 mV.
(G) A graph showing the $V_{1/2}$ values for each Kv_{Synth} channel/holding potential condition, plotted against the pH of the intracellular solution. Values were derived from the Boltzmann fits in (Fig 15A), and error bars correspond to one standard deviation.

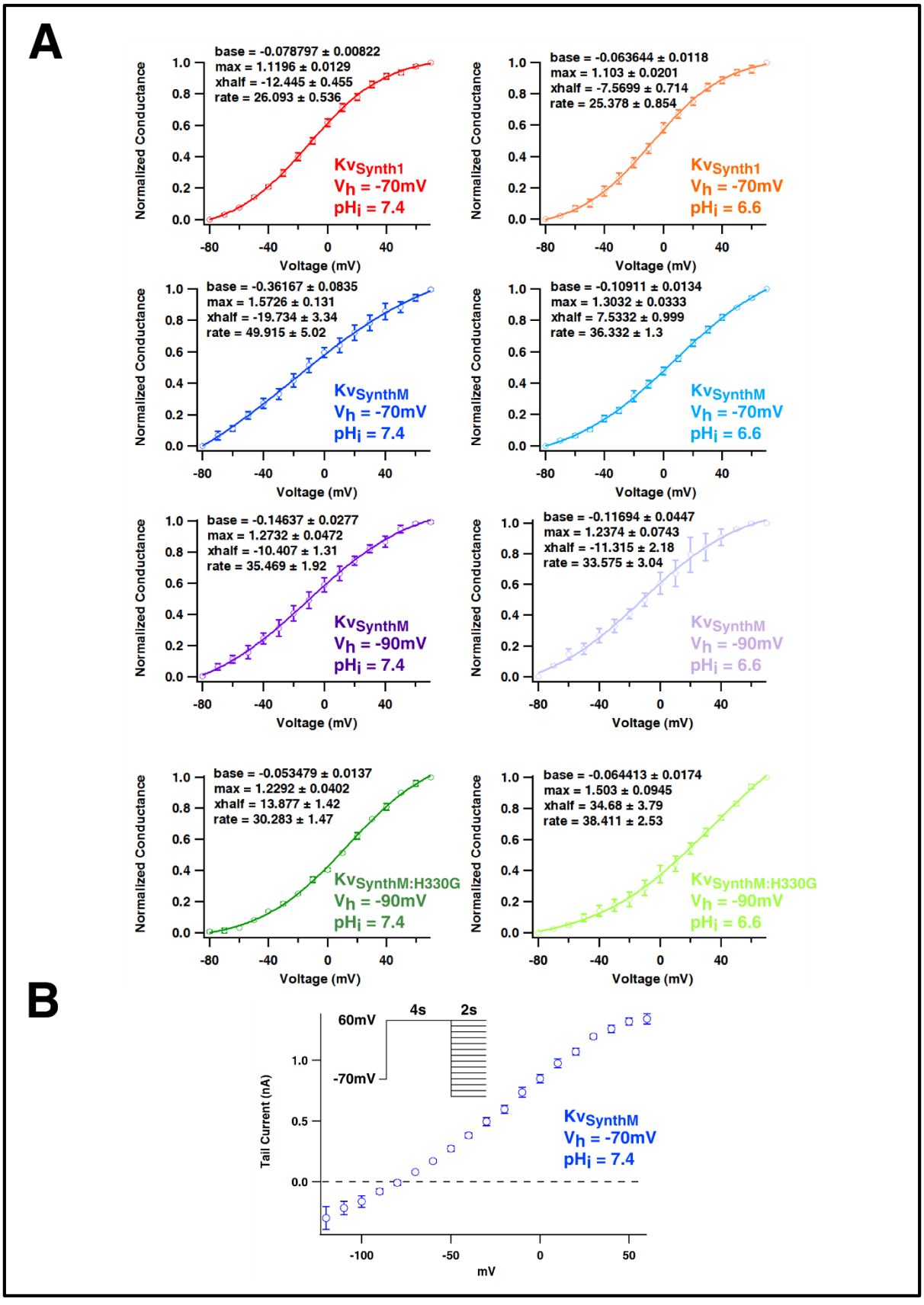
A
base = -0.078797 ± 0.00822
max = 1.1196 ± 0.0129
xhalf = -12.445 ± 0.455
rate = 26.093 ± 0.536
KvSynth1
Vh = -70mV
pHi = 7.4
base = -0.063644 ± 0.0118
max = 1.103 ± 0.0201
xhalf = -7.5699 ± 0.714
rate = 25.378 ± 0.854
KvSynth1
Vh = -70mV
pHi = 6.6
base = -0.36167 ± 0.0835
max = 1.5726 ± 0.131
xhalf = -19.734 ± 3.34
rate = 49.915 ± 5.02
KvSynthM
Vh = -70mV
pHi = 7.4
base = -0.10911 ± 0.0134
max = 1.3032 ± 0.0333
xhalf = 7.5332 ± 0.999
rate = 36.332 ± 1.3
KvSynthM
Vh = -70mV
pHi = 6.6
base = -0.14637 ± 0.0277
max = 1.2732 ± 0.0472
xhalf = -10.407 ± 1.31
rate = 35.469 ± 1.92
KvSynthM
Vh = -90mV
pHi = 7.4
base = -0.11694 ± 0.0447
max = 1.2374 ± 0.0743
xhalf = -11.315 ± 2.18
rate = 33.575 ± 3.04
KvSynthM
Vh = -90mV
pHi = 6.6
base = -0.053479 ± 0.0137
max = 1.2292 ± 0.0402
xhalf = 13.877 ± 1.42
rate = 30.283 ± 1.47
KvSynthM:H330G
Vh = -90mV
pHi = 7.4
base = -0.064413 ± 0.0174
max = 1.503 ± 0.0945
xhalf = 34.68 ± 3.79
rate = 38.411 ± 2.53
KvSynthM:H330G
Vh = -90mV
pHi = 6.6
Normalized Conductance
Voltage (mV)
B
60mV
4s
2s
-70mV
Tail Current (nA)
KvSynthM
Vh = -70mV
pHi = 7.4
mV

Figure 15: Boltzmann curve fit parameters and reversal potential measurements of Kv_{Synth} channels

(A) Shown are conductance-voltage relationship (G-V) curves for cells expressing Kv_{Synth} channels. Each G-V curve corresponds to the indicated channel and recording conditions. Tail currents were normalized using the maximum and minimum tail currents recorded in each cell, to provide a measure of normalized channel conductance between 0 and 1. In the inserts, the values of the Boltzmann parameters are listed +/- one standard deviation, obtained by fitting the function

$$P_O = base+(max/(1+exp((xhalf-x)/rate)))$$

to the observed G-V relationships. Note that because the x-axis is in units of mV, the variable *xhalf* is equivalent to the measure $V_{1/2}$ discussed in the text. The data are the same as shown in (Fig 14C-F). Max and base values obtained from these fits were used to standardize the data for presentation in (Fig 14C-F) to facilitate visual comparison of the curves.
(B) The reversal potential of Kv_{SynthM} shows it conducts potassium. Instantaneous Kv_{SynthM} tail current amplitudes were measured at a range of voltages after a 4 second activating pulse to +60 mV. Tail currents were plotted versus the voltage at which they were measured to determine the reversal potential of Kv_{SynthM} currents. The pulse protocol is shown in the inset. The average reversal potential (~-80) was near the reversal potential of potassium given the recording solutions used. Error bars indicate standard error of the mean (n=3).

from which the test pulses were applied. Except where noted, I held HEK293T/17 cells at -70 mV to model the neuronal resting membrane potential, whereas the oocyte membranes were held at -20 mV (Arrigoni et al., 2013).

Compared to the Ci-VSP-based Kv_{Synth1}, the Mm-VSP-based Kv_{SynthM} showed activation at more hyperpolarized potentials, with a $V_{1/2}$ of approximately -20mV (Fig 15A). Furthermore, Kv_{SynthM} also demonstrated weaker voltage dependence than Kv_{Synth1} (Fig 14D). In the Boltzmann equation used to fit the G-V relationship, the strength of the voltage dependence corresponds to the variable designated *rate* (Fig 15A). In this form of the Boltzmann equation, *rate* is equal to RT/zF, where R is the universal gas constant, T is temperature in degrees Kelvin, F is the faraday constant, and z is the equivalent charge movement. Although these experiments do not directly measure charge movement of the voltage sensor, the estimated value of z serves as a convenient way to compare voltage sensitivities between proteins and recording conditions. A larger value for z corresponds to more equivalent charge movement in response to a given depolarization, hence proteins with larger z values can be said to have stronger voltage dependence. For Kv_{Synth1} the rate derived from the Boltzmann fit corresponds to a value for z of approximately 1, similar to the value given by measurements of Ci-VSP gating currents (Murata et al., 2005). In comparison, Kv_{SynthM} showed much weaker voltage dependence, with an estimated z value of approximately 0.52.

The voltage sensor of Mm-VSP is modulated by intracellular pH

To attempt to explain the basis of the differences in the voltage-dependent properties of Kv_{Synth1} and Kv_{SynthM}, I compared the residues of the S4 between Mm-VSP and Ci-VSP. This revealed that Mm-VSP is lacking one of the gating charge residues present in Ci-VSP (Fig 14A), which likely contributes to the weaker voltage sensitivity of the Mm-VSP voltage sensor. This

comparison also revealed that the Mm-VSP voltage sensor contains a histidine residue (H330) on the same face of the S4 alpha helix, which is conserved in the human VSPs, but absent from Ci-VSP. The pKa of a histidine side chain (6.0) is such that it can be protonated at low physiological pH, which has the effect of adding positive charge to the histidine side chain. This property of histidines has allowed them to be used as pH-titratable gating charges, and substituting the gating charge residues of the *Shaker* potassium channel with histidines produces pH-titratable changes in voltage-dependent properties (Starace et al., 1997; Starace and Bezanilla, 2001). Similar results have recently been reported with histidine substitutions of the predicted gating charge residues in the Ci-VSP voltage sensor (Villalba-Galea et al., 2013).

The presence of a conserved histidine in the S4 of human VSPs is therefore notable, and I hypothesized that this residue might act as an endogenous pH-titratable gating charge. Based on an alignment of S4 from Mm-VSP with Ci-VSP's S4, for which the structure of the voltage sensor is known, this histidine residue is most likely near the cytoplasmic side of the S4. This predicts that changing the intracellular pH should affect the voltage dependent properties of Kv_{SynthM}. To test this possibility, I repeated the G-V experiments that had been performed with intracellular solutions of pH 7.4, using instead intracellular solutions of pH 6.6.

When G-V relationships were measured for the Ci-VSP-based Kv_{Synth1}, decreasing the intracellular pH (pH_i) from 7.4 to 6.6 had very little effect on either the $V_{1/2}$ or the strength of voltage dependence observed (Figs 14C and 15A, red traces). In contrast, the Mm-VSP-based Kv_{SynthM} demonstrated drastically different voltage-dependent properties based on the pH of the intracellular solution (Figs 14D and 15A, blue traces). The $V_{1/2}$ increased from -20 mV with pH_i of 7.4, to approximately 8 mV with pH_i of 6.6, and the value for *z* increased from 0.52 with pH_i of 7.4, to approximately 0.72.

Although these results are consistent with the interpretation that H330 acts as a titratable gating charge, the pH-dependent gating properties of Kv_{SynthM} cannot be explained by H330 alone. Mutation of H330 to a glycine (H330G) in Kv_{SynthM} did not abolish the pH-dependent shift in $V_{1/2}$ of Kv_{SynthM}, as would be expected if H330 were entirely responsible for the pH-dependent effects. At pH_i of 7.4 the G-V relationship of Kv_{SynthM}:H330G had a $V_{1/2}$ of 14 mV, and at pH_i of 6.6 the $V_{1/2}$ increased to 35 mV (Fig 14F and 15A, green traces). Furthermore, the magnitude of this pH-dependent shift in $V_{1/2}$ is almost identical between Kv_{SynthM} and Kv_{SynthM}:H330G (Fig 14G). It should be noted that at neutral pH, the H330G mutant had a positively-shifted G-V compared to the wild-type Kv_{SynthM}, indicating that this histidine destabilizes the resting state of the voltage sensor. Intriguingly, holding the membrane at the more negative potential of -90 mV abolished the pH-dependent shift of the $V_{1/2}$ for Kv_{SynthM}, resulting in measured $V_{1/2}$s of -10 mV at pH_i of 7.4, and -11 mV at pH_i of 6.6 (Figs 14E and 15A, purple traces). This suggests that the conformational changes associated with Kv_{SynthM} gating and the accessibility of key protonatable residues may differ at the two holding potentials.

Conclusions regarding the structure and function of the Mm-VSP voltage sensor

The Kv_{SynthM} chimera demonstrates that the transmembrane segments from Mm-VSP do in fact form a voltage-regulated domain, capable of gating a potassium pore. However, the voltage-dependent properties of Mm-VSP's voltage sensor are distinct from those of Ci-VSP's voltage sensor, indicating again that the mammalian VSPs are likely functionally divergent from the VSPs of non-mammals. In particular, Ci-VSP's voltage sensor appears to be have stronger voltage-sensitivity than the voltage sensor in Mm-VSP, and the Mm-VSP voltage sensor also exhibits pH-dependent modulation of activity that is not seen with the Ci-VSP voltage sensor. These findings are particularly interesting given the apparent localization of Mm-VSP to the ER

and Golgi. The Golgi is not thought to use membrane voltage as a major signaling mechanism, however changes in pH are an important means of regulating Golgi function. The pH-sensitivity of Mm-VSP may therefore represent a physiologically-important mechanism for mammalian VSP activation.

III. Voltage-regulated activity of the Mm-VSP phosphatase domain

The phosphatase domain of Mm-VSP inhibits PI(4,5)P_2-sensitive M currents

Now that Mm-VSP has been shown to contain a functional voltage sensor, the question of what the voltage-regulated phosphatase activity is follows naturally. However, analyzing the voltage-regulated phosphatase activity in the context of the native Mm-VSP is problematic. Both full-length Mm-VSP and the splice variant expressed in the adult mouse brain localize to intracellular membranes in primary neurons (Fig 9) and in heterologous expression systems (Fig 11). While Mm-VSP can be made to traffic to the plasma membrane by truncation of the amino terminus, as in the Kv_{SynthM} channel, assessment of Mm-VSP's voltage sensor activity indicates that Mm-VSP will be activated at the resting membrane potentials of all cells (Fig 14). As sustained lipid phosphatase activity can be detrimental to cell health, this makes establishing an expression system for Mm-VSP technically challenging.

To circumvent these issues and characterize the voltage-regulated phosphatase activity of Mm-VSP, I exploited the modularity of the VSP phosphatase domain. It has been shown that both VSP phosphatase domains and PTEN can be attached to the voltage sensors of other species' VSPs to generate functional voltage-controlled enzymes (Lacroix et al., 2011; Halaszovich et al., 2012). As would be expected, these chimeric proteins exhibit the substrate specificity of the phosphatase domain, and the voltage dependency of the voltage sensor domain.

The Dr-VSP voltage sensor is known to traffic readily to the plasma membrane of HEK293T/17 cells, and Dr-VSP is known to require potentials above 0 mV to become activated (Hossain et al., 2008). Because of these properties, Dr-VSP contains a voltage sensor ideally-suited for use in HEK293T/17 cells. I therefore generated a chimera, termed Dr-VSTpte, in which the phosphatase from Mm-VSP is fused to the VSD of Dr-VSP (Fig 16A).

As a readout of phosphatase activity, the amplitude of M currents was used. These currents modulate the excitability of neurons, and are named for the fact that they are suppressed by the activation of muscarinic acetylcholine receptors (mAChRs) (Brown and Adams, 1980). M current modulation by mAChRs has been found to be due to the sensitivity of the M current to $PI(4,5)P_2$ (Zhang et al., 2003). $PI(4,5)P_2$ acts to facilitate opening of voltage-gated potassium channels formed by the KCNQ2 and KCNQ3 subunits, which are the proteins responsible for producing the M current. Decreases in $PI(4,5)P_2$ such as those resulting from mAChR activation consequently decrease M current amplitude. As a result, the amplitudes of M currents serve as a sensitive electrophysiological readout of the $PI(4,5)P_2$ concentration in the plasma membrane.

To establish that HEK293T/17 cells contain no endogenous mechanisms to cause a voltage-induced depletion of $PI(4,5)P_2$, cells were co-transfected with KCNQ2, KCNQ3, and the empty pIRES2-EGFP vector as a negative control. Co-transfection with these constructs generated appreciable M currents when cells were voltage clamped in whole-cell mode, then held at -60 mV and depolarized to -20 mV (Fig 16B,C, black). Repeated measurements of the tail currents in single cells demonstrated that M current amplitude did not show much variability (Fig 16E, black), indicating that the concentration of $PI(4,5)P_2$ at the plasma membrane was stable over time as well. Additionally, M current amplitude was stable when currents were

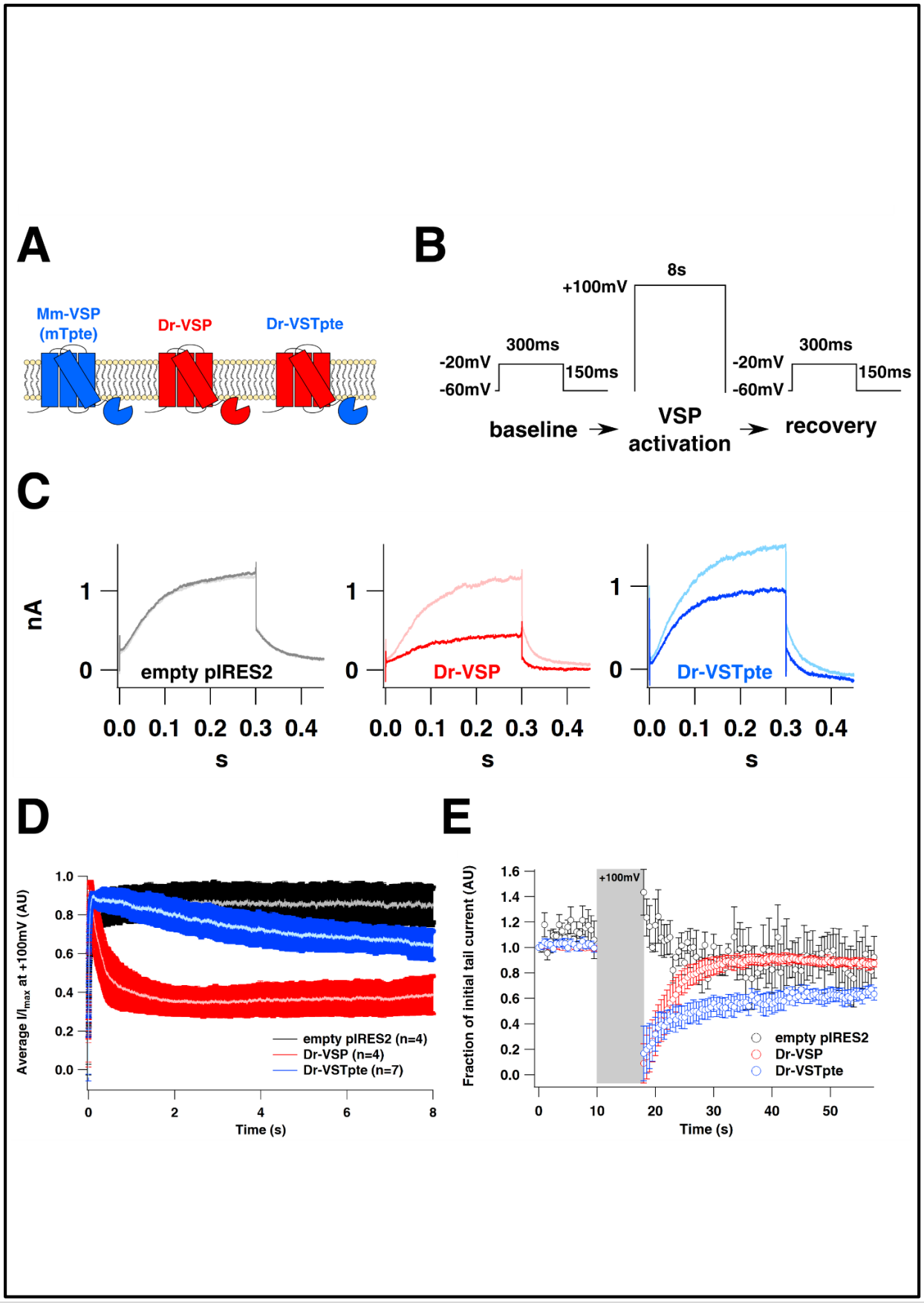
A
Mm-VSP
(mTpte)
Dr-VSP
Dr-VSTpte
B
8s
+100mV
300ms
-20mV
-60mV
150ms
300ms
-20mV
-60mV
150ms
baseline
VSP
activation
recovery
C
nA
1
0
empty pIRES2
Dr-VSP
Dr-VSTpte
0.0 0.1 0.2 0.3 0.4
s
D
Average I/I$_{max}$ at +100mV (AU)
1.0
0.8
0.6
0.4
0.2
0.0
empty pIRES2 (n=4)
Dr-VSP (n=4)
Dr-VSTpte (n=7)
0 2 4 6 8
Time (s)
E
Fraction of initial tail current (AU)
1.6
1.4
1.2
1.0
0.8
0.6
0.4
0.2
0.0
+100mV
empty pIRES2
Dr-VSP
Dr-VSTpte
0 10 20 30 40 50
Time (s)

Figure 16: The activity of the Mm-VSP phosphatase domain slowly inhibits KCNQ2/3 currents in HEK cells

(A) Schematic depicting the topology of the Dr-VSTpte chimera (right). The Dr-VSTpte chimera was generated by fusing the Mm-VSP phosphatase domain from Mm-VSP (left, blue) to the voltage sensor of Dr-VSP (red, center).
(B) The voltage protocol used to probe VSP-based inhibition of $PI(4,5)P_2$-dependent M currents. Baseline tail current amplitude was established by activating M currents at -20 mV for 300 ms and then measuring instantaneous currents when the cell was repolarized to -60 mV. Measurements were taken once every 500 ms for 10 seconds. Cells were then depolarized to +100 mV for 8 seconds to activate VSP activity. Following VSP activation, tail currents were again recorded once every 500 ms for 40 seconds.
(C) Representative currents recorded from HEK293T/17 cells co-transfected with KCNQ2, KCNQ3, and either an empty vector (black), Dr-VSP (red) or Dr-VSTpte (blue). Traces recorded immediately before depolarizing cells to +100 mV are shown in lighter colors, and traces recorded immediately after depolarization are shown in darker colors.
(D) Average normalized M current (I/I_{max}) of cells held at +100 mV. The lighter center of each trace represents the average I/I_{max} of 4-7 cells, while darker bars represent per-timepoint standard error of the mean.
(E) Normalized tail currents amplitudes plotted over time. Amplitudes were normalized to the initial tail current in each cell. Error bars are standard error of the mean for the same 4-7 cells shown in panel D.

continuously recorded for 8 seconds at +100 mV (Fig 16D, black), and tail current amplitudes were not suppressed following the +100 mV pulse (Fig 16C,E, black).

As a positive control for VSP activity, HEK293T/17 cells were co-transfected with KCNQ2, KCNQ3, and Dr-VSP. As in the absence of Dr-VSP, robust M currents were evoked by depolarizing from -60 mV to -20 mV (Fig 16B,C, red). Repeated measurement of tail currents at these potentials again showed very little variability, confirming that Dr-VSP is not active under these conditions (Fig 16E, red). However when cells expressing Dr-VSP were depolarized to +100 mV, M currents were rapidly suppressed (Fig 16D, red). Repolarizing cells and continuing to repeatedly measure tail currents after the +100 mV step revealed that the tail current amplitude was strongly inhibited by the strong depolarization. Furthermore, tail current amplitude recovered over time, indicating the resynthesis of $PI(4,5)P_2$ by the action of endogenous lipid kinases (Fig 16E, red). When M current rundown and tail current recovery after Dr-VSP activation were fit with single exponentials (Table 3), the time constants from the fits ($\tau_{inhibition}$=0.3s $\tau_{recovery}$=4.4s) were in good agreement with those previously reported (Falkenburger et al., 2010).

As expected, these control data confirm that measurement of M currents in HEK293T/17 cells is a robust system with which to investigate the phosphatase activity of VSPs against the substrate $PI(4,5)P_2$. To test whether the Mm-VSP phosphatase is capable of causing a voltage-dependent decrease in $PI(4,5)P_2$, HEK293T/17 cells were co-transfected with KCNQ2, KCNQ3, and the Dr-VSTpte chimera containing the Mm-VSP phosphatase. As before, M current measurements were stable over time before depolarization to +100 mV (Fig 16E, blue). When cells were depolarized to +100 mV the M current was again seen to be suppressed over time (Fig

	M Current Inhibition ($y = y_0+A(exp[(-x-x_0)/\tau]$)				M Current Recovery ($y = y_0+A(exp[(-x-x_0)/\tau]$)					
Dr-VSP	y_0	A	τ	x_0	y_0	A		τ		x_0
	0.36274 ± 8.99e-005	0.54042 ± 0.000846	0.30129 ± 0.000697	0.05	0.90158 ± 0.00292	-0.8724 ± 0.0118		4.4488 ± 0.106		18
	M Current Inhibition ($y = y_0+A(exp[(-x-x_0)/\tau]$)				M Current Recovery ($y = y_0+A_1(exp[(-x-x_0)/\tau_1]+A_2\ (exp[(-x-x_0)/\tau_2]$)					
Dr-VSTpte	y_0	A	τ	x_0	y_0	A_1	A_2	τ_1	τ_2	x_0
	0.60017 ± 0.000552	0.30054 ± 0.000457	4.4791 ± 0.0178	0.05	0.67201 ± 0.0296	-0.2604 ± 0.0474	-0.26312 ± 0.028	2.5391 ± 0.646	18.581 ± 7.31	18

Table 3: Fit parameters of M current inhibition and recovery

The average time courses of M current inhibition and recovery shown in Figs 16D and 16E were fit with either a single or double exponential as noted in the table, generating the listed values for the fit parameters. Values are reported +/- one standard deviation, as derived from the fit.

16C, blue), however the Mm-VSP phosphatase domain decreased the current amplitude at a much slower rate than Dr-VSP ($\tau_{inhibition}$=4.5s). Even after 8 seconds at +100 mV, M current amplitude was not decreased to the same level seen with Dr-VSP. This difference in the rates of M current amplitude decrease could simply be due to lower expression levels of the chimera. However, the recovery of tail currents following inhibition by the Mm-VSP phosphatase also occurred much more slowly than following inhibition by Dr-VSP. Furthermore, the time course of tail current recovery after Mm-VSP phosphatase activation required a double exponential with two time constants to fit the data, compared to the single exponential used to fit the recovery after Dr-VSP activation (Table 3). The faster time constant of recovery was comparable to that observed following Dr-VSP activation ($\tau_{fast\ recovery}$=2.5s), however the second time constant was about seven times slower ($\tau_{slow\ recovery}$=18.6s).

Time course of tail current recovery suggests a novel VSP phosphatase activity for Mm-VSP

One interpretation of the ability of the chimera to inhibit KCNQ2/3 currents is that the Mm-VSP phosphatase uses $PI(4,5)P_2$ as a substrate, and as a result directly depletes the $PI(4,5)P_2$ pool available to KCNQ2/3 channels (Fig 18). Support for this model comes analogy to the activities of the non-mammalian VSPs, which act as 3' and 5' phosphatases on the substrates $PI(3,4,5)P_3$, $PI(3,4)P_2$, and $PI(4,5)P_2$. While this model was expected based on the activity of other VSPs, it fails to provide a mechanism for the biphasic recovery of $PI(4,5)P_2$ in the plasma membrane. Because $PI(4,5)P_2$ resynthesis by endogenous lipid kinases should take place in a single step, using the precursor PI(4)P, this model predicts that the tail current recovery time course should be well-fit with an exponential equation containing a single time constant.

An alternative explanation of the KCNQ2/3 current inhibition is that the Mm-VSP phosphatase acts to deplete a pool of phosphoinositides that serves as a precursor for $PI(4,5)P_2$

synthesis (Fig 19). It has recently been shown that by depleting PI(4)P in either the plasma membrane or Golgi, the plasma membrane pool of $PI(4,5)P_2$ is slowly and indirectly depleted (Dickson et al., 2014). This is because the concentrations of PI(4)P and $PI(4,5)P_2$ are maintained in a dynamic equilibrium within the cell, and PI(4)P serves as a direct precursor to $PI(4,5)P_2$ by acting as a substrate for PI(4)P 5-kinases. In a model where Mm-VSP utilizes PI(4)P as a substrate, the slow inhibition of KCNQ2/3 current can be interpreted as indirect depletion of $PI(4,5)P_2$ by the Mm-VSP phosphatase as the equilibrium between the two phosphoinositides shifts. In this model, the rapid phase of KCNQ2/3 current recovery would be indicative of $PI(4,5)P_2$ resynthesis by PI 5-kinases acting on a remaining pool of PI(4)P. The slow phase of current recovery would then indicate exhaustion of the available pool of PI(4)P. Recovery of the basal $PI(4,5)P_2$ concentration would then require resynthesis of PI(4)P from PI by PI 4-kinases, followed by resynthesis of $PI(4,5)P_2$ by PI(4)P 5-kinases. This model is able to directly account for both the slow time course of KCNQ2/3 inhibition and the biphasic, slow time course of KCNQ2/3 current recovery, and is supported by previous analyses of the kinetics of PI(4)P and $PI(4,5)P_2$ synthesis (Willars et al., 1998).

Mm-VSP's phosphatase domain is unable to cause translocation of the PLCδ1-PH domain

It should be noted that I have so far been unable to detect changes in the localization of the $PI(4,5)P_2$-binding PLCδ1-PH domain (Table 1) in response to activation of the Dr-VSTpte chimera (Fig 17). Dr-VSP is able to cause a robust and rapid movement of the PLCδ1-PH domain from the plasma membrane to the cytosol (Fig 17A), but the Dr-VSTpte chimera does not after either 5 or 10 seconds of activation (Fig 13B,C), despite the observed ability of Dr-VSTpte to inhibit the $PI(4,5)P_2$-sensitive KCNQ2/3 channels.

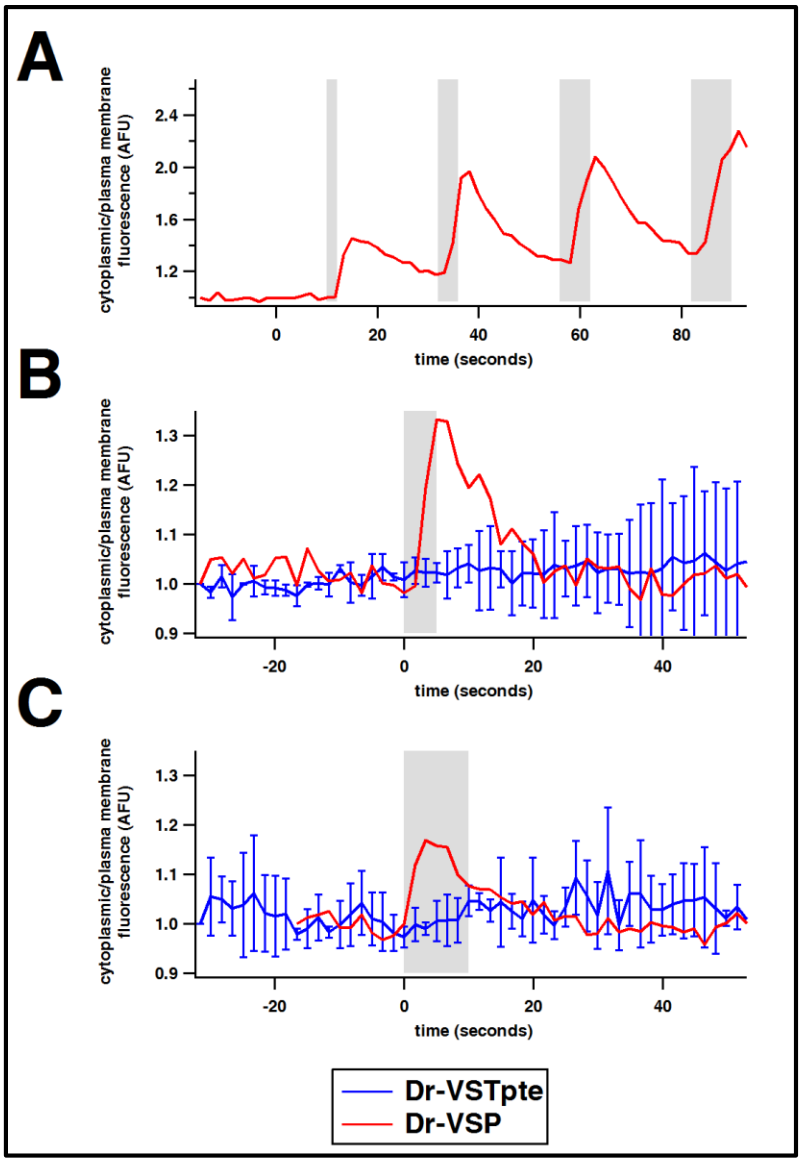

Figure 17: The Dr-VSTpte chimera does not affect the localization of the PLCδ1-PH domain

Shown are fluorescence measurements over time recorded from HEK293T/17 cells expressing a CFP-tagged PLCδ1-PH domain, which binds to $PI(4,5)P_2$. Cells were patch clamped in whole-cell mode and held at -60 mV. Fluorescence data over time are represented here as normalized cytoplasmic fluorescence divided by normalized plasma membrane fluorescence.
(A) A representative response from a cell coexpressing Dr-VSP with PLCδ1-PH-CFP. Gray bars indicate times when the cell was depolarized to +80 mV.
(B) A representative response from a cell coexpressing Dr-VSP with PLCδ1-PH-CFP (red), compared with a cohort of 2-3 cells coexpressing Dr-VSTpte with PLCδ1-PH-CFP (blue). A characteristic translocation of PLCδ1-PH-CFP was seen when Dr-VSP was activated by depolarizing to +100 mV for 5 seconds (grey bar), but not when Dr-VSTpte was activated.
(C) As in (B), but with depolarization to +100 mV for 10 seconds (gray bar).

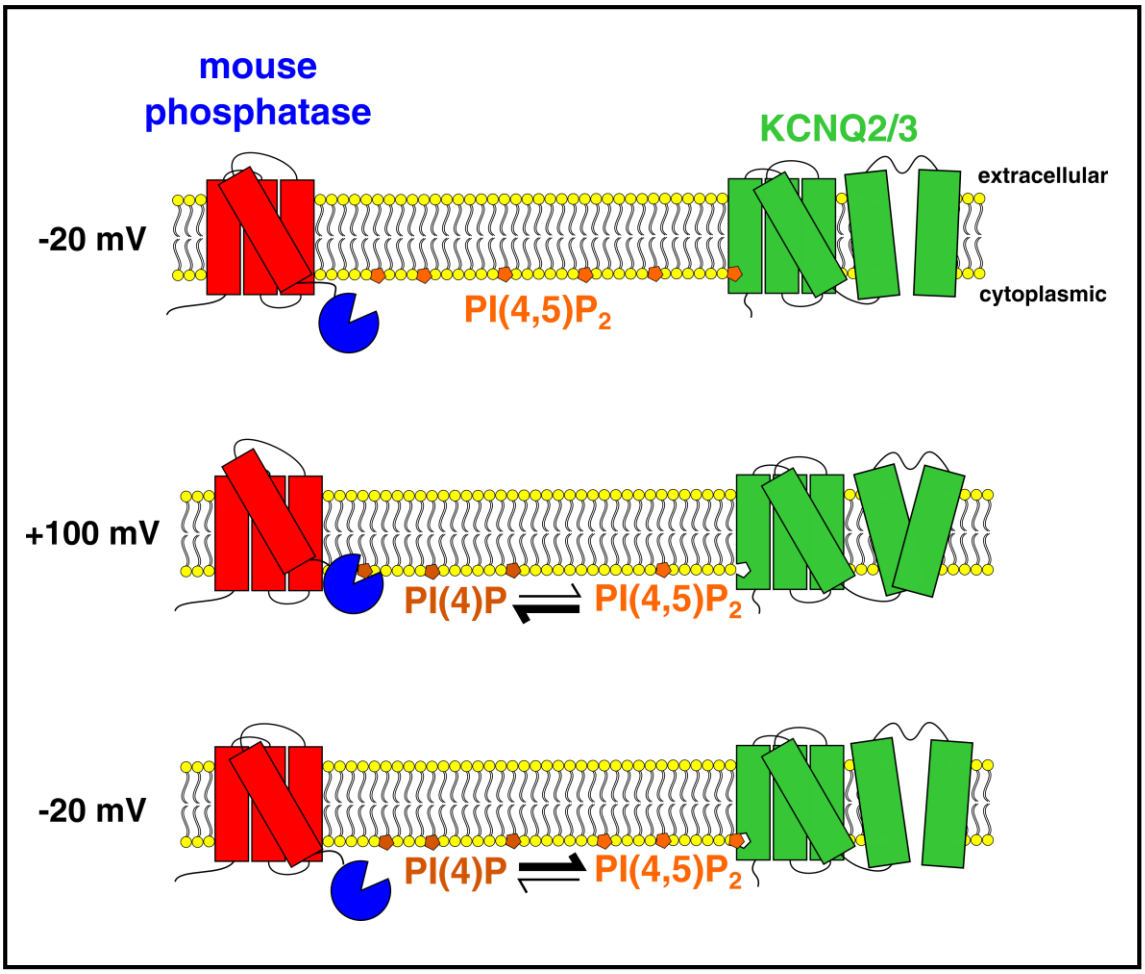

Figure 18: Direct model for a VSP-mediated decrease of PI(4,5)P_2

Shown is a cartoon depicting a model in which the Mm-VSP phosphatase domain directly dephosphorylates PI(4,5)P_2. At -20 mV, the VSP voltage sensor is in a resting state and the phosphatase domain is inactive, preserving the pool of PI(4,5)P_2 at the plasma membrane and thereby allowing KCNQ2/3 channels to open (top). At +100 mV, the VSP becomes active, dephosphorylating PI(4,5)P_2 to generate PI(4)P (middle). This decrease in PI(4,5)P_2 leads to KCNQ2/3 channel closure. Returning the cell to -20 mV deactivates the VSP, allowing PI(4,5)P_2 to be resynthesized from PI(4)P in a single step, through the activity of endogenous lipid kinases (bottom).

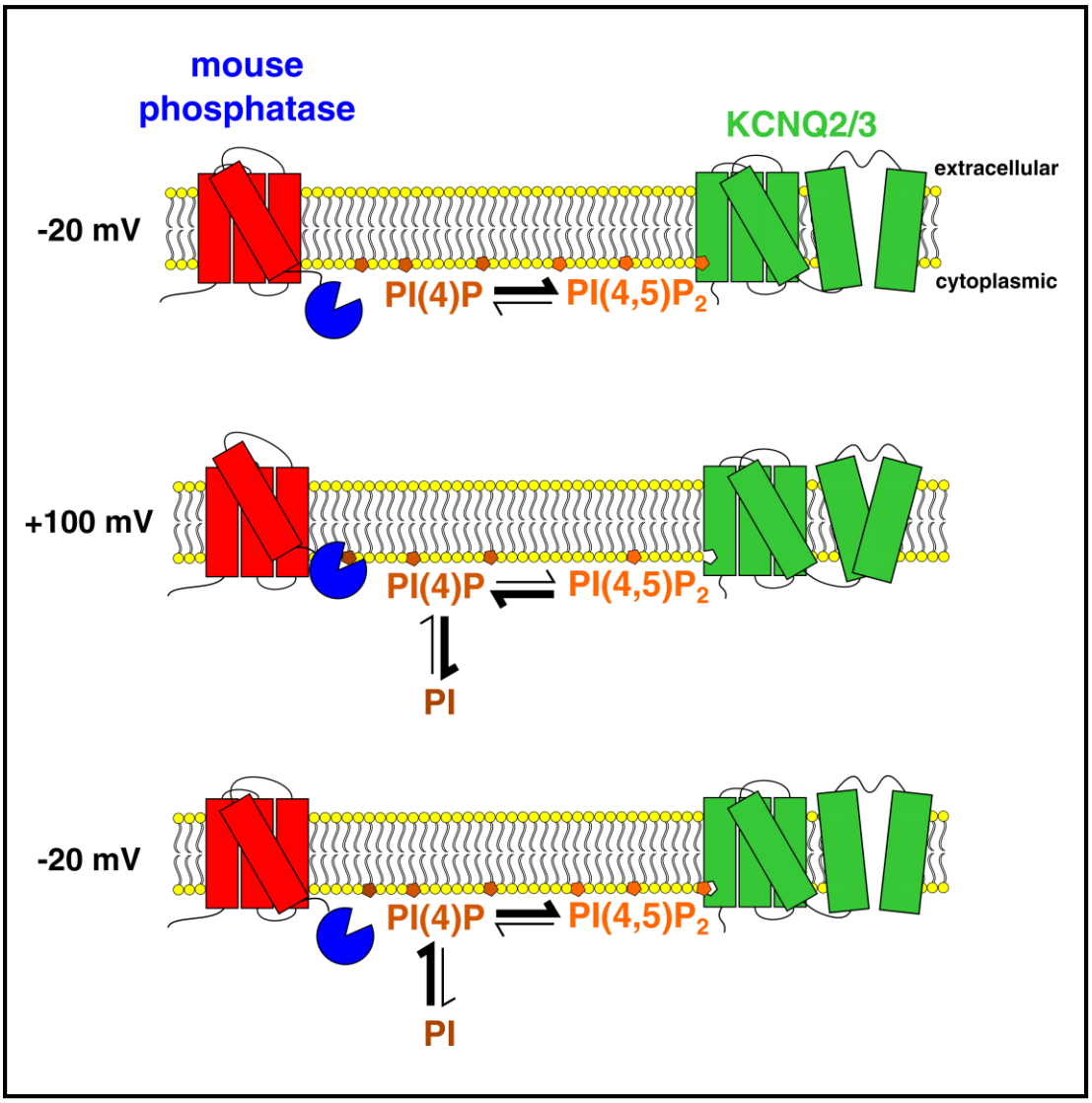

Figure 19: Indirect model for a VSP-mediated decrease of $PI(4,5)P_2$

Shown is a cartoon depicting a model in which the Mm-VSP phosphatase domain dephosphorylates PI(4)P, leading to an indirect decrease in $PI(4,5)P_2$. At -20 mV, the VSP voltage sensor is in a resting state and the phosphatase domain is inactive, preserving the pool of $PI(4,5)P_2$ at the plasma membrane and thereby allowing KCNQ2/3 channels to open (top). At +100 mV, the VSP becomes active, dephosphorylating PI(4)P to generate PI (middle). PI(4)P and $PI(4,5)P_2$ are maintained in a dynamic equilibrium at the plasma membrane, and so the decrease in PI(4)P levels leads to an indirect increase in $PI(4,5)P_2$. This decrease in $PI(4,5)P_2$ leads to KCNQ2/3 channel closure. Returning the cell to -20 mV deactivates the VSP, allowing PI(4)P to be resynthesized from PI, and $PI(4,5)P_2$ to be resynthesized from PI(4)P, through the activity of endogenous lipid kinases (bottom). This model predicts that resynthesis of $PI(4,5)P_2$ by lipid kinases will occur in two steps.

This apparent discrepancy can potentially be explained by the differences in affinity of the KCNQ2/3 channel and the PLCδ1-PH domain for $PI(4,5)P_2$ Inhibition of KCNQ2/3 current upon VSP activation is faster than translocation of the PLCδ1-PH away from the plasma membrane, and conversely PLCδ1-PH domain localization at the plasma membrane recovers more quickly than KCNQ2/3 currents (Falkenburger et al., 2010). Accordingly, in a kinetic model describing $PI(4,5)P_2$ metabolism Falkenburger *et al.* assigned KCNQ2/3 channels a K_D value 1000 times higher than the K_D of the PLCδ1-PH domain. The inability to detect changes in the localization of the PLCδ1-PH domain after activation of the Mm-VSP phosphatase domain is therefore likely due to the fact that small, slow changes in $PI(4,5)P_2$ levels are below the threshold for detection by PLCδ1-PH domain probes.

Conclusions regarding the phosphatase activity of Mm-VSP

Most of the VSP proteins that have been characterized so far are known to dephosphorylate $PI(4,5)P_2$. This activity has most often been measured by analyzing translocation of the $PI(4,5)P_2$-binding PLCδ1-PH domain and inhibition of $PI(4,5)P_2$-sensitive ion channels, such as the KCNQ2/3 channel. Although no voltage-dependent translocation of the PLCδ1-PH domain was observed in response to activation of the Mm-VSP phosphatase domain (Fig 17), Mm-VSP's phosphatase domain was able to cause a measurable decrease in the amplitude of currents generated by the KCNQ2/3 channel. While this indicates that the phosphatase activity of Mm-VSP leads to a decrease in $PI(4,5)P_2$, the kinetics of the current inhibition and recovery suggest that this may not be due to Mm-VSP directly dephosphorylating $PI(4,5)P_2$. One possibility for an alternative substrate is PI(4)P, the precursor of $PI(4,5)P_2$. Because endogenous kinases and phosphatases maintain $PI(4,5)P_2$ and PI(4)P in a dynamic

equilibrium (Dickson et al., 2014), decreases in PI(4)P can indirectly affect the concentration of $PI(4,5)P_2$.

While further studies will be required to provide stronger evidence in support of this substrate specificity, it is interesting to consider that one proposed role for VSPs is in regulating formation of neurite-like outgrowths (Yamaguchi et al., 2014) – a process in which PI 4-kinases and PI(4)P 5-kinases are known to play a role (Yamazaki et al., 2002; Hernandez-Deviez et al., 2004; Clayton et al., 2013). Moreover, the isoform of Mm-VSP expressed in the adult mouse brain localizes to the Golgi, where PI(4)P is the predominant phosphoinositide (Overduin et al., 2001). All the current data are therefore consistent with the possibility that Mm-VSP dephosphorylates PI(4)P.

IV. Possible physiological roles of Mm-VSP

Regulated electrical signaling and phospholipid signaling are both ubiquitously involved in physiological and pathophysiological phenomena, and VSPs are so far the only known proteins to directly couple these two signaling mechanisms. There is a clear motivation to understand the impact these proteins have on cellular physiology. Nevertheless, information regarding the activity of these proteins, particularly in mammals, has been difficult to acquire, and it remains unclear how many of the biophysical properties observed in non-mammalian VSPs are conserved in the VSPs from mammals.

In the work presented here, I have shown that the mammalian VSPs are evolutionarily very divergent from the best characterized VSPs in non-mammals (Fig 4). Accordingly, the subcellular localization, voltage-sensitivity, and phosphatase activity of Mm-VSP, a model mammalian VSP, are all distinct from the properties observed in non-mammalian VSPs. Therefore to address what the roles of mammalian VSPs are in regulating various aspects of cell

signaling, it will be important to consider the specific properties of the mammalian proteins. Based on the data I have presented here, I will now speculate on possible roles for Mm-VSP in the mouse central nervous system.

Mm-VSP to intracellular membranes of neurons suggests a novel function

I have shown that the mRNA encoding Mm-VSP, as well as the Mm-VSP protein are indeed both expressed in the mouse brain (Fig 7). Expression of both the transcript and protein is developmentally-regulated and – at least for the protein – expression is neuron-specific in the central nervous system (Fig 9). Taken together with the widespread distribution of neuronal subtypes that express Mm-VSP (Fig 10), these results strongly suggest an important role for mammalian VSPs in neurons. Given the importance of electrical and phosphoinositide signaling in neurons this is perhaps unsurprising. What was unexpected was the localization of the majority of Mm-VSP to intracellular membranes (Fig 9). While the possibility of an undiscovered splice variant or trafficking partner of Mm-VSP that would induce plasma membrane localization cannot be ruled out, both full-length and exon 9-lacking Mm-VSP clearly localize to intracellular membranes in HEK293T/17 cells (Fig 11). This is striking, as Ci-VSP, Dr-VSP, and certain isoforms of the human VSPs all traffic readily to the plasma membrane in this cell type.

One possible role for intracellular Mm-VSP is regulation of trafficking between intracellular membranes. Mm-VSP's own subcellular localization appears to be affected by both developmentally-regulated splicing and its own phosphatase activity (Fig 11), suggesting that Mm-VSP may regulate the trafficking of other proteins as well. It is possible that the C458S phosphatase-inactivating mutation results in a change in localization for reasons unrelated to the phosphatase activity. However, the analogous mutation in Ci-VSP (C363S) results in a protein

that is electrophysiologically (Villalba-Galea et al., 2009a) and structurally (Liu et al., 2012) comparable to the wild-type, making this possibility seem less likely. Future studies that analyze the effect of Mm-VSP on the trafficking of other proteins through the endoplasmic reticulum and Golgi should be able to address this possibility

Changes in pH: a secondary activation mechanism for Mm-VSP

Technical limitations have prohibited measurement of Mm-VSP's voltage sensitivity using the full Mm-VSP protein. To circumvent this challenge, I have used the Kv_{SynthM} chimeric potassium channel to characterize the Mm-VSP voltage sensor. The results from this characterization are extremely provocative, and suggest that the mammalian VSPs have voltage-dependent properties completely distinct from the non-mammalian proteins. Moreover the properties of the Mm-VSP voltage sensor are also consistent with the possibility that the primary role of Mm-VSP is at intracellular membranes. The voltage range of Mm-VSP's voltage sensor activation suggests that Mm-VSP would be chronically active at the resting membrane potentials of all cells. If Mm-VSP were expressed at the plasma membrane, this would lead to depletion of the concentration of $PI(4,5)P_2$, disrupting the many processes that rely on the phospholipid's presence (for reviews, see eg. (Czech, 2000; Gamper and Shapiro, 2007; Suh and Hille, 2008)).

In the Golgi however, $PI(4,5)P_2$ levels are low (Watt et al., 2002) despite evidence that the cell is capable of producing $PI(4,5)P_2$ on the Golgi membrane (Godi et al., 1999; Jones et al., 2000; Siddhanta et al., 2000). Hence while the Kv_{SynthM} results indicate that Mm-VSP will be chronically active at the Golgi membrane as well, which is predicted to have a transmembrane potential near 0 mV (Schapiro and Grinstein, 2000), this chronic activity is consistent with the phosphoinositide composition of the organelle. Although the Golgi is not thought to undergo fluctuations in transmembrane voltage comparable to those at the plasma membrane, the

discovery that activation of Mm-VSP's voltage sensor is affected by intracellular pH provides an alternate mechanism for protein regulation. The pH sensitivity of Mm-VSP also supports a possible Golgi-centric role for Mm-VSP. Regulation of intracellular pH has long been known to play an important role in Golgi trafficking and morphology (Cosson et al., 1989; Yoshida et al., 1999). As a provocative correlation, it has also been shown that changes in the phosphoinositides of intracellular membranes also affect Golgi trafficking and morphology (Siddhanta et al., 2000; Sweeney et al., 2002), and interactions between neuronal activity and intracellular pH have also been characterized (reviewed in (Chesler and Kaila, 1992; Chesler, 2003; Ruffin et al., 2014)). These findings are consistent with pH regulation of Mm-VSP as a physiologically important mechanism, and future studies to investigate the roles of Mm-VSP at intracellular membranes will likely be able to exploit this regulation by intracellular pH.

The slow phosphatase activity of Mm-VSP may hint at a divergent function

Recordings from $PI(4,5)P_2$-sensitive M currents demonstrate that the phosphatase domain of Mm-VSP can decrease the plasma membrane concentration of $PI(4,5)P_2$ in a voltage-dependent manner (Fig 16). However, Mm-VSP performs this function much more slowly than Dr-VSP, even when the same voltage sensor is used to activate both enzymes. Furthermore, the recovery of the $PI(4,5)P_2$ concentration takes place with distinct kinetics, depending on which phosphatase was activated. The biphasic recovery of $PI(4,5)P_2$ suggests that Mm-VSP may not directly dephosphorylate $PI(4,5)P_2$, and might instead utilize PI(4)P as a substrate (Fig 19). This possibility is particularly interesting given that the isoform of Mm-VSP expressed in adult brain localizes to the Golgi, where the major membrane phosphoinositide is PI(4)P (Overduin et al., 2001). Future work will doubtlessly be able to address this enticing possibility by analyzing the effect of Mm-VSP activation on the localization of PI(4)P-binding probes.

Epilogue

The discovery of the voltage-sensitive phosphatases demonstrated definitively and elegantly that the voltage sensing domain is a modular structure not restricted by nature to use in ion channels. The fact that VSPs function as monomers has made them far easier to work with than the multimeric channels, and significant insights into the structural nature of voltage sensing have been made using VSPs as model proteins. These include the discovery that the amino terminus of the VSD undergoes significant movement in response to changes in voltage (Tsutsui et al., 2013), and the observation of active and resting structures of the same voltage sensor (Li et al., 2014). VSPs have also proven to be extremely useful experimental tools, rapidly and specifically depleting pools of phosphoinositides. The unprecedented temporal control VSPs offer in manipulating phosphoinositides has provided invaluable information about the signaling roles that these phosphoinositides play (Klein et al., 2008; Falkenburger et al., 2010; Itsuki et al., 2012).

Yet, the great achievements made in the field of VSP research are rivaled by a single overarching question – what is it that VSPs *do*? How does the movement of the voltage sensor increase the activity of the phosphatase domain, and once it does, what does that mean for the cells in which VSPs are expressed? The ubiquitous biological importance of both phosphoinositide signaling and electrical signaling predicts that VSPs will play a marked role in the physiology of whatever cells they are found in, but exactly what this contribution is remains a mystery.

The best evidence so far for physiological roles of VSPs remains circumstantial, and varies significantly between the species in which VSPs are found. In some species the voltage

sensitivity, phosphatase activity, and expression profile of VSPs are consistent with a role in sperm-egg fusion (Ratzan et al., 2011), while in others these data are incompatible with such a role (Mutua et al., 2014). In some species the primary substrate of VSPs appears to be $PI(4,5)P_2$, (Murata and Okamura, 2007; Halaszovich et al., 2009), while other species have VSPs that seem to prefer $PI(3,4,5)P_2$ (Kurokawa et al., 2012; Yamaguchi et al., 2014).

To form a basis of work on which to investigate the physiological roles of VSPs in the central nervous system of mammals, I have presented an initial characterization of the mouse VSP family member, Mm-VSP. I have demonstrated an unequivocal expression in the neurons of the mouse brain, where the protein is developmentally regulated in multiple ways. I have addressed the functionality of the voltage sensor domain, demonstrating that the protein's activity is regulated by both voltage and intracellular pH. Similarly, I have shown that the phosphatase domain is an active lipid phosphatase whose activity can be controlled by voltage, and that is capable of inhibiting the physiologically important M currents. Based on the data regarding the localization and functionality of Mm-VSP, I speculate that the protein has a physiologically important role in the intracellular membranes of neurons. The importance of PI(4)P and $PI(4,5)P_2$ signaling pathways in the Golgi, as well as the importance of pH regulation, provide attractive possibilities for what actions VSPs might have in intracellular membranes. In particular, regulation of protein trafficking between intracellular membranes is an interesting possible role for Mm-VSP that warrants further investigation. This and other such possibilities will need to be systematically explored in future work, so as to provide further insight into the biological importance of the remarkable VSPs.

Appendix

I. Materials and Methods

Phylogenetic clustering

Phylogenetic protein sequence clustering was performed using ClustalW algorithm on the EMBL-EBI web server (McWilliam et al., 2013). Sequences were clustered based on the 4 transmembrane helices that form the voltage sensor, from the alignments reported by (Musset et al., 2011). Input sequences were platypus VSP (accession: gi_149635858), Xt-VSP (accession: gi_62859843), Gg-VSP (accession: gi_ 118084924), Dr-VSP (accession: gi_70887553), Xl-VSP1 (accession: gi_148230800), rat VSP (accession: gi_157820295), Mm-VSP (accession: gi_40549440), dog VSP (accession: gi_73993164), human TPIP (accession: gi_213972591), human TPTE (accession: gi_40549435), and Ci-VSP (accession: gi_76253898).

Crystal structure representation

Residues 1-116 from the crystal structure of the NavAb voltage-gated sodium channel were used as a structural example of an S4-based voltage sensor (PDB ID 3RVY_A). The PDB file was visualized and colored using PyMOL (Schrödinger, LLC).

Protein sequence alignment

For amino acid sequence comparisons, the COBALT algorithm (Papadopoulos and Agarwala, 2007) was used to align the sequences of Mm-VSP (accession: NP_954866.2), Ci-VSP (accession: BAD98733.1), Dr-VSP (accession: BAG50379.1), human TPTE (accession: NP_954868.1), human TPIP (accession: AAP45146.1), and *Drosophila* Shaker (accession: CAA29917.1). Alignments were visualized and annotated using Jalview (Waterhouse et al., 2009).

RT-PCR

RNA was purified from mouse whole brain homogenate using a spin column system (NucleoSpin, Machery-Nagel). RT-PCR primers against the Mm-VSP mRNA sequence (accession: NM_199257.2) were designed using the Primer-BLAST software (Ye et al., 2012). The three primer pairs used were 5'-CGACTTCTGAGCCCAAGCAGCC-3' with 5'-TGTCGTAGCCAGTGCTGCCATTTA-3', 5'-GGGGAGCTTCGAGCA GCACAAC-3' with 5'-ACCGAGGACACAAGGATGCGCA-3', and 5'-GTCTGTAGAAGGGAGACGGCGC-3' with 5'-GCGGACCCTGTAGTGGAAGTGC-3'. Reverse transcription and PCR were carried out in a 1-step procedure using the SuperScript III with Platinum *Taq* kit (Invitrogen). PCR products were separated by electrophoresis on a 1.5% agarose gel and visualized with ethidium bromide. For sequencing of selected amplicons, bands were cut from the agarose gel, purified using a spin column (QIAquick Gel Extraction Kit, Qiagen), and sequenced in the forward and reverse direction using the associated RT-PCR primers.

Molecular biology

The GalT-oxBFP construct was a generous gift of Dr. Erik Snapp at Albert Einstein College of Medicine. Kv_{Synth1}-psGEM was graciously given to us by the Moroni Lab at the University of Milan. KCNQ2, KCNQ3, and Dr-VSP-encoding constructs were kindly provided by the Hille Lab at the University of Washington. A BluntII-TOPO plasmid containing the DNA for Mm-

VSP was purchased from Open Biosystems (clone ID 40054415). Additional constructs were engineered and subcloned based on these plasmids using standard molecular cloning techniques.

To generate Mm-VSP constructs fused to a fluorescent tag, a common reverse primer was designed for amplifying all sequences, with the sequence 5'-AAAGGCGCGCCCCGTTCTCACCAAAATCCACC-3' (Mm-VSP-reverse). Full-length Mm-VSP was amplified using Mm-VSP- reverse and 5'-AAAAAGCTTGGATCCATGTATGGAGAAAAGAAGAGCCATTTG-3' (Mm-VSP-forward). An Mm-VSP amplicon lacking exon 9 was generated in two PCR steps: first, using the primers 5'-TGAATTCCTTGAGTGAAGTATCGAAAGAAATCAAAATCCCAAGTACACTGCAAACG-3' with Mm-VSP- reverse and 5'-CGTTTGCAGTGTACTTGGGATTTTGATTTCTTTCGATACTTCACTCAAGGAATTCA-3' with Mm-VSP-forward, and then by amplifying the combined resultant fragments with Mm-VSP-forward and Mm-VSP- reverse. The resulting Mm-VSP construct amplicons were cloned into pcDNA3 between the AscI and HindIII restriction sites, with DNA encoding GFP in-frame at the 3' end. Catalytically inactive Mm-VSP-Ex9 was generated by QuikChange mutagenesis (Stratagene) using the primers 5'- GCGATTCACTCTAAGGGAGGAAAAGGAAGAACTGG-3' and 5'-TCCTCCCTTAGAGTGAATCGCGACAACATTTTCAGG-3'.
For immunocytochemistry experiments, a sequence to encode full-length Mm-VSP with an N-terminally-fused FLAG epitope was generated using the primers 5'-AAACCCGGGATGGACTACAAGGACGATGACGACAAGTATGGAGAAAAGAAGAGCCATTTG-3' and 5'-GGATCCCTGCAGCTAGTTCTCACCAAAATCCAC-3'. The resulting amplicon was cloned into the pRRL vector between the PstI and BamHI restriction sites.
The original Kv_{Synth1} construct was amplified from an oocyte expression vector using the primers 5'- AAGCTTGGATCCATGGAGGGATTCGACGGT-3' and 5'-AAACGGCGCGCCCCTAAAGTTAGAACGATGAA-3' (Kv_{Synth} reverse), then subcloned into pcDNA3 for expression in mammalian cells between the BamHI and AscI restriction sites, with DNA encoding GFP in-frame at the 3' end. To generate Kv_{SynthM}, DNA encoding the Kcv pore was amplified from Kv_{Synth1} using the primers 5'-AAATTAATTAAAATGTTAGTGTTTAGTAAA-3' and Kv_{Synth} reverse. The VSD DNA from Mm-VSP was amplified using the primers 5'- AAAAAGCTTATGGAAATCAAAATCCCA-3' and 5'-AAATTAATTAATTGTCTCTTTTGATGAGC-3', then fused to the Kcv pore using the PacI restriction site to generate the full Kv_{SynthM} sequence. This was cloned into pcDNA3 between the HindIII and AscI restriction sites, with DNA encoding GFP in-frame at the 3' end.
Dr-VSTpte was generated by amplifying DNA encoding the Dr-VSP VSD using the primers 5'-AAAAAGCTTATGACGTCTGTGCATTTT-3' and 5'-AAAGGTACCCTCTCTCTTCTGCGAGGC-3', and by amplifying DNA encoding the Mm-VSP phosphatase using the primers 5'-AAAGGTACCCTCGAAAGGCTGACCAGG-3' and 5'-AAATTAATTAATTGTCTCTTTTGATGAGC-3'. The two fragments were ligated together using an engineered KpnI site, then inserted into pcDNA3 between the HindIII and AscI restriction sites. The engineered KpnI site, encoding two additional amino acids, was removed by QuikChange mutagenesis using the primers 5'-CTGGCCTCGCAGAAGAGAGAGCTCGAAAGGCTGACCAGGAAG-3' and 5'-CTTCCTGGTCAGCCTTTCGAGCTCTCTCTTCTGCGAGGCCAG-3'. Dr-VSTpte was then amplified and subcloned into pIRES2-EGFP (pIRES2) between the SacI and PstI restriction sites

using the primer pair 5'-GGGGAGCTCATGACGTCTGTGCATTTTAACCCTGGGTTA-3' and 5'-GGGCTGCAGCTAGTTCTCACCAAAATCCACCTCTACTGCAAA-3'.
All DNA constructs were verified by sequencing.

Cell culture

HEK293T/17 cells were grown at 37°C with 5% CO2 saturation in DMEM supplemented with 10% fetal bovine serum and 1% penicillin/streptomycin. For live-cell imaging and electrophysiology, cells were transfected with DNA using calcium phosphate, and experiments were conducted 24-48 hours later. Primary cultures of mouse cortical neurons and astrocytes were obtained at postnatal day 0-1. Cells were dissociated using papain trituration. Astrocytes were grown under the same conditions as HEK293T/17 cells until confluent. Neurons were cultured on top of a confluent layer of astrocytes at 37°C with 5% CO2 saturation in MEM supplemented with 1X Glutamax, 10% fetal horse serum, 25mM HEPES, 20mM glucose, 1% penicillin/streptomycin, 1% N2 supplement, 1% B27 supplement, and 1mM sodium pyruvate. For lentiviral infection, lentivirus particles were produced by transfecting HEK293T/17 cells with three packaging vectors (pLP1, pLP2, pLP_VSG) and FLAG-Mm-VSP-pRRL using calcium phosphate. Virions were harvested daily between 24 and 72 hours after transfection by collecting the culture medium. Virions were concentrated by centrifugation at 6690 RCF overnight at 4°C. Virions were applied to cultures between 24 and 72 hours after plating the cells. Experiments were conducted 14-17 days post-infection.

Microscopy

Immunolabeled samples were imaged on a Nikon Eclipse 90i with a 40x (cultured neurons) or 10x (sagittal brain slice) objective, and standard filter sets for GFP (excitation: 450-490nm, dichroic: 495nm, emission: 500-550nm), RFP (excitation: 530-560nm, dichroic: 570nm, emission: 590-650nm), and DAPI (excitation: 325-375nm, dichroic: 400nm, emission: 435-485nm). Images were acquired with a Cool Snap HQ2 cooled CCD camera (Photometrics) controlled through NIS-Elements software (Nikon). Live cell imaging was conducted on a Zeiss inverted laser scanning confocal microscope with a 40x objective. The oxBFP protein was excited with 405nm light, and emitted light was collected from 438-484nm. GFP was excited with 488nm light, and emitted light was collected from 504-552nm. Images were collected using ZEN software (Zeiss).

Antibody development

DNA encoding the first 113 amino acids of Mm-VSP was amplified using the PCR primers 5'-GGGGGATCCGAATTCATGTATGGAGAAAAGAAGAGCCAT-3' and 5'-GGGGAATTCAAGCTTCTGCAGCTACAGTTCATACAGGGTTGTGCTGCT-3'. This was inserted into the bacterial expression vector pRSF between the HindIII and EcoRI sites, generating a construct encoding a fusion protein with 6X-His and maltose binding protein (His-MBP) at the amino terminus. The resulting construct was electroporated into BL21 *E.coli*, and recombinant peptide containing Mm-VSP amino acids 1-113 was purified using the His-MBP dual affinity tag system, then cleaved from the tags using an engineered tobacco etched virus cleavage site. The identity of the protein was confirmed via mass spectrometry, and was then injected as an antigen into two different rabbits, h5535 and h5536, by New England Peptides. Antibody-containing serum from each rabbit had ELISA titers of 63,100 and 13,000, and both rabbits' sera were validated for use in immunocytochemistry experiments (Fig 8C). Serum h5536 was chosen for affinity purification to generate pure polyclonal antibodies for use in Western blotting. The immunizing peptide was immobilized through an N-terminal linkage on NHS-activated agarose beads (Pierce). Serum h5536 diluted 1:1 in binding buffer (25mM Tris,

150mM NaCl, pH 7.2) was passed over the peptide beads, allowing the antibodies to bind the peptide. The antibodies were eluted using high salt buffer (2.5M KCl, pH 7.7). Eight fractions were collected and tested for immunoreactivity via western blot against mouse whole brain homogenate. The fraction with the highest immunoreactivity was verified by incubating the antibody with the immunizing peptide before probing the Western blot, which blocked the majority of the band intensity at the expected size of Mm-VSP (Fig 8A). The blot shown is representative of 4 repeated peptide blocking experiments.

Western blotting

Mouse brains were dissected from animals and homogenized in 1ml buffer (0.32M sucrose, 5mM HEPES, pH7.4, 1X Roche EDTA-Free cOmplete protease inhibitor) per 100mg tissue. For samples treated with PNGaseF, the manufacturer's protocol was followed (New England Biolabs). Whole brain homogenate samples were run out on polyacrylamide gels, and transferred to nitrocellulose membranes. Membranes were probed first with the affinity purified Mm-VSP rabbit polyclonal antibody, then with a MAP2 monoclonal antibody raised in mouse (Sigma). Both antibodies were diluted 1:1000 in PBST with 1% BSA. Secondary goat anti-rabbit or goat anti-mouse IgG conjugated to horseradish peroxidase (Invitrogen) was diluted 1:1000 in PBST and incubated with the blot, then exposed using Clarity ECL substrate (BioRad) and imaged using a Kodak IS440CF digital imager.

Histological samples

Whole mouse brains were dissected out of adult animals, and then embedded in Tissue-Tek O.C.T. (Sakura) and frozen. 12.5um sagittal sections were taken using a Leica CM1850 cryostat, and kept frozen on coverglass under dessicating conditions until they were labeled.

Immunolabeling

Cell cultures and brain sections were fixed with 4% paraformaldehyde, then permeabilized and blocked in blocking buffer (2% normal goat serum, 0.4% saponin, 1% bovine serum albumin, in phosphate-buffered saline (PBS)). The sera containing rabbit polyclonal antibodies generated against Mm-VSP were used at 1:200 in blocking buffer. Both sera were validated to have high immunoreactivity and specificity in immunolabeling (Fig 8C), and were thus used interchangeably. Mouse monoclonal antibodies against FLAG (Sigma), MAP2 (Sigma), GFAP (Sigma), and SV2 (Buckley and Kelly, 1985) were all used at 1:1000. Alexa dyes 488 and 568 conjugated to goat anti-rabbit or goat anti-mouse secondary antibodies were used to visualize primary antibody labeling at dilutions between 1:1000 and 1:2500. Hoechst dye was used at 1:10000 in blocking buffer to label cell nuclei. For all samples, a corresponding control sample in which only secondary antibodies were added was used to assess the background fluorescence.

Fluorescence-detection size-exclusion chromatography

HEK293T/17 cells were transiently transfected with either mTpte-CFP-pcDNA3 or mTpte-Ex9-pcDNA3 and allowed to grow for 48 hours. Cells were then harvested in lysis buffer (25mM HEPES, pH 7.4, 150mM NaCl, 1mM EDTA, 1.5% dodecyl maltoside, and 2X protease inhibitor (cOmplete ULTRA, Roche)) to promote formation of mixed micelles containing the expressed proteins. Samples were passed over a Superdex 200 10/300 GL gel filtration column at a flow rate of 0.5mL/minute in running buffer (20mM HEPES, 150mM NaCl, 0.05mM EDTA, 0.08% dodecyl maltoside) using an automated FPLC system with fluorescence detector (Shimadzu).

Electrophysiology

HEK293T/17 cells were plated on a poly-lysine-coated coverslip at low density 4-24 hours before experiments began. For measurement of sensing currents, cells were continuously perfused with an extracellular solution of (in mM) 75 NMDG, 1 $CaCl_2$, 1 $MgCl_2$, and 180

HEPES, pH 7.0 with methanesulfonic acid. Cells were recorded from in whole-cell voltage clamp mode after achieving a gigaohm seal using a borosilicate patch pipette, with an intracellular solution of (in mM) 65 NMDG, 1 $MgCl_2$, and 100 HEPES, pH 7.0 with methanesulfonic acid. A P/5 leak subtraction protocol was applied to all sensing current measurements. For measurements of ionic currents, cells were continuously perfused with an extracellular solution of (in mM) 160 NaCl, 2.5 KCl, 2 $CaCl_2$, 1 $MgCl_2$, 10 HEPES, and 8 glucose, pH 7.4 with NaOH. Cells were recorded from in whole-cell voltage clamp mode after achieving a gigaohm seal using a borosilicate patch pipette, with an intracellular solution of (in mM) 175 KCl, 5 $MgCl_2$, 5 HEPES, 0.1 K_4BAPTA, 3 Na_2ATP, and 0.1 Na_3GTP, pH 7.4 with KOH, or 6.6 where noted (from (Falkenburger et al., 2010)). Recordings were collected by an EPC9 amplifier controlled by Pulse software (HEKA), and were filtered at 2.9 kHz. Data were collected with sample intervals of 0.1 ms (KCNQ2/3 tail currents), 0.4 ms (Kv_{Synth} currents), or 5 ms (current decay at +100 mV). Access resistance was kept below 10 MΩ, and 70% of series resistance was compensated after compensation of the capacitance. For Kv_{Synth} recordings, cells were held at -70 mV (or -90 mV, where noted). 4s long depolarizing pulses were then applied from -80 mV to +70 mV. The cell was then repolarized to -40 mV to measure tail currents. Recordings occurred once every 10 seconds to allow the channels to completely deactivate. For KCNQ2/3 (M current) recordings, cells were held at -60 mV. 300 ms depolarizations to -20 mV, followed by repolarization to -60 mV for 150 ms were applied every 500 ms for 10 seconds. KCNQ2/3 tail currents were measured instantly after repolarizing the cell. The cells were then pulsed to +100 mV for 8 seconds, and the current decay (if any) at +100 mV was recorded. The tail current measurement protocol then resumed for 40 seconds to observe recovery of any current inhibition. Traces were analyzed using IGOR Pro version 6.3.4.1 (Wavemetrics) after being imported using the PPT library (Dr. Francisco Mendez and Frank Würriehausen, Max-Planck Institute).

II. Abbreviations

- Akt — alternative name for protein kinase B (PKB)
- BFP — blue fluorescent protein
- Btk — Bruton's tyrosine kinase
- CFP — cyan fluorescent protein
- Ci-VSP — voltage-sensitive phosphatase from *Ciona intestinalis*
- Cp-VSP — voltage-sensitive phosphatase from *Cynops pyrrhogaster*
- Dr-VSP — voltage-sensitive phosphatase from *Danio rerio*
- ER — endoplasmic reticulum
- FSEC — fluorescence-detection size exclusion chromatography
- GFP — green fluorescent protein
- Hn-VSP — voltage-sensitive phosphatase from *Hynobius nebulosus*
- Mm-VSP — voltage-sensitive phosphatase from *Mus musculus*
- PBM — phosphoinositide-binding motif
- PD — pore domain
- PH domain — pleckstrin homology domain
- PI3K — phosphatidylinositol 3-kinase

- $PI(3,4)P_2$ phosphatidylinositol 3,4-bisphosphate
- $PI(3,4,5)P_3$ phosphatidylinositol 3,4,5-trisphosphate
- $PI(4,5)P_2$ phosphatidylinositol 4,5-bisphosphate
- PKB protein kinase B
- PLCδ1 phospholipase C, delta 1
- PTEN phosphatase and tensin homolog deleted on chromosome ten
- PTP protein tyrosine phosphatase
- TAPP1 tandem PH-domain-containing protein 1
- TEVC two-electrode voltage clamp
- TLC thin layer chromatography
- TPIP TPTE and PTEN homologous inositol lipid phosphatase
- TPTE transmembrane phosphatase with tensin homology
- VC voltage clamp
- VSD voltage sensing domain
- VSP voltage-sensitive phosphatase
- Xl-VSP voltage-sensitive phosphatase from *Xenopus laevis*
- Xt-VSP voltage-sensitive phosphatase from *Xenopus tropicalis*

III. Acknowledgements

Regarding the work I have presented here, I would like to thank Eamonn Dickson, Bertil Hille, Anna Moroni, and Erik Snapp for providing invaluable materials used in this project. Thanks also to all of my wonderful lab mates, past and present. In particular I would like to acknowledge Micaela Gomez, Pat Kensel-Hammes, and Jia Yao for their assistance with this project. Further thanks go to Bill Catterall, Marcus Collins, Rich Gardner, Fernando Gonzalez, Mika Munari, Fernando Santana, Todd Scheuer, Jane Sullivan, Carmen Ufret-Vincenty, Carlos Villalba-Galea, and Bill Zagotta for your extremely helpful discussions, feedback and overall support throughout the years.

On a more personal note, I have had the great luxury of being helped along my academic path by a number of remarkable people at many stages of my life. Without the support of these amazing individuals, I know that I would not have ended up where I am.

I must first acknowledge my family, and in particular my mother. You've encouraged me to achieve my goals for as long as I can remember, and you've always fostered a sense of wonder and curiosity about the world that I deeply appreciate. My adopted families, both legal and honorary, are also included in this category. I hope that you all know that your rank in my life is in no way secondary to questions of genetics. You have all been more supportive and incredible than I ever could have asked for, and I love you all.

My friends, who I am so fortunate to have too many of to name – you too are a family to me, and another amazing and supportive one at that. You've helped me tolerate the lows, celebrate the highs, and continue along the path to get where I am. I thank you all, and I look forward to enjoying the future with you.

My next thanks go to my scientific mentors, past and present:

Bill Gerthoffer – You served as my first scientific inspiration, and a wonderful life role model in general. You're responsible for first introducing me to what pharmacology was, and to how incredibly rewarding scientific pursuits could be.

Rochelle Wagner – You always pushed me to achieve my full potential, and laid the groundwork for my academic interests long before I could fully appreciate the quality of the teaching you were providing.

Pancho Bezanilla – You were the first person to show me the elegance of biophysics, and you provided a phenomenal learning and research environment. Furthermore, it's you who I have to thank for initiating my enduring fascination with ion channels and VSPs.

Sharona Gordon – I've immensely enjoyed our collaboration and friendship, and I certainly couldn't have performed the kind of work I've presented here without your help and support. I very much look forward to continuing our collaboration in the future.

Finally, Sandy Bajjalieh – I doubt whether many labs in the world would have allowed me the support and freedom to pursue my personal research interests that you have. I've always admired your dedication to scientific inquiry, and I could not have asked for a more encouraging environment to do my graduate work. I've been given the chance to achieve a childhood dream, and I couldn't have done that without the support you've given me. I feel that it's been a very productive and very fun few years working with you and your lab, and I will always appreciate the opportunities and training you've given me.

To all those listed here, thank you. This work is truly dedicated to you.

IV. References

Armstrong, C.M., and F. Bezanilla. 1973. Currents related to movement of the gating particles of the sodium channels. *Nature*. 242:459-461.

Arrigoni, C., I. Schroeder, G. Romani, J.L. Van Etten, G. Thiel, and A. Moroni. 2013. The voltage-sensing domain of a phosphatase gates the pore of a potassium channel. *The Journal of general physiology*. 141:389-395.

Barford, D., A.K. Das, and M.P. Egloff. 1998. The structure and mechanism of protein phosphatases: insights into catalysis and regulation. *Annual review of biophysics and biomolecular structure*. 27:133-164.

Bezanilla, F. 2000. The voltage sensor in voltage-dependent ion channels. *Physiological reviews*. 80:555-592.

Billups, D., B. Billups, R.A. Challiss, and S.R. Nahorski. 2006. Modulation of Gq-protein-coupled inositol trisphosphate and Ca2+ signaling by the membrane potential. *The Journal of neuroscience : the official journal of the Society for Neuroscience*. 26:9983-9995.

Brown, D.A., and P.R. Adams. 1980. Muscarinic suppression of a novel voltage-sensitive K+ current in a vertebrate neurone. *Nature*. 283:673-676.

Buckley, K., and R.B. Kelly. 1985. Identification of a transmembrane glycoprotein specific for secretory vesicles of neural and endocrine cells. *J Cell Biol*. 100:1284-1294.

Campbell, R.B., F. Liu, and A.H. Ross. 2003. Allosteric activation of PTEN phosphatase by phosphatidylinositol 4,5-bisphosphate. *The Journal of biological chemistry*. 278:33617-33620.

Cantley, L.C. 2002. The phosphoinositide 3-kinase pathway. *Science*. 296:1655-1657.

Catterall, W.A. 1986. Molecular properties of voltage-sensitive sodium channels. *Annual review of biochemistry*. 55:953-985.

Chen, H., C. Rossier, M.A. Morris, H.S. Scott, A. Gos, A. Bairoch, and S.E. Antonarakis. 1999. A testis-specific gene, TPTE, encodes a putative transmembrane tyrosine phosphatase and maps to the pericentromeric region of human chromosomes 21 and 13, and to chromosomes 15, 22, and Y. *Human genetics*. 105:399-409.

Chesler, M. 2003. Regulation and modulation of pH in the brain. *Physiological reviews*. 83:1183-1221.

Chesler, M., and K. Kaila. 1992. Modulation of pH by neuronal activity. *Trends in neurosciences*. 15:396-402.

Clayton, E.L., S. Minogue, and M.G. Waugh. 2013. Mammalian phosphatidylinositol 4-kinases as modulators of membrane trafficking and lipid signaling networks. *Progress in lipid research*. 52:294-304.

Cosson, P., I. Decurtis, J. Pouyssegur, G. Griffiths, and J. Davoust. 1989. Low Cytoplasmic Ph Inhibits Endocytosis and Transport from the Trans-Golgi Network to the Cell-Surface. *J Cell Biol*. 108:377-387.

Czech, M.P. 2000. PIP2 and PIP3: complex roles at the cell surface. *Cell*. 100:603-606.

De Matteis, M.A., A. Godi, and D. Corda. 2002. Phosphoinositides and the Golgi complex. *Curr Opin Cell Biol*. 14:434-447.

de Sousa Abreu, R., L.O. Penalva, E.M. Marcotte, and C. Vogel. 2009. Global signatures of protein and mRNA expression levels. *Molecular bioSystems*. 5:1512-1526.

Dickson, E.J., J.B. Jensen, and B. Hille. 2014. Golgi and plasma membrane pools of PI(4)P contribute to plasma membrane PI(4,5)P2 and maintenance of KCNQ2/3 ion channel current. *Proceedings of the National Academy of Sciences of the United States of America*. 111:E2281-2290.

Dowler, S., R.A. Currie, D.G. Campbell, M. Deak, G. Kular, C.P. Downes, and D.R. Alessi. 2000. Identification of pleckstrin-homology-domain-containing proteins with novel phosphoinositide-binding specificities. *The Biochemical journal*. 351:19-31.

Falkenburger, B.H., J.B. Jensen, and B. Hille. 2010. Kinetics of PIP2 metabolism and KCNQ2/3 channel regulation studied with a voltage-sensitive phosphatase in living cells. *The Journal of general physiology*. 135:99-114.

Fernandez, J.M., F. Bezanilla, and R.E. Taylor. 1982. Distribution and kinetics of membrane dielectric polarization. II. Frequency domain studies of gating currents. *The Journal of general physiology*. 79:41-67.

Fujiwara, Y., T. Kurokawa, K. Takeshita, M. Kobayashi, Y. Okochi, A. Nakagawa, and Y. Okamura. 2012. The cytoplasmic coiled-coil mediates cooperative gating temperature sensitivity in the voltage-gated H(+) channel Hv1. *Nature communications*. 3:816.

Gamper, N., and M.S. Shapiro. 2007. Role of PIP2 in regulating versus modulating Ca2+ channel activity - Reply. *J Physiol-London*. 583:1167-1167.

Godi, A., P. Pertile, R. Meyers, P. Marra, G. Di Tullio, C. Iurisci, A. Luini, D. Corda, and M.A. De Matteis. 1999. ARF mediates recruitment of PtdIns-4-OH kinase-beta and stimulates synthesis of PtdIns(4,5)P-2 on the Golgi complex. *Nat Cell Biol*. 1:280-287.

Gray, A., J. Van Der Kaay, and C.P. Downes. 1999. The pleckstrin homology domains of protein kinase B and GRP1 (general receptor for phosphoinositides-1) are sensitive and selective probes for the cellular detection of phosphatidylinositol 3,4-bisphosphate and/or phosphatidylinositol 3,4,5-trisphosphate in vivo. *The Biochemical journal*. 344 Pt 3:929-936.

Guipponi, M., C. Tapparel, O. Jousson, N. Scamuffa, C. Mas, C. Rossier, P. Hutter, P. Meda, R. Lyle, A. Reymond, and S.E. Antonarakis. 2001. The murine orthologue of the Golgi-localized TPTE protein provides clues to the evolutionary history of the human TPTE gene family. *Human genetics*. 109:569-575.

Guy, H.R., and P. Seetharamulu. 1986. Molecular model of the action potential sodium channel. *Proceedings of the National Academy of Sciences of the United States of America*. 83:508-512.

Halaszovich, C.R., M.G. Leitner, A. Mavrantoni, A. Le, L. Frezza, A. Feuer, D.N. Schreiber, C.A. Villalba-Galea, and D. Oliver. 2012. A human phospholipid phosphatase activated by a transmembrane control module. *Journal of lipid research*. 53:2266-2274.

Halaszovich, C.R., D.N. Schreiber, and D. Oliver. 2009. Ci-VSP is a depolarization-activated phosphatidylinositol-4,5-bisphosphate and phosphatidylinositol-3,4,5-trisphosphate 5'-phosphatase. *The Journal of biological chemistry*. 284:2106-2113.

Hernandez-Deviez, D.J., M.G. Roth, J.E. Casanova, and J.M. Wilson. 2004. ARNO and ARF6 regulate axonal elongation and branching through downstream activation of phosphatidylinositol 4-phosphate 5-kinase alpha. *Molecular biology of the cell*. 15:111-120.

Hille, B. 2001. Ion channels of excitable membranes. 3rd.ed. Sinauer, Sunderland, Mass. xviii, 814 p. pp.

Hobiger, K., T. Utesch, M.A. Mroginski, and T. Friedrich. 2012. Coupling of Ci-VSP modules requires a combination of structure and electrostatics within the linker. *Biophysical journal*. 102:1313-1322.
Hobiger, K., T. Utesch, M.A. Mroginski, G. Seebohm, and T. Friedrich. 2013. The linker pivot in Ci-VSP: the key to unlock catalysis. *PloS one*. 8:e70272.
Hodgkin, A.L., and A.F. Huxley. 1952. A quantitative description of membrane current and its application to conduction and excitation in nerve. *The Journal of physiology*. 117:500-544.
Hopp, T.P., and K.R. Woods. 1981. Prediction of protein antigenic determinants from amino acid sequences. *Proceedings of the National Academy of Sciences of the United States of America*. 78:3824-3828.
Horn, R. 2002. Coupled movements in voltage-gated ion channels. *The Journal of general physiology*. 120:449-453.
Hossain, M.I., H. Iwasaki, Y. Okochi, M. Chahine, S. Higashijima, K. Nagayama, and Y. Okamura. 2008. Enzyme domain affects the movement of the voltage sensor in ascidian and zebrafish voltage-sensing phosphatases. *The Journal of biological chemistry*. 283:18248-18259.
Itsuki, K., Y. Imai, Y. Okamura, K. Abe, R. Inoue, and M.X. Mori. 2012. Voltage-sensing phosphatase reveals temporal regulation of TRPC3/C6/C7 channels by membrane phosphoinositides. *Channels*. 6:206-209.
Iwasaki, H., Y. Murata, Y. Kim, M.I. Hossain, C.A. Worby, J.E. Dixon, T. McCormack, T. Sasaki, and Y. Okamura. 2008. A voltage-sensing phosphatase, Ci-VSP, which shares sequence identity with PTEN, dephosphorylates phosphatidylinositol 4,5-bisphosphate. *Proceedings of the National Academy of Sciences of the United States of America*. 105:7970-7975.
Jaffe, L.A. 1976. Fast block to polyspermy in sea urchin eggs is electrically mediated. *Nature*. 261:68-71.
Jaffe, L.A., A.P. Sharp, and D.P. Wolf. 1983. Absence of an electrical polyspermy block in the mouse. *Developmental biology*. 96:317-323.
Jones, D.H., J.B. Morris, C.P. Morgan, H. Kondo, R.F. Irvine, and S. Cockcroft. 2000. Type I phosphatidylinositol 4-phosphate 5-kinase directly interacts with ADP-ribosylation factor 1 and is responsible for phosphatidylinositol 4,5-bisphosphate synthesis in the golgi compartment. *The Journal of biological chemistry*. 275:13962-13966.
Kandel, E.R., J.H. Schwartz, and T.M. Jessell. 2000. Principles of neural science. 4th.ed. McGraw-Hill, Health Professions Division, New York. xli, 1414 p. pp.
Kawate, T., and E. Gouaux. 2006. Fluorescence-detection size-exclusion chromatography for precrystallization screening of integral membrane proteins. *Structure*. 14:673-681.
Keynes, R.D., and E. Rojas. 1974. Kinetics and steady-state properties of the charged system controlling sodium conductance in the squid giant axon. *The Journal of physiology*. 239:393-434.
Klein, R.M., C.A. Ufret-Vincenty, L. Hua, and S.E. Gordon. 2008. Determinants of molecular specificity in phosphoinositide regulation. Phosphatidylinositol (4,5)-bisphosphate (PI(4,5)P2) is the endogenous lipid regulating TRPV1. *The Journal of biological chemistry*. 283:26208-26216.
Koch, H.P., T. Kurokawa, Y. Okochi, M. Sasaki, Y. Okamura, and H.P. Larsson. 2008. Multimeric nature of voltage-gated proton channels. *Proceedings of the National Academy of Sciences of the United States of America*. 105:9111-9116.
Kohout, S.C., S.C. Bell, L. Liu, Q. Xu, D.L. Minor, Jr., and E.Y. Isacoff. 2010. Electrochemical coupling in the voltage-dependent phosphatase Ci-VSP. *Nature chemical biology*. 6:369-375.
Kohout, S.C., M.H. Ulbrich, S.C. Bell, and E.Y. Isacoff. 2008. Subunit organization and functional transitions in Ci-VSP. *Nature structural & molecular biology*. 15:106-108.
Kumanovics, A., G. Levin, and P. Blount. 2002. Family ties of gated pores: evolution of the sensor module. *FASEB journal : official publication of the Federation of American Societies for Experimental Biology*. 16:1623-1629.
Kurokawa, T., S. Takasuga, S. Sakata, S. Yamaguchi, S. Horie, K.J. Homma, T. Sasaki, and Y. Okamura. 2012. 3' Phosphatase activity toward phosphatidylinositol 3,4-bisphosphate [PI(3,4)P2] by voltage-sensing phosphatase (VSP). *Proceedings of the National Academy of Sciences of the United States of America*. 109:10089-10094.

Kuzmenkin, A., F. Bezanilla, and A.M. Correa. 2004. Gating of the bacterial sodium channel, NaChBac: voltage-dependent charge movement and gating currents. *The Journal of general physiology*. 124:349-356.

Lacroix, J., C.R. Halaszovich, D.N. Schreiber, M.G. Leitner, F. Bezanilla, D. Oliver, and C.A. Villalba-Galea. 2011. Controlling the activity of a phosphatase and tensin homolog (PTEN) by membrane potential. *The Journal of biological chemistry*. 286:17945-17953.

Lacroix, J.J., and F. Bezanilla. 2012. Tuning the voltage-sensor motion with a single residue. *Biophysical journal*. 103:L23-25.

Lee, S.Y., J.A. Letts, and R. Mackinnon. 2008. Dimeric subunit stoichiometry of the human voltage-dependent proton channel Hv1. *Proceedings of the National Academy of Sciences of the United States of America*. 105:7692-7695.

Leslie, N.R., X.S. Yang, C.P. Downes, and C.J. Weijer. 2007. PtdIns(3,4,5)P-3-dependent and -independent roles for PTEN in the control of cell migration. *Curr Biol*. 17:115-125.

Levine, T.P., and S. Munro. 2002. Targeting of Golgi-specific pleckstrin homology domains involves both PtdIns 4-kinase-dependent and -independent components. *Curr Biol*. 12:695-704.

Li, J., C. Yen, D. Liaw, K. Podsypanina, S. Bose, S.I. Wang, J. Puc, C. Miliaresis, L. Rodgers, R. McCombie, S.H. Bigner, B.C. Giovanella, M. Ittmann, B. Tycko, H. Hibshoosh, M.H. Wigler, and R. Parsons. 1997. PTEN, a putative protein tyrosine phosphatase gene mutated in human brain, breast, and prostate cancer. *Science*. 275:1943-1947.

Li, Q., S. Wanderling, M. Paduch, D. Medovoy, A. Singharoy, R. McGreevy, C.A. Villalba-Galea, R.E. Hulse, B. Roux, K. Schulten, A. Kossiakoff, and E. Perozo. 2014. Structural mechanism of voltage-dependent gating in an isolated voltage-sensing domain. *Nature structural & molecular biology*. 21:244-252.

Liu, L., S.C. Kohout, Q. Xu, S. Muller, C.R. Kimberlin, E.Y. Isacoff, and D.L. Minor, Jr. 2012. A glutamate switch controls voltage-sensitive phosphatase function. *Nature structural & molecular biology*. 19:633-641.

Maehama, T., and J.E. Dixon. 1998. The tumor suppressor, PTEN/MMAC1, dephosphorylates the lipid second messenger, phosphatidylinositol 3,4,5-trisphosphate. *The Journal of biological chemistry*. 273:13375-13378.

Mahaut-Smith, M.P., J.F. Hussain, and M.J. Mason. 1999. Depolarization-evoked Ca2+ release in a non-excitable cell, the rat megakaryocyte. *The Journal of physiology*. 515 (Pt 2):385-390.

Mason, M.J., and M.P. Mahaut-Smith. 2001. Voltage-dependent Ca2+ release in rat megakaryocytes requires functional IP3 receptors. *The Journal of physiology*. 533:175-183.

McWilliam, H., W. Li, M. Uludag, S. Squizzato, Y.M. Park, N. Buso, A.P. Cowley, and R. Lopez. 2013. Analysis Tool Web Services from the EMBL-EBI. *Nucleic acids research*. 41:W597-600.

Murata, Y., H. Iwasaki, M. Sasaki, K. Inaba, and Y. Okamura. 2005. Phosphoinositide phosphatase activity coupled to an intrinsic voltage sensor. *Nature*. 435:1239-1243.

Murata, Y., and Y. Okamura. 2007. Depolarization activates the phosphoinositide phosphatase Ci-VSP, as detected in Xenopus oocytes coexpressing sensors of PIP2. *The Journal of physiology*. 583:875-889.

Musset, B., S.M. Smith, S. Rajan, D. Morgan, V.V. Cherny, and T.E. Decoursey. 2011. Aspartate 112 is the selectivity filter of the human voltage-gated proton channel. *Nature*. 480:273-277.

Mutua, J., Y. Jinno, S. Sakata, Y. Okochi, S. Ueno, H. Tsutsui, T. Kawai, Y. Iwao, and Y. Okamura. 2014. Functional diversity of voltage-sensing phosphatases in two urodele amphibians. *Physiological reports*. 2.

Ogasawara, M., M. Sasaki, N. Nakazawa, A. Nishino, and Y. Okamura. 2011. Gene expression profile of Ci-VSP in juveniles and adult blood cells of ascidian. *Gene expression patterns : GEP*. 11:233-238.

Okamura, Y., Y. Murata, and H. Iwasaki. 2009. Voltage-sensing phosphatase: actions and potentials. *The Journal of physiology*. 587:513-520.

Okamura, Y., A. Nishino, Y. Murata, K. Nakajo, H. Iwasaki, Y. Ohtsuka, M. Tanaka-Kunishima, N. Takahashi, Y. Hara, T. Yoshida, M. Nishida, H. Okado, H. Watari, I.A. Meinertzhagen, N. Satoh, K. Takahashi, Y. Satou, Y. Okada, and Y. Mori. 2005. Comprehensive analysis of the ascidian genome reveals novel insights into the molecular evolution of ion channel genes. *Physiological genomics*. 22:269-282.

Olcese, R., R. Latorre, L. Toro, F. Bezanilla, and E. Stefani. 1997. Correlation between charge movement and ionic current during slow inactivation in Shaker K+ channels. *The Journal of general physiology*. 110:579-589.

Overduin, M., M.L. Cheever, and T.G. Kutateladze. 2001. Signaling with phosphoinositides: better than binary. *Molecular interventions*. 1:150-159.

Papadopoulos, J.S., and R. Agarwala. 2007. COBALT: constraint-based alignment tool for multiple protein sequences. *Bioinformatics*. 23:1073-1079.

Payandeh, J., T. Scheuer, N. Zheng, and W.A. Catterall. 2011. The crystal structure of a voltage-gated sodium channel. *Nature*. 475:353-358.

Piper, D.R., A. Varghese, M.C. Sanguinetti, and M. Tristani-Firouzi. 2003. Gating currents associated with intramembrane charge displacement in HERG potassium channels. *Proceedings of the National Academy of Sciences of the United States of America*. 100:10534-10539.

Plugge, B., S. Gazzarrini, M. Nelson, R. Cerana, J.L. Van Etten, C. Derst, D. DiFrancesco, A. Moroni, and G. Thiel. 2000. A potassium channel protein encoded by chlorella virus PBCV-1. *Science*. 287:1641-1644.

Raftopoulou, M., S. Etienne-Manneville, A. Self, S. Nicholls, and A. Hall. 2004. Regulation of cell migration by the C2 domain of the tumor suppressor PTEN. *Science*. 303:1179-1181.

Ratzan, W.J., A.V. Evsikov, Y. Okamura, and L.A. Jaffe. 2011. Voltage sensitive phosphoinositide phosphatases of Xenopus: their tissue distribution and voltage dependence. *Journal of cellular physiology*. 226:2740-2746.

Reddy, R., D. Smith, G. Wayman, Z. Wu, E.C. Villacres, and D.R. Storm. 1995. Voltage-sensitive adenylyl cyclase activity in cultured neurons. A calcium-independent phenomenon. *The Journal of biological chemistry*. 270:14340-14346.

Redfern, R.E., D. Redfern, M.L. Furgason, M. Munson, A.H. Ross, and A. Gericke. 2008. PTEN phosphatase selectively binds phosphoinositides and undergoes structural changes. *Biochemistry*. 47:2162-2171.

Reymond, A., V. Marigo, M.B. Yaylaoglu, A. Leoni, C. Ucla, N. Scamuffa, C. Caccioppoli, E.T. Dermitzakis, R. Lyle, S. Banfi, G. Eichele, S.E. Antonarakis, and A. Ballabio. 2002. Human chromosome 21 gene expression atlas in the mouse. *Nature*. 420:582-586.

Ruffin, V.A., A.I. Salameh, W.F. Boron, and M.D. Parker. 2014. Intracellular pH regulation by acid-base transporters in mammalian neurons. *Frontiers in physiology*. 5:43.

Sakata, S., M.I. Hossain, and Y. Okamura. 2011. Coupling of the phosphatase activity of Ci-VSP to its voltage sensor activity over the entire range of voltage sensitivity. *The Journal of physiology*. 589:2687-2705.

Sakata, S., and Y. Okamura. 2014. Phosphatase activity of the voltage-sensing phosphatase, VSP, shows graded dependence on the extent of activation of the voltage sensor. *The Journal of physiology*. 592:899-914.

Salim, K., M.J. Bottomley, E. Querfurth, M.J. Zvelebil, I. Gout, R. Scaife, R.L. Margolis, R. Gigg, C.I. Smith, P.C. Driscoll, M.D. Waterfield, and G. Panayotou. 1996. Distinct specificity in the recognition of phosphoinositides by the pleckstrin homology domains of dynamin and Bruton's tyrosine kinase. *The EMBO journal*. 15:6241-6250.

Schapiro, F.B., and S. Grinstein. 2000. Determinants of the pH of the Golgi complex. *Journal of Biological Chemistry*. 275:21025-21032.

Schneider, M.F., and W.K. Chandler. 1973. Voltage dependent charge movement of skeletal muscle: a possible step in excitation-contraction coupling. *Nature*. 242:244-246.

Shirokov, R., R. Levis, N. Shirokova, and E. Rios. 1992. Two classes of gating current from L-type Ca channels in guinea pig ventricular myocytes. *The Journal of general physiology*. 99:863-895.
Siddhanta, A., J.M. Backer, and D. Shields. 2000. Inhibition of phosphatidic acid synthesis alters the structure of the Golgi apparatus and inhibits secretion in endocrine cells. *Journal of Biological Chemistry*. 275:12023-12031.
Starace, D.M., and F. Bezanilla. 2001. Histidine scanning mutagenesis of basic residues of the S4 segment of the shaker k+ channel. *The Journal of general physiology*. 117:469-490.
Starace, D.M., E. Stefani, and F. Bezanilla. 1997. Voltage-dependent proton transport by the voltage sensor of the Shaker K+ channel. *Neuron*. 19:1319-1327.
Steck, P.A., M.A. Pershouse, S.A. Jasser, W.K. Yung, H. Lin, A.H. Ligon, L.A. Langford, M.L. Baumgard, T. Hattier, T. Davis, C. Frye, R. Hu, B. Swedlund, D.H. Teng, and S.V. Tavtigian. 1997. Identification of a candidate tumour suppressor gene, MMAC1, at chromosome 10q23.3 that is mutated in multiple advanced cancers. *Nature genetics*. 15:356-362.
Suh, B.C., and B. Hille. 2008. PIP2 is a necessary cofactor for ion channel function: how and why? *Annual review of biophysics*. 37:175-195.
Sutton, K.A., M.K. Jungnickel, L. Jovine, and H.M. Florman. 2012. Evolution of the voltage sensor domain of the voltage-sensitive phosphoinositide phosphatase VSP/TPTE suggests a role as a proton channel in eutherian mammals. *Molecular biology and evolution*. 29:2147-2155.
Sweeney, D.A., A. Siddhanta, and D. Shields. 2002. Fragmentation and re-assembly of the Golgi apparatus in vitro - A requirement for phosphatidic acid and phosphatidylinositol 4,5-bisphosphate synthesis. *Journal of Biological Chemistry*. 277:3030-3039.
Tapparel, C., A. Reymond, C. Girardet, L. Guillou, R. Lyle, C. Lamon, P. Hutter, and S.E. Antonarakis. 2003. The TPTE gene family: cellular expression, subcellular localization and alternative splicing. *Gene*. 323:189-199.
Tombola, F., M.H. Ulbrich, and E.Y. Isacoff. 2008. The voltage-gated proton channel Hv1 has two pores, each controlled by one voltage sensor. *Neuron*. 58:546-556.
Tsutsui, H., Y. Jinno, A. Tomita, and Y. Okamura. 2013. Optically detected structural change in the N-terminal region of the voltage-sensor domain. *Biophysical journal*. 105:108-115.
Vanhaesebroeck, B., S.J. Leevers, K. Ahmadi, J. Timms, R. Katso, P.C. Driscoll, R. Woscholski, P.J. Parker, and M.D. Waterfield. 2001. Synthesis and function of 3-phosphorylated inositol lipids. *Annual review of biochemistry*. 70:535-602.
Varnai, P., and T. Balla. 1998. Visualization of phosphoinositides that bind pleckstrin homology domains: calcium- and agonist-induced dynamic changes and relationship to myo-[3H]inositol-labeled phosphoinositide pools. *J Cell Biol*. 143:501-510.
Villalba-Galea, C.A., L. Frezza, W. Sandtner, and F. Bezanilla. 2013. Sensing charges of the Ciona intestinalis voltage-sensing phosphatase. *The Journal of general physiology*. 142:543-555.
Villalba-Galea, C.A., F. Miceli, M. Taglialatela, and F. Bezanilla. 2009a. Coupling between the voltage-sensing and phosphatase domains of Ci-VSP. *The Journal of general physiology*. 134:5-14.
Villalba-Galea, C.A., W. Sandtner, D. Dimitrov, H. Mutoh, T. Knopfel, and F. Bezanilla. 2009b. Charge movement of a voltage-sensitive fluorescent protein. *Biophysical journal*. 96:L19-21.
Villalba-Galea, C.A., W. Sandtner, D.M. Starace, and F. Bezanilla. 2008. S4-based voltage sensors have three major conformations. *Proceedings of the National Academy of Sciences of the United States of America*. 105:17600-17607.
Walker, S.M., C.P. Downes, and N.R. Leslie. 2001. TPIP: a novel phosphoinositide 3-phosphatase. *The Biochemical journal*. 360:277-283.
Walker, S.M., N.R. Leslie, N.M. Perera, I.H. Batty, and C.P. Downes. 2004. The tumour-suppressor function of PTEN requires an N-terminal lipid-binding motif. *The Biochemical journal*. 379:301-307.
Waterhouse, A.M., J.B. Procter, D.M. Martin, M. Clamp, and G.J. Barton. 2009. Jalview Version 2--a multiple sequence alignment editor and analysis workbench. *Bioinformatics*. 25:1189-1191.

Watt, S.A., G. Kular, I.N. Fleming, C.P. Downes, and J.M. Lucocq. 2002. Subcellular localization of phosphatidylinositol 4,5-bisphosphate using the pleckstrin homology domain of phospholipase C delta(1). *Biochemical Journal*. 363:657-666.

Wilkins, M.R., E. Gasteiger, A. Bairoch, J.C. Sanchez, K.L. Williams, R.D. Appel, and D.F. Hochstrasser. 1999. Protein identification and analysis tools in the ExPASy server. *Methods in molecular biology*. 112:531-552.

Willars, G.B., S.R. Nahorski, and R.A. Challiss. 1998. Differential regulation of muscarinic acetylcholine receptor-sensitive polyphosphoinositide pools and consequences for signaling in human neuroblastoma cells. *The Journal of biological chemistry*. 273:5037-5046.

Wu, Y., D. Dowbenko, M.T. Pisabarro, L. Dillard-Telm, H. Koeppen, and L.A. Lasky. 2001. PTEN 2, a Golgi-associated testis-specific homologue of the PTEN tumor suppressor lipid phosphatase. *The Journal of biological chemistry*. 276:21745-21753.

Yamaguchi, S., T. Kurokawa, I. Taira, N. Aoki, S. Sakata, Y. Okamura, and K.J. Homma. 2014. Potential role of voltage-sensing phosphatases in regulation of cell structure through the production of PI(3,4)P2. *Journal of cellular physiology*. 229:422-433.

Yamazaki, M., H. Miyazaki, H. Watanabe, T. Sasaki, T. Maehama, M.A. Frohman, and Y. Kanaho. 2002. Phosphatidylinositol 4-phosphate 5-kinase is essential for ROCK-mediated neurite remodeling. *The Journal of biological chemistry*. 277:17226-17230.

Ye, J., G. Coulouris, I. Zaretskaya, I. Cutcutache, S. Rozen, and T.L. Madden. 2012. Primer-BLAST: a tool to design target-specific primers for polymerase chain reaction. *BMC bioinformatics*. 13:134.

Yoshida, T., T. Kamiya, K. Imanaka-Yoshida, and T. Sakakura. 1999. Low cytoplasmic pH causes fragmentation and dispersal of the Golgi apparatus in human hepatoma cells. *Int J Exp Pathol*. 80:51-57.

Yu, F.H., V. Yarov-Yarovoy, G.A. Gutman, and W.A. Catterall. 2005. Overview of molecular relationships in the voltage-gated ion channel superfamily. *Pharmacological reviews*. 57:387-395.

Zhang, H.L., L.C. Craciun, T. Mirshahi, T. Rohacs, C.M.B. Lopes, T.H. Jin, and D.E. Logothetis. 2003. PIP2 activates KCNQ channels, and its hydrolysis underlies receptor-mediated inhibition of M currents. *Neuron*. 37:963-975.